Eidgenössische Technische Hochschule Zürich
Swiss Federal Institute of Technology Zurich

WSL-Institut für Schnee- und Lawinenforschung SLF

Forest and Snow Avalanche Dynamics

Application and Evaluation of the RAMMS Forest Detrainment Function in the Back-Simulation of the 1951 Forest Avalanches in Engadin.

Valentina Berchier
May 2018

Master Thesis
Department of Environmental Systems Science
Forest and Landscape Management
ETH Zürich

Supervisor
Dr. Peter Bebi
WSL-Institute for Snow and Avalanche Research SLF
Dr. Perry Bartelt
WSL-Institute for Snow and Avalanche Research SLF

Front page: Picture of the study area Zernez after the avalanche event in 1951.

Zusammenfassung

Lawinen stellen eine grosse Bedrohung für Strassen und Siedlungen dar. Eine der am weitesten verbreiteten und effektiven Schutzmassnahmen gegen diese Gefahr ist der Wald, dies obwohl er bei extremen Lawinen oft auch selbst gefährdet sein kann. Trotz der Waldschäden deuten mehrere Studien auf eine Auslaufverkürzung und –verlangsamung der durch den Wald fliessenden Lawinen hin. In der Gefahrenkartierung werden heutzutage Modelle für die Lawinensimulation breit angewendet. Dabei wird die Wirkung des Waldes lediglich als zusätzlicher Reibungsfaktor betrachtet. Im Fall von extremen Lawinen wird die Wirkung komplett vernachlässigt. Einen unterschiedlichen Ansatz für die genauere Berücksichtigung der Waldwirkung wurde am SLF im Rahmen der neuen Forschungsversion der Software RAMMS (Rapid Mass Movement Simulation) entwickelt. Dabei besteht die Wirkung der Bäume im Zurückhalten von Schneemasse, die direkt aus der Lawine in Funktion der Fliessgeschwindigkeit und der Waldstruktur (als K-Wert definiert) entzogen wird. Der neue Waldansatz impliziert, dass die Lawinenschutzwirkung von Bergwäldern in direktem Zusammenhang mit der Lawinengrösse steht.

In dieser Arbeit wurde die Forschungsversion von RAMMS in der Nachsimulierung von grossen bis extremen Lawinen, die den Wald über den Dörfern La Punt, Susauna und Zernez im Engadin im Jahre 1951 zerstörten, angewendet und ausgewertet. Die vorliegende Arbeit zielt darauf ab, die Veränderung der Lawinenschutzfunktion seit 1951 zu überprüfen und die Wirkung der Waldbedingungen im Jahre 2018 in der Simulation von entsprechenden extremen Lawinen zu untersuchen.
In der Forschungsversion von RAMMS ist es möglich, zusätzliche Prozesse wie z.B. die Schneeaufnahme im Transitbereich, zu berücksichtigen. Die Sensitivität der Resultate im Bezug auf den Koeffizienten für die Parametrisierung dieses Prozesses und die Waldparameter wurde anhand von Simulationen im Jahre 1951 verglichen. Anschliessend wurde den Einsatz von landesweit verfügbaren Fernerkundungsdaten (Kronenhöhenmodell und SwissALTI3D-Geländemodell) für die Klassifizierung der Waldparameter und für die in den Simulationen gebrauchten K-Werte geprüft.

Lawinenanrissgebiete, Waldstruktur und Parameter für die Nachsimulierung in 1951 wurden anhand von Lawinenberichten, Orthophotos, historischen Dokumenten und Daten aus der Messtationen definiert. Für die Simulationen im Jahre 2018 wurden die Anrissgebiete aufgrund der heutigen Waldstruktur angepasst. Die Bremswirkung des Waldes (K-Wert) wurde mithilfe von Orthophotos, Bestandeskarten und Feldemessungen klassifiziert. Insgesamt wurden die Koordinaten, Waldtyp, Deckungsgrades und Bodenrauigkeit von 84 Stichproben erhoben. Gleichzeitig wurden Baumart und BHD (Brusthöhendurchmesser) aller Bäume vermerkt, sowie die Höhe ausgewählter Bäume gemessen. Fernerkundungsdaten wurden auf Unterschiede mit Felddaten untersucht und mittels Regressionsanalyse für die Walderfassung angewendet.

Die Veränderung der Waldstruktur hat seit 1951 potentielle Anrissgebiete nur zu einem geringen Teil tangiert. Aufgrund der Daten und der Literatur wird angenommen, dass die Ausbreitung von Legföhren, Arven, Lärchen und Bergföhren im Waldgrenzenbereich seit 1951 die Anrissgebiete für

kleinere Lawinen verkleinert hat, nicht aber für grössere Lawinen. Der Wald konnte trotzdem die Auslaufdistanz und die maximale Drücke der Lawinen in alle drei Untersuchungsgebiete reduzieren. Die Waldwirkung im Jahre 1951 zeigte generell 70-120 m kürzere Auslaufdistanzen an der Lawinenfront in La Punt und Susauna und 40-50 m in Zernez. Im Vergleich zur Erfassung von 1951 führt die veränderte Waldstruktur im Jahre 2018 generell zu einer grösseren Auslaufverkürzung. Der Unterschied liegt aber vor allem an den detaillierteren Informationen zur Klassifizierung der Bodenrauigkeit im Jahre 2018, was zur Zuordnung von generell höheren K-Werte zu den Waldbeständen führte. Aufgrund der simulierten Auslaufweiten ist zu erwarten, dass Gebiete mit gefährdeten Gebäuden im Jahre 1951 weiterhin auch im Jahre 2018 durch extreme Ereignisse gefährdet sind. Mit Ausnahme eines Gebäudes in Susauna, wird erwartet, dass die Siedlungen von kleinen und häufigeren Lawinen nicht betroffen sind.

Die Simulationen der Ereignisse im Untersuchungsgebiet Susauna im Jahre 1951 zeigen, dass Lawinenausläufe und Maximaldrücke im gleichen Mass von den Parameter für die Schneeaufnahme wie von der Klassifizierung der Bodenrauigkeit im Wald abhängen. Die Klassifikation des Deckunggsgrades beeinflusst die Resultate weniger als die Bodenrauigkeit.

Die Anwendung von Fernerkundungsdaten führt, im Vergleich zur manuellen Klassifikation des Waldes im Jahre 2018, generell zu einer Unterschätzung des K-Wertes. Der Vergleich mit den Simulationen des Jahres 1951 deutet dennoch darauf hin, dass die Klassifizierung des Waldes und des K-Wertes mit den derzeit verfügbaren Fernerkundungsdaten für die Simulation von extremen Lawinen, bei denen die Bodenrauigkeit durch die Schneeansammlungen geglättet wird, zuverlässig sein kann.

Summary

Snow avalanches represent a major threat to roads and settlements in mountain areas. One of the most extensive and effective protective measures against this hazard is given by forests, although often being themselves endangered in the case of extreme avalanches. Despite the forest damages, several studies suggest runout shortening and deceleration of extreme avalanches flowing through forest. Nowadays, avalanche simulation models are widely used in hazard mapping, but the effect of forest is merely considered as additional friction factor. In the case of extreme avalanches it is disregarded. The detrainment function developed at the SLF provides a new approach to consider the effect of forest in avalanche simulations with the extended version of the Software RAMMS (Rapid Mass Movement Simulation). Thereby, snow mass is detrained behind trees and is directly removed from the avalanche as a function of the flowing velocity and the braking power of the forest stands (defined as K-Value). The new forest approach implies that the effectiveness of mountain forests to stop avalanches is directly related to avalanche size.

In this thesis, the extended version of RAMMS was applied and evaluated in the back-simulation of large to extreme avalanches that destroyed the forest in the slopes over the villages of La Punt, Susauna and Zernez in Engadin in 1951. The thesis aims to examine the changes in the protective function since 1951 and to investigate the effect of the forests condition in 2018 in the simulation of similar extreme avalanches.
In the extended version of RAMMS, it is also possible to account for additional processes, such as snow entrainment along the track. The sensitivity of the results to the entrainment coefficients as well as the forest parameters was compared using simulations in 1951. In conclusion, the possibility of using widely available remote sensing data (Canopy height model and SwissALTI3D terrain model) for the classification of forest parameters and K-Values used in the simulations was tested.

Avalanche release areas, forest structure and parameters for the back-simulation of the 1951 events were defined using avalanche reports, orthophotos, historical documents and data from the measuring stations. For the simulations in 2018, release areas were adjusted to account for the current forest structure. The K-Value of the forest was classified using orthophotos, stand maps and field measurements. Coordinates, forest type, canopy coverage and ground roughness were collected for 84 sample plots distributed over all three study areas. At the same time, tree species and DBH (diameter at breast height) of all trees were noted and the height of selected trees measured. Remote sensing data was examined for differences to the field data and applied for classification of forest characteristics by means of regression analysis.

The changes in forest structure since 1951 affected only a small proportion of the possible release areas. Based on the field data and the literature, the growth of dwarf mountain pines, young larches, mountain pines and Swiss stone pines at the treeline is assumed to have reduced possible release areas for frequent and small avalanches but not for extreme events. Nevertheless, forests were able to reduce runout distance and maximum pressure of extreme avalanches in all three

study areas. In the back-simulation of 1951, forest generally lead to 70-120 m shorter runouts at the avalanche front in La Punt and Susauna and 40-50 m in Zernez. The changed forest structure in 2018 in the avalanche tracks had a greater impact on the avalanche runouts compared to the forest classification in 1951. This is mostly due to the more detailed information for the classification of ground roughness in 2018, which resulted in the assignment of higher K-Values to the forest stands. However, simulated avalanche runouts showed that areas with buildings endangered in 1951 are expected to remain in the possible runouts of extreme events also in 2018. When considering snow detrainment in forest, small avalanches are expected to stop before settlements, with the exception for one building in Susauna at the front edge of the avalanche runout.

Simulations of the 1951-events in the study area Susauna show, that avalanche runouts and maximum pressures are affected similarly by changes in entrainment parameters as by changes in forest ground roughness. The classification of canopy coverage has a smaller effect on the simulation results compared to ground roughness.

Compared to the manual classification of forest characteristics in 2018, the use of remote sensing data results in a general underestimation of the K-Value in the forest stands. However, the comparison with the 1951 simulations indicates that the classification of forest and the K-Value with the currently available remote sensing data can be reliable for the simulation of extreme avalanches, where ground roughness is smoothed by snow accumulations.

Table of Contents

Abbreviations

CHM	Canopy height model
DBH	Diameter at breast height
DSM	Digital surface model
DTM	Digital terrain model
K-Value	Forest detrainment coefficient
Lidar	Laser Imaging Detection and Ranging
RAMMS:	Rapid Mass Movement Simulation
RKE	Random Kinetic Energy
SLF	Swiss Federal Institute of Snow and Avalanche Research
SwissALTI3D	Digital terrain model of Swisstopo
VS	Voellmy-Salm
VRM	Vector Rudgeness Method

1. Introduction

Snow avalanches are gravity driven natural processes representing a major threat to roads and settlements in snow covered mountain areas (Laternser and Pfister, 1997; Schweizer et al., 2015). Mitigation strategies, such as snow supporting structures, protection forest and technical measures are widely used to reduce avalanche hazard and risk (Bründl and Margreth, 2015). In terms of area, mountain forest is considered the most extensive and important protection measure in the Alps (Bründl and Margreth, 2015; Margreth, 2004). In Switzerland, the protective function of forest was firstly established in the 14th century, with the prohibition of clear cutting on the slopes over Andermatt (Margreth, 2004). At present, 36% of the forested area in the country is prioritized as a protective forest against natural hazards (Brändli, 2010).

Although the primary effect of forest on the stabilization of the snow cover and prevention of avalanche formation has been recognised since the Middle ages, the effect on flowing avalanches is still being investigated (Schneebeli and Bebi, 2004; Teich et al., 2012). For small to medium avalanches the effect is limited to runout shortening and deceleration, whereas theoretical models and observations showed that large snow avalanches can destroy entire forests with only small energy consumption and no significant deceleration (Bartelt and Stöckli, 2001; Teich et al., 2012). The destructive power of extreme avalanches was observed during the catastrophic winters of 1951 and 1999, where almost 160'000 m^3 of timber forest were completely destroyed (Margreth, 2004; SLF, 1951a; SLF, 2000). Nevertheless, recent studies indicate that large avalanches are potentially decelerated when flowing through forest areas (Anderson and McClung, 2012; Takeuki et al., 2011; Teich et al., 2012).

After the 1951 winter, modern avalanche control and protective measures were developed. With the introduction of hazard maps in the 60s, land-use planning was applied as a mitigation measure in Switzerland (Bründl and Margreth, 2015). A one-dimensional model based on two frictional parameters and differential equations of motion ("Voellmy-Model") further improved by Salm ("Voellmy-Salm-Model") was firstly applied in order to predict avalanche impact pressures and runout distances in endangered areas (Feistl, 2015; Salm et al., 1990). Nowadays, three dimensional computer programs such as RAMMS (Rapid Mass Movements Simulation) allow to consider more complex topography with multiple avalanche release and flow paths (Christen et al., 2008; Christen et al., 2010b). However, the simulation results depend strongly on the initial parameters, in particular on release areas, fracture depth, friction coefficients and snow entrainment along the track (Christen et al., 2010b). Therefore, historical data and observations from extreme events of winter 1951 or 1999 represent valuable information for avalanche simulations and hazard mapping (Gruber and Margreth, 2001). Currently, forest is considered in simulations as additional roughness factor but this method hardly models the observed reduction of avalanche runouts (Feistl, 2015; Feistl et al., 2014b; Teich et al., 2014). The new approach developed by Feistl. et al. (2014b) in the extended version of RAMMS considers forest avalanche interactions by assuming that mass is stopped behind trees or tree groups and is directly removed from the flowing ava-

lanche as a function of forest structure. This allows distinguishing for different braking effects depending on the forest stand characteristics like canopy coverage, forest type and ground roughness (Feistl et al., 2014b; Teich et al., 2014). In this study, the new approach is applied in avalanche-dynamics calculations in three different areas of the Engadin, where in 1951 extensive forest destruction was recorded after the events.

With the more detailed consideration of forest in avalanche simulations, there is also an increase in the effort to record the forest parameters. Currently, these are classified using orthophotos, stand maps and sporadic field measurements, which can be time consuming. With the increasing availability of remote sensing data (e.g. digital terrain models and canopy height models), opportunities to map forest characteristics are arising.

1.1 Research Question

In this study, the 1951 avalanches in the areas of La Punt, Susauna, and Zernez are used to evaluate the forest detrainment approach and assess the braking effect of forests against extreme avalanches. Release areas, snow depth, meteorological conditions and forest characteristics are reconstructed based on historical data. The results will show the effect of forest on runout distance and avalanche pressure and will be evaluated in regard to archive data and damage records. The important question whether and to which extend similar avalanches can be expected under the current state of the forest is also addressed. Therefore, the forest structure in 2018 is determined with the aid of orthophotos, field work and stand maps and the effect in the simulation of extreme events and more frequent ones is investigated. The advantages and limitations of currently available remote sensing data for the acquisition of forest parameters are shown in comparison to field data. Therefore, this thesis aims to investigate the following questions:

1. What is the effect of forest in the simulations of extreme snow avalanches deposition length and pressures?
    - How does the actual forest structure (2018) affect the release area and deposition compared to 1951?
    - What is the effect of the current forest structure on smaller avalanches with higher frequency?
2. What is the effect of forest parameters compared to avalanche simulation parameters?
3. How precise is the detection of forest parameters needed in the simulations (K-Value, DBH) using widely available remote sensing data? What are the differences in the simulated runouts compared to manual classification with field work?

2. Theory

2.1 Snow avalanches

Avalanche release is mainly differentiated between two types: loose snow avalanches and snow slab avalanches. The first originate from a point of cohesionsless dry- or wet-snow and descend entraining snow mass and spreading in the lateral direction forming a triangular shape. Although generally small while involving only near surface layers, in the case of a snow cover saturated with water they can grow to larger and damaging avalanches as more snow mass is entrained. However, fatalities are mainly caused by slab avalanches as they involve larger snow volumes and are harder to predict (McClung and Schaerer, 2009; Schweizer et al., 2015; Schweizer et al., 2003). Among the three differentiated slab avalanche release types (dry-snow, wet snow and glide snow avalanches), dry-snow avalanches represent the most hazardous ones (Schweizer et al., 2003). The prerequisite for dry-slab avalanche formation is the presence of a cohesive slab over a persistent weak layer. Overloading of the weak layer initiates fractures, which can propagate and lead to the collapse of the overlying slab on the bed surface. When the slab detaches, fracture occurs at five different surfaces: the crown (uphill fracture line), flanks, between the slab and the sliding bed surface (terrain or old snow) and at the stauchwall (lower fracture line) (McClung and Schaerer, 2009; Schweizer et al., 2015; Schweizer et al., 2003). Slab avalanches release when the slope is steep enough for the stress due to gravity to overcome the frictional resistance, which is usually on terrain with more than 30° angle. Releases from slope angles under this threshold are rare and only few have been observed in the avalanche winters of 1999 and 1951 (Ammann, 2000; Schweizer et al., 2003; SLF, 1951a). In the case of large new snow avalanches, the 3-day sum of new snow is the most critical parameter (Schweizer et al., 2003). New snow depths of more than 1 m deposited during a storm usually lead to extreme avalanches, whereas 30-50 cm are generally critical for all natural avalanches (Schweizer et al., 2015; Schweizer et al., 2003). Other factors affecting slab avalanche formation are terrain roughness, wind, temperature, snowpack stratigraphy and vegetation (Schweizer et al., 2015; Schweizer et al., 2003).

2.2 Forest and snow interaction

The protective effect of forest on slopes prone to avalanche release is based on the direct stabilization of the snow cover and the prevention of avalanche formation (Margreth, 2004). Multiple processes modify the mechanical properties of the snow on the ground of mountain forests compared to open unforested terrain. Trees interception lowers the amount of snow on the ground and creates a heterogeneous snowpack when falling from the branches. The canopy reduces temperature fluctuations and the formation of surface hoar, which contributes to prevent the building of weak layers considered as a major cause for slab avalanche release. Additionally, trees reduce the near surface wind speed preventing heterogeneous accumulation of snow masses (Schneebeli and Bebi, 2004; Teich, 2013). The main variables for assessing the protective effectiveness of forest against avalanche release are tree species, canopy coverage, gap dimension and

number of tree stems per hectare (Bebi et al., 2009; Margreth et al., 2008; Meyer-Grass and Schneebeli, 1992). Forests exert a reliable protective function when tree heights exceed the maximum snow cover height by 1.5-2 times (Frehner et al., 2005; Saeki and Matsuoka, 1969) and canopy coverage is above 50-60% (Margreth et al., 2008). Avalanches may occur in openings wider than 15 m and longer than 25-60 m in the line of slope depending on slope inclination (Hubler and Rychetnik, 1991). However, canopy interception and radiation are less effective in the case of extreme snowfall events. The optimal and critical stem densities required to stabilize the snowpack and hinder the formation of slab avalanches was defined by Meyer-Grass and Schneebeli (1992) for different forest types with strong variations depending on slope angle and gap dimensions. Generally, in mixed evergreen and larch or pure larch forests the stem density for avalanche prevention should reach at least 280 trees per hectare with DBH above 16 cm, whereas 200 trees per hectare are regarded as critical (Meyer-Grass and Schneebeli, 1992). Differently, Salm (1978) considered only the mechanical support of the snow cover by tree stems and calculated that forests with more than 1000 stems per hectare can prevent avalanche release. The terrain roughness underneath the forest canopy (e.g stumps and lying stems) also influences avalanche formation if the snow depth is smaller than the highest elements (Bebi et al., 2009; Frey and Thee, 2002).

Once the snow cover is set in motion, the effect of forest is limited to runout and speed reduction due to increased friction along the track (Margreth, 2004; Teich, 2013). Avalanches starting more than 150 m above the treeline are assumed to be able to break or uproot trees (Bebi et al., 2009; Margreth, 2004; Margreth et al., 2008). Bartelt and Stöckli (2001) showed, that entrainment of debris along the track decelerate avalanches more than the fracturing of trees, which consumes only little of the avalanche's energy.

2.3 Avalanche modelling

Hazard zones are determined based on impact pressures of avalanches based on different scenarios with typical return periods of 30 and 300 years (BFF und SLF, 1984; Bründl and Margreth, 2015; Schweizer et al., 2015). Since 1950 different approaches to estimate runout of extreme events have been developed. In statistical models, measured extreme runouts are used to estimate the probability of runout distance past a reference point in the lower avalanche track. However, in such models the estimated runouts are independent on terrain features, vegetation and release area (Jamieson et al., 2008). Differently, dynamic models are based on the mathematical solution of equation of mass and momentum and calculate avalanche velocity along a simplified track. The model can be applied to back-calculate historical events, where friction coefficients and release depth are adjusted to obtain same runout as the historical record. Alternatively, runout and impact pressure of extreme events are estimated using calibrated frictional values and release depth (Jamieson et al., 2008).

2.3.1 RAMMS

RAMMS: AVALANCHE (Rapid Mass Movement Simulation) is a depth-averaged dynamic model developed by Christen et al. (2010b) to simulate flowing snow in three-dimensional terrain. The version currently available for practitioners and recommended by the Swiss guidelines applies the Voellmy-Salm (VS) approach and models avalanches using two parameters for the basal shear. Thereby, the frictional resistance S (Pa) is split into a velocity independent dry Coloumb friction (coefficient μ) and a velocity driven viscous-turbulent friction (coefficient ξ):

$$S = \mu \rho H g cos(\phi) + \frac{\rho g U^2}{\xi} \quad (1)$$

where ρ is the density, g the gravitational acceleration, H the flow height and U the flow velocity. Coefficient μ is proportional to the normal stress at the bottom and depends mainly on the snow properties (temperature, density and water content). It dominates in the runout zone when the avalanche is close to stopping. The parameter ξ controls the flow in the transition zone where the avalanche velocity is high and is mostly given by the terrain geometry (Bartelt et al., 2011; Christen et al., 2010b; Salm, 1993; Salm et al., 1990). Currently, practitioners are provided with a set of calibrated values depending on altitude, return period, avalanche volume and track type (Bartelt et al., 2011; Gruber and Bartelt, 2007). The frictional resistance function was later modified to include cohesion of the snow in flowing avalanches with low values for dry- and higher values for wet-snow (Bartelt et al., 2017; Platzer et al., 2007).

The extended version of RAMMS additionally accounts for velocity gradients between front and tail of the avalanche, snow entrainment along the track and flow of mixed flowing/powder avalanches. The applied RKE model (Random Kinetic Energy) describes the frictional parameters as a function of the random kinetic energy, which is determined by the production of the particles fluctuation energy from basal shear work (α) and its decay through the inelastic collision and interaction of the granules (β). This allows to represent the variation of friction parameters along the avalanche length (Bartelt et al., 2012; Christen et al., 2008; Christen et al., 2010b). In this model, the avalanche is divided into the core (ϕ) and the cloud (Π) (Figure 1). The random movement of particles leads to expansion of the avalanche core and air intake, especially at the front (so called saltation layer). The cloud arises from the core as heavier particles settle and a mix of air and dust is blown out. In mixed flowing/powder avalanches three mass exchanges occurs: air entrainment, ice-dust blow out from the core and snow entrainment into the avalanche core (Bartelt et al., 2016; Stoffel et al., 2016). In the last process, the mass uptake and acceleration of snow along the track to the avalanche velocity is parametrized by the erodibility coefficient (K) using slope or velocity driven laws. Small erodibility parameters (K <1) indicate basal erosion, whereas higher values between 1-5 represent entrainment at the avalanche head (“ploughing”) (Christen et al., 2010a). The amount of energy in the entrainment process that goes directly into heat or random kinetic energy is parametrized by the elasticity coefficient ε (Bartelt et al., 2018).

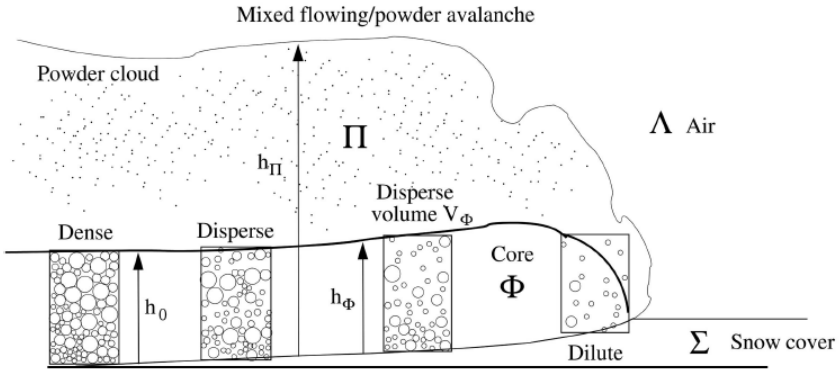

Figure 1: Representation of a mixed flowing/powder avalanche which contains the core (ϕ) and the cloud (Π). Snow (Σ) and air (Λ) are entrained by the avalanche (Bartelt et al., 2016).

Through entrainment, heat energy flows into the avalanche core and can lead to a melting process. In the extended version, an additional function accounts for the decrease in dry friction related to meltwater production and lubrification processes (Vera Valero et al., 2015). Currently, two snow layers with different snow height, density, temperature and entrainment rate can be defined by users with the top layer representing the new snow and the bottom the older layers (Christen et al., 2010b).

2.3.2 Forest module in RAMMS

In practical applications of avalanche models, users are suggested to disregard forest where avalanches reach pressures above 50 kPa as complete destruction is assumed (Christen et al., 2010a; Margreth et al., 2008). According to the Swiss guidelines, forest is considered by reducing the turbulent friction (ξ) to 400 m/s^2 (Margreth, 2004; Salm et al., 1990) but other studies also apply an increment of 0.02-0.05 to the dry friction (μ) in forested terrain (Bartelt et al., 2011; Christen et al., 2010a; Feistl et al., 2014b; Gruber and Bartelt, 2007).

Alternatively, forest interactions are described assuming that snow mass is stopped by material jamming behind trees or tree groups. In the new function (forest detrainment function) developed by Feistl et al. (2014b) at the SLF, mass is directly removed from the flowing avalanche and the change in total momentum is related to the momentum of the mass detrained per unit area M_d:

$$\frac{dM_d}{dt} = -\frac{K}{\|V\|} \qquad (2)$$

where *V* is the depth averaged velocity of the avalanche and *K* the detrainment coefficient (Feistl et al., 2014b). Multiple analysis of forest avalanches provided calibration of the K-Values in function of forest type and structure (Feistl et al., 2014b; Teich et al., 2014), which are shown in the look up table in Figure 2.

forest type	crown coverage*	roughness**	K-value***	Code
evergreen / mixed	dense (> 70%) coverage	rough (stumps/shrubs/saplings); height > 100 cm	48	A
		knobby (scree/stepped/seedlings); height 20 - 100 cm	38	B
		smooth (grass/leaves/smooth rock); height < 20 cm	28	C
	scattered, grouped (40% - 70%) coverage	rough (stumps/shrubs/saplings); height > 100 cm	43	D
		knobby (scree/stepped/seedlings); height 20 - 100 cm	33	E
		smooth (grass/leaves/smooth rock); height < 20 cm	23	F
	open (20% - 40%) coverage	rough (stumps/shrubs/saplings); height > 100 cm	38	G
		knobby (scree/stepped/seedlings); height 20 - 100 cm	28	H
		smooth (grass/leaves/smooth rock); height < 20 cm	18	I
larch / deciduous trees	dense (> 70%) coverage	rough (stumps/shrubs/saplings); height > 100 cm	35	J
		knobby (scree/stepped/seedlings); height 20 - 100 cm	25	K
		smooth (grass/leaves/smooth rock); height < 20 cm	15	L
	scattered, grouped (40% - 70%) coverage	rough (stumps/shrubs/saplings); height > 100 cm	30	M
		knobby (scree/stepped/seedlings); height 20 - 100 cm	20	N
		smooth (grass/leaves/smooth rock); height < 20 cm	10	O
	open (20% - 40%) coverage	rough (stumps/shrubs/saplings); height > 100 cm	25	P
		knobby (scree/stepped/seedlings); height 20 - 100 cm	15	Q
		smooth (grass/leaves/smooth rock); height < 20 cm	5	R

* Can be determined analysing orthophotos. Pictures below show example cases.
** Quantity for ground roughness as well as small vegetation and dead wood in the avalanche path. Examples below.
*** K in [Pa] represents the braking power per square meter that the forest exerts on the avalanche flow. It can be chosen manually if forest structure is not clear or in between two classes.

Crown coverage:

dense

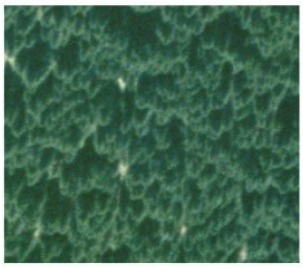

scattered, grouped

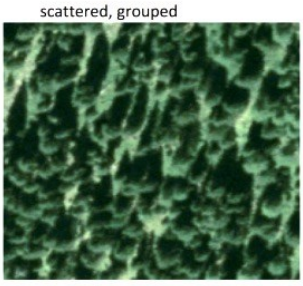

open

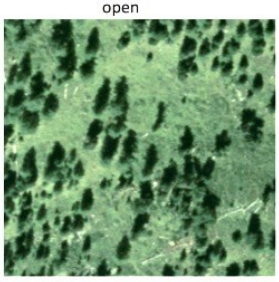

Figure 2: Table for assigning K-values to forest polygons according to RAMMS. The pictures show examples of crown coverage in orthophotos. Examples of ground roughness are shown in Section 3.2.1.

When forest is destructed, snow mass is not detrained behind trees but the increase in turbulent friction and the entrainment of tree stems and roots can decelerate the avalanche (Bartelt and Stöckli, 2001). Therefore, the user can choose to set the detrainment coefficient to a percentage of the original value and increase friction (μ, ξ parameters) as a function of K-Value. Forest destruction is introduced when the bending strength of the trees is exceeded by the bending stress applied by the avalanche, which depends on the avalanche flow regime and tree type (Feistl et al., 2015). Mixed powder avalanche pressures are regarded differently for the flowing core (ϕ) and the powder cloud (Π). In the first case, the impact height is limited to the tree trunk, whereas in the second case the cloud is assumed to be higher than the tree. Bending stresses (σ) exerted by a dry-snow avalanche are:

- avalanche core: $\sigma_{\Phi}^{d} = c_{\Phi}\rho_{\Phi}^{d}\frac{8u_{\Phi}^{2}}{\pi d^{2}}h_{a}^{2}\cos(\gamma)$ (3)
- powder cloud: $\sigma_{\Pi}^{d} = c_{\Pi}\rho_{\Pi}\frac{8u_{\Pi}^{2}}{\pi d^{3}}wH^{2}\cos(\gamma)$ (4)

where c = 1.5, γ is the slope angle, u the flow or powder velocity, ρ the avalanche density, d the stem diameter, h_a the impact height, H tree height and w tree width (Feistl et al., 2015).

For the forest file, users provide only mean diameter at breast height (DBH) or mean height (H) of the forest stands and the model assumes a general relation:

$$H = DBH^{0.8} <-> DBH = H^{1.25} \quad (5)$$

Detailed description of the implementation of tree breaking and forest detrainment function is provided in Feistl et al. (2015; 2014a).

2.4 Winter 1950-1951

In the Alps the winter 1950-1951 was characterized by extreme snowfalls, which resulted in periods of intense avalanche activity and catastrophic events (Laternser and Ammann, 2001; SLF, 1951a). In Switzerland, 1'300 avalanches caused the loss of 98 people, damaged around 1'500 constructions and destroyed more than 1'945 ha of forest (SLF, 1951a). After the heavy November snowfalls, the cold and dry December lead to an unfavourable development of the snowpack into a loose base layer (SLF, 1951a). In January, a northerly barrage brought extensive snowfalls over the north and central Alps. The precipitation exceeded the normal January precipitation by 200%. In the regions of Ticino, mid and south Grisons, the snowfalls measured up to 300-400% of the normal January level (Laternser and Ammann, 2001; Laternser and Pfister, 1997). The extreme amount of new snow and the strong NW-storm combined with the low air temperature led to the accumulations of wind drifted snow, which worsened the situation and resulted in an extraordinary avalanche period between the 19th and 22nd January 1951. Strongly affected by disasters were the cantons of Uri, part of Valais and Grisons (Laternser and Ammann, 2001; Laternser and Pfister, 1997; SLF, 1951a). Differently, the south barrage and the long period of foehn in February mainly affected the southern cantons of Switzerland, causing intensive avalanche activity from 11th-14th February (Laternser and Pfister, 1997).

One of the Swiss regions severely tested during the January snowfalls was the Engadin, a valley located in Southern Grisons. Additionally to tragic events with human losses, the damage to forest stands was extensive. At the beginning of the avalanche period, the released slab avalanches developed over short distances into highly fluid and dust streams. The low impact pressure in the upper avalanche tracks left open forest stands undamaged, while the forest stands situated downwards were completely destroyed (SLF, 1951a). Toward the end of the January avalanche period, avalanches with heavy densified snow released often. Although the release areas consisted of cold and dry-snow, the avalanches flowed into areas with more compacted snow. The major forest disasters, such as the one in the forest over Zernez, were presumably caused by similar avalanches (SLF, 1951a).

3. Materials and Methods

3.1 Study areas

The investigated areas of La Punt, Susauna and Zernez are all situated on the orographic left side of the Engadin valley in the canton of Grisons (Switzerland). They were suggested by the canton of Grisons as examples of the 1951 avalanches, which released far up or at the treeline and reached the valley bottom after destroying mature and young forest stands. All three study areas well represent the typical texture of subalpine mixed larch, Swiss stone pine, mountain pine and spruce stands. The diffuse treeline of dwarf mountain pine, mountain pine, Swiss stone pine and larch is present in both study areas La Punt and Susauna.

3.1.1 La Punt

At the end of the 19th century, the area of "God Arschaida" was intensely reforested and protective structures, such as stone walls and impalements, were constructed in the mid-east slopes. However, the effective height of the structures was small and in 1935 one avalanche reached the shooting range (Pitsch, 2015). According to the avalanche report, on the 20th January 1951 at 11 a.m. four large and two smaller avalanches released from 2000 to 2200 m.a.s.l. and reached the grassland destroying the shooting range and damaging the cottage "Acla Buob" (SLF, 1951b). Around 8 ha of 40 to 75 years old larch, Swiss stone pine, mountain pine and spruce forest were damaged. Although no exact informations on the avalanche depositions were available, the avalanche report does not indicate damages to the village and I can presume the avalanches stopped between the lower timber line and the railroad at 1780 m.a.s.l. (SLF, 1951b). Between 1990 and 1995 the area was part of a project for avalanche control. Steel snow bridges and wooden rakes were built on the slopes and the area was reforested (Pitsch, 2015).

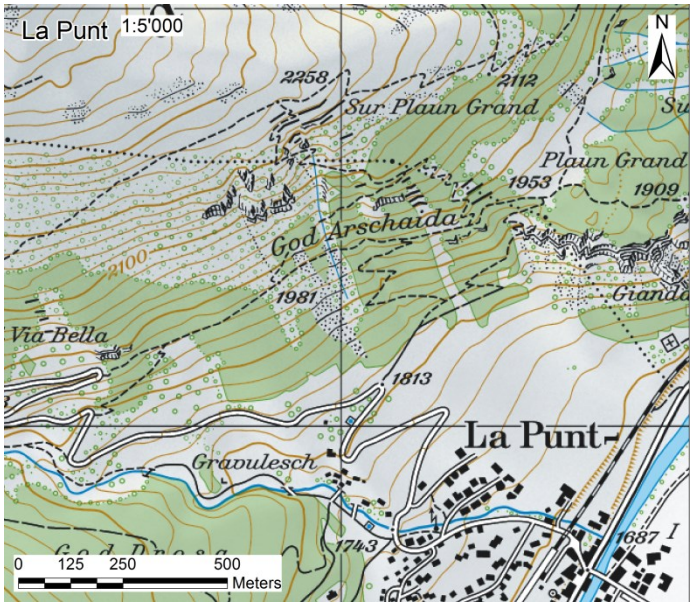

Figure 3: Study area La Punt (Swisstopo ©, 2017).

3.1.2 Susauna

On the 20th January 1951 at 10 p.m., avalanches releasing at the upper treeline at around 2350 m.a.s.l. damaged seven buildings in the underlying village of Susauna (1682 m.a.s.l.) (SLF, 1951b). Recollections from an old inhabitant indicate, that the avalanche core completely destroyed a barn and slightly compressed the walls of a building in the west part of the village. The same building remained untouched in the south-east facing side (Simon Luzi, 2018). The air impact caused most of the damages, especially in the lower forest part. In the forests of "God Susauna-God Murter" the avalanche destroyed 14 ha and damaged 6 ha of larch, Swiss stone pine and spruce stands of 35-75 years old. The 5 ha of afforestation were destroyed as well (SLF, 1951b; Wirtschaftsplan S-chanf, 1955). The grassland in the valley was covered by a mix of snow, rocks and timber transported up to the river (Simon Luzi, 2018; SLF, 1951b). The stone walls for avalanche protection constructed in 1927 on the ridge were revealed to be too small (Simon Luzi, 2018; SLF, 1951b). After the event, numerous avalanche protection structures were built from the upper treeline to the ridge and the area was reforested. Steel snow bridges were built also in the middle of "God Murter", where the previous afforestation was destroyed and new regeneration was planted between the structures (Schutzbautenkataster Kanton Graubünden, 2018c; Swisstopo ©, 2017).

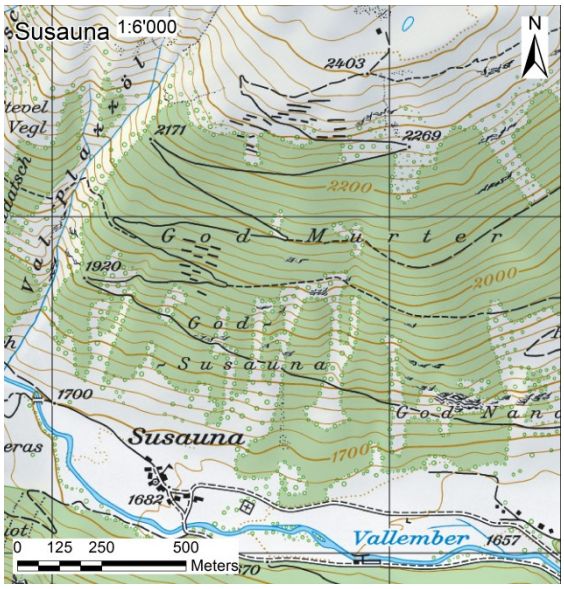

Figure 4: Study area Susauna (Swisstopo ©, 2017).

3.1.3 Zernez

The forest stands above the village of Zernez ("God Tretschinas–God Bugnaidas–Las Ognas") were damaged on the 21st January 1951 at 9 a.m. According to the avalanche report, the avalanche initiated with the fall of a snow cornice on the extension of Piz d'Urezza at 2850 m.a.s.l. (SLF, 1951b). The avalanche followed then the two existing avalanche tracks "Vallanzun" and "Vallun Quadratscha" and opened a completely new track further north destroying mixed spruce, larch and Swiss stone pine timber forest of over 100-120 years old (SLF, 1951b). The avalanche report indicates, that due to unfrozen terrain most of the trees were uprooted and not broken (SLF,

1951b). The grassland between the treeline and the river (1471 m.a.s.l.) was covered by snow, rocks and timber material (Meliorationsamt und Vermessungsamt Graubünden, 1951).

After 1951 the area was reforested but no others avalanche protection measures were taken into consideration. On the 6th January 2018 the "Vallanzun" avalanche released from the slope above the gully and on the 22nd a slab avalanche starting from the ridge destroyed the afforestations in the track "Vallun Quadratscha"(Figure 5). The stands at the upper treeline were damaged as well but no forest destruction in the new avalanche track of 1951 occurred.

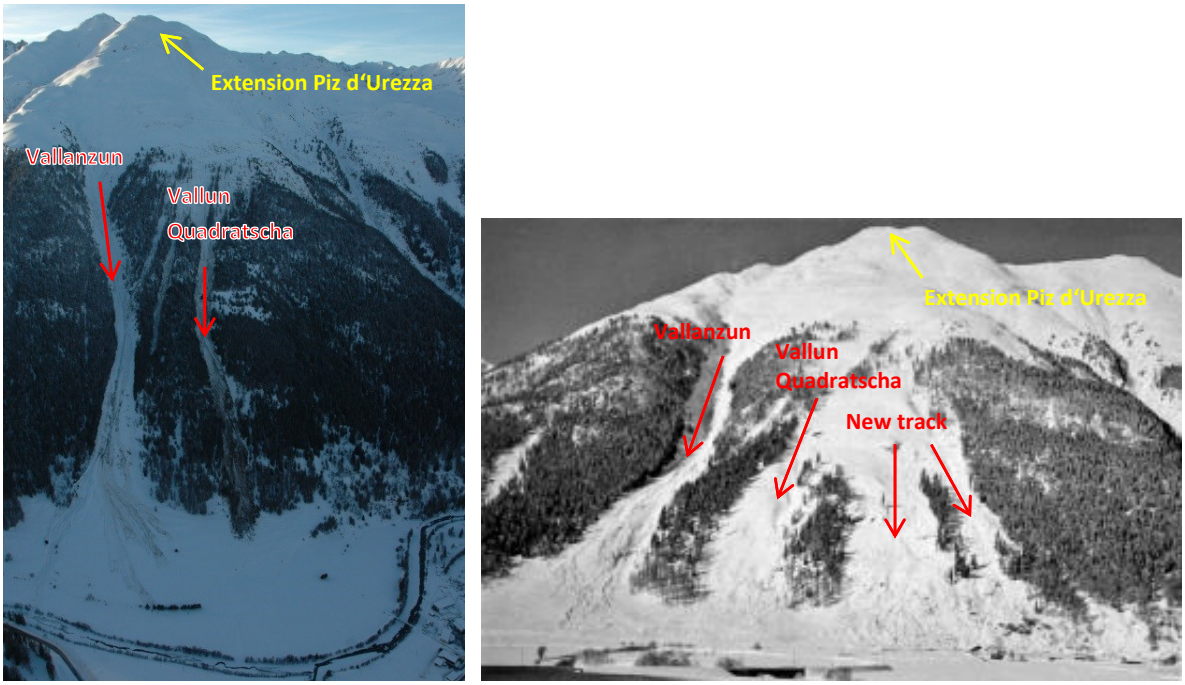

Figure 5: Study area Zernez after the avalanche in January 2018 (left, (Martin Keiser AWN GR, 2018)) and after the 1951 avalanche (right, (Archive Zernez, 1951)).

3.2 Forest and terrain parameters

3.2.1 Field data collection

For each of the study areas field work was carried out in autumn 2017. Sample plots of 6 m radius were defined in ArcGIS 10.2 by laying a grid of 150 m per 200 m over the forest. The resulting samples where then checked for accessibility in the field and relocated or deleted manually if necessary. Before entering the field, I roughly defined the polygons for different forest structures based on orthophotos from 2017 (Swisstopo ©, 2017). For major forest stands with a texture different from all the already selected sample plots, an additional plot was added. For the areas of Susauna and Zernez, 30 samples each were collected. For the smaller area La Punt the samples were 24. The exact coordinates of each point were measured in the centre with a GPS Trimble and their position can be seen in the Appendix A. The DBH (Diameter at Breast Height) of all trees above 1.3 m height was measured and social position of the tree (dominant, codominant, under-storey, young forest/shrubs) assigned. The position of dominant trees in the plot was noted in order to have possible control of sample location when looking at orthophotos. Crown coverage of

the sample was estimated standing in the centre as well. For time reasons, the height was measured only for dominant, codominant and selected understorey trees using a VERTEX IV. For smaller trees or dwarf mountain pine, the height was measured manually. Terrain ground roughness was estimated according to Table 1.

Table 1: Table to classify ground roughness in forest polygons according to RAMMS look up table. For each category elements height (H), examples (e.g.) and an example picture are shown. Elements should be present every few meters. If this was not the case, one category lower was used.

	rough	**knobby**	**smooth**
H [cm]	> 100	20 – 100	< 20
e.g.	stumps, shrubs, saplings	scree, stepped, seedlings, dwarf mountain pine	grass, leaves, smooth rock
			

Major roughness obstacles such as stumps, saplings, scree or rocks were described on the sampling sheets. The obstacles showed a small scale spatial variability. For example, saplings are described as a rough obstacle and often grow in regeneration groups instead of homogeneously distributed. Therefore, it was possible to have smooth samples in a generally rough forest polygon. To estimate the right roughness for the polygons I also described roughness for the area in which I collected the samples.

3.2.2 Remote sensing

3.2.2.1 Canopy height model

Ginzler and Hobi (2015) generated a canopy height model using aerial stereo imagery taken from airplanes flights over Switzerland by the Federal Office of Topography (Swisstopo) between Mai and September. The automated image matching approach generates dense point clouds, which are used to create a digital surface model (DSM) of 1x1 m resolution for the entire country. As all the images are regularly updated maximum every six years, the process offers the possibility to continuously actualize the digital surface model (Ginzler and Hobi, 2015). The canopy height model (CHM) is the difference between the digital surface model (DSM) and the digital terrain model (DTM). For the last, the swissALTI3D of Swisstopo acquired with Lidar data and resampled to 1 m resolution was used (Ginzler and Hobi, 2015). As the SwissALTI3D model showed inaccuracies and a large band with a resolution of 25 m instead of the usual 2 m in the upper part of the study area Susauna, 11 sampling plots were excluded for the remote sensing analysis.

For this study, the cell values of the CHM derived from stereo images acquired between 2007 and 2012 (denominated CHM 2012) and the updated version (denominated CHM 2016) were extracted

in ArcGIS for each sampling plot. Maximum tree height measured in the field was compared to the maximum height detected by the model in each sampling plot. I defined this difference as ΔHmax (negative values indicate underestimation of maximum heights by the canopy height model). Statistics of the CHM values at plot level were compared to maximum tree height and mean height of the (co-)dominant trees measured in the field. To investigate possible systematic errors in height detection two parameters used to define the goodness of the canopy height model and the accuracy of the GPS in the terrain were investigated. Distance to nadir (point directly below the camera on the airplane) indicates how far the plot is from the centre of the image used for the digital surface model. Completeness of match (COMP) determines the image fitting process in the workflow of model creation (best = 1) (personal communication Christian Ginzler, December 2018; Ginzler and Hobi, 2015). Canopy coverage was calculated as the percentage of cells above 3 m height (Ginzler and Hobi, 2016; Waser et al., 2015) and analysed related to canopy coverage estimations in the field. In the results, the range of canopy coverage with remote sensing is shown for each class observed in the field.

3.2.2.2 Terrain ground roughness

Terrain roughness was computed using the approach of Rickenbach (2018) with the SwissALTI3D terrain model of 2 m resolution according to the vector rudgeness measure (VRM) suggested by Sappington et al. (2007). The method uses vectors normal to each grid cell of the DTM and divides the normalized resulting vector by the number of neighbourhood cells (in this study 5x5). The obtained value is subtracted from 1, resulting in a range between 0 (smooth) and 1 (most rough). Maximum and median values at each sampling plot are classified using the smallest divisions and observations from several studies (Sappington et al., 2007; Veitinger et al., 2016; Veitinger and Sovilla, 2016) into smooth (< 0.01), knobby (0.01-0.02) and rough (> 0.02). The roughness classification with remote sensing was compared to the classification in the field. Additionally, roughness elements from the vegetation (saplings, stumps, seedlings) were excluded for a new classification of field roughness without elements from the vegetation. The result was also compared to the remote sensing classification.

3.2.3 Statistical analysis

All the statistical analysis were done with the statistic software R version 3.3.2. Data was grouped according to tree species, forest type, canopy coverage or study area. Interactions between explanatory and predictor variables were first investigated using the Spearman's rank correlation. Groups were tested for significant ($p < 0.05$) effect on prediction variables with the F-test in ANOVA (Crawley, 2007).

The formula used in RAMMS (Equation 5) was tested for differences in predicted height compared to field data using the paired student's t-test with a significance level of 0.05. The functions "lm" and "nls"were used to fit linear and power regressions between tree height and DBH mesured in the field for each tree type (Swiss stone pine, larch, spruce, dwarf mountain pine and mountain pine) and a general equation for multiple tree species (Swiss mountain pine, larch, spruce, mountain pine). The regression lines were then compared to the general formula used in RAMMS (Equa-

tion 5). In the same way, the function “lm” and “nls” were used to fit linear natural logarithmic and power regressions between statistics of the CHM and mean DBH in each sampling plot accounting for forest type as factor (Bates and Pinheiro, 1998; Christian and Streibig, 2009; Crawley, 2007). Regression models were compared using the F-test in ANOVA where possible and the Akaike information criterion (AIC) in the other cases. Models with lower AIC are supposed to better represent the data. In the results, only the models with best fit are shown. Canopy coverage as well as roughness values were compared for differences in mean of each field classification group using the F-test in ANOVA and a significance level of $p < 0.05$.

The assumptions of normal distribution and constancy of variance were visually inspected with plot of standardized residuals against fitted values and sample quantiles against theoretical quantiles (QQ-plot)(Christian and Streibig, 2009).

3.2.4 Classification of forest and ground roughness parameters

After the field work, the polygons for forest stands were adjusted in ArcGIS 10.2. For each polygon in the RAMMS forest file, tree type, DBH and K-Value are necessary. For the last, the look up table (Figure 2 in in Section 2.3.2) provides an overview of the values in function of forest type, canopy coverage and ground roughness.

The forest type and coverage for 2018 was defined using the field data and by analysing orthophotos from 2017 (representing 2018, (Swisstopo ©, 2017)). As the RAMMS look up table indicates only K-Values for evergreen or larch/deciduous forest, a mean value between the two options was used for mixed forest stands. I distinguished between four types: larch, evergreen, mixed and dwarf mountain pine forests. I used the notations in the field to classify the roughness in each polygon. Dwarf mountain pine in understorey was considered as a knobby element as suggested by RAMMS for seedlings and not rough due to its very flexible trunk. Stands with no field information, where terrain features were not visible in orthophotos, were classified as smooth. Tree type of larch-dominated forests with only small rates (below ca. 20 %) of other tree species was classified as “larch”. Otherwise, pine, spruce or larch were assigned according to majorly represented tree type. Dwarf mountain pine forests were classified as “birch”, because this vegetation category presents the highest bending strength available in the model. The DBH was classified using the mean value of field data. However, field sampling plots were selected randomly and were not always representative of the entire forest stand. Therefore, stand maps of the canton of Grisons (Bestandeskarte Kanton Graubünden, 2018a), and orthophotos were also used. The selected DBH ranges are shown in Figure 6.

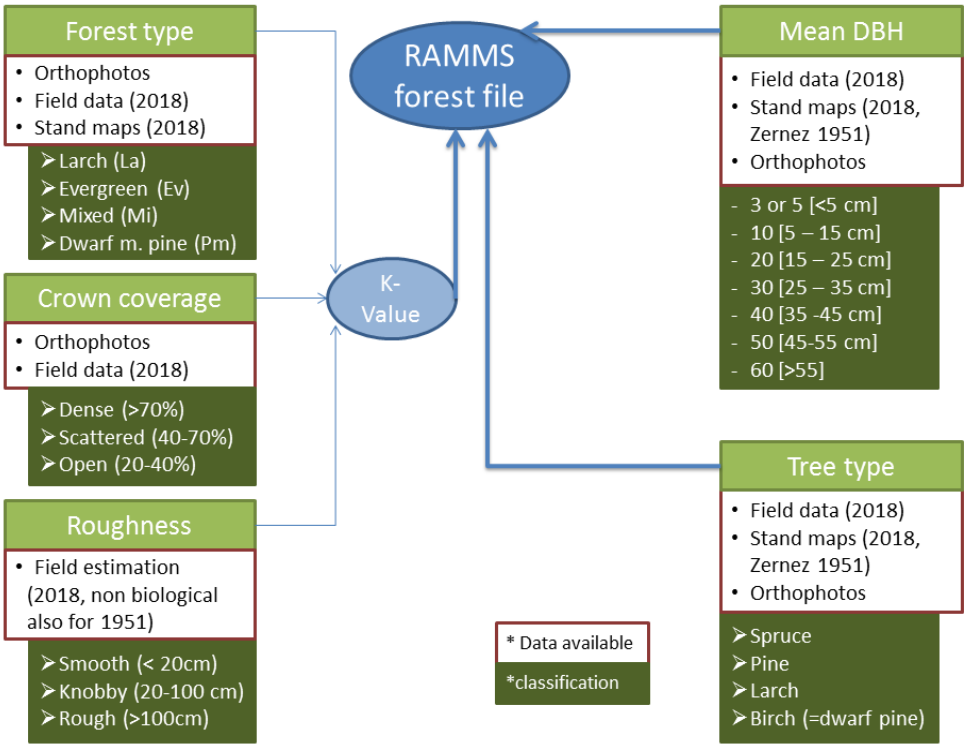

Figure 6: Parameters needed in the forest file for RAMMS. Classification classes of each parameter and the data available are shown in the squares.

Pure dwarf mountain pine forest stands were not considered in the forest shapefile of extreme snow avalanches. However, dwarf mountain pine associated with larch, Swiss stone pine and transitional forms between mountain pine and dwarf mountain pine were frequently observed (especially in the study area of La Punt). In similar stands, dwarf mountain pine reached heights of 5 m with DBH of 10-15 cm. These stands were classified as open forest (K-Value = 15) and were also considered in the classification for extreme events. Smaller dwarf mountain pine stands, considered only in the shapefile of more frequent avalanches, were attributed the lowest K-Value of 5. Observations in winter showed, that these stands are completely bent on the ground by the snow load. Figure 7 and 8 display examples of stands with K = 15 and K = 5 in autumn and in winter.

Figure 7: Examples of dwarf mountain pine stands with K-Value 15 (left) and 5 (right) in autumn.

Figure 8: Examples of dwarf mountain pine stands with K-Value 15 (left) and 5 (right) in winter.

The classification of the polygons for the shapefile of 1951 was performed by analysing orthophotos of 1946 (Swisstopo ©, 1946). Ground roughness and DBH were assigned based on assumptions. The field notations in autumn 2017 were used for the classification but dead wood, recent stumps or small vegetation were not considered. Only elements like rocks or terrain irregularities contributed to the definition of roughness. The DBH was reconstructed by comparison of orthophotos from 1946, 1956 and 2017 (representing the forest stand in 2018)(Swisstopo ©, 1946; Swisstopo ©, 1956; Swisstopo ©, 2017). For stands that were not destructed in 1951, DBH was assumed as one class smaller than in 2018. For the destructed stands, DBH was estimated with orthophotos and damage descriptions (SLF, 1951b; Wirtschaftsplan S-chanf, 1955).

In the area of Zernez full scaling and delineation of the forest divisions as well as description of forest types and terrain vegetation from 1943 was available (Wirtschaftsplan Zernez, 1924). The average DBH of each stand polygon was calculated using the mean values of full scaling. The resulting DBH was also compared to actual stand maps (Kanton Graubünden, 2018a). Ground vegetation and forest regeneration in the site description (Wirtschaftsplan Zernez, 1924) were also used to estimate ground roughness in Zernez.

3.2.4.1 Classification of K-Values using remote sensing

The polygons manually defined for the study area Zernez are used to show an example of classification of K-Value and DBH with remote sensing data. Thereby, the information of polygon area and forest type (from orthophotos) of each polygon was taken from the manual classification. Canopy height model cell values and terrain roughness according to the method of Sappington et al. (2007) were extracted in ArcGIS and evaluated in R. For each forest type, canopy coverage and roughness classes for remote sensing (Section 4.1.3) were calculated and the corresponding K-Values was assigned to each polygon. However, roughness was defined using the mean values and not the maximum as the larger forest area also included rockwalls or roads and this would have resulted in extreme high roughness values for each polygon. For tree type the manual definition was used and the DBH was calculated using the linear regression of CHM values and mean DBH presented in Section 4.1.3.

3.3 Avalanche simulations and scenarios

The extended version of RAMMS:AVALANCHE version 2.7.08 was used to back-simulate the 1951 avalanches under reconstruction of release areas, fracture depth, meteorological conditions and forest structure at each test site (scenario *T1951*). To investigate the question, whether today similar events would be mitigated by the growth of forest in the release zone or by changes in forest structure, avalanches were simulated with same snow and meteorological conditions as in 1951 but with consideration of forest stands in 2018. This scenario is termed *T300* (similar to 300 year return period). The effect of forest in 2018 on the release and runout distance of more frequent and smaller avalanches is investigated using the scenario *T30* (30 year return period). Only for the test site Zernez, the observed avalanche on the 22nd January 2018 (scenario *T22J*) is back-simulated instead of the two fictive scenarios for 2018.

3.3.1 Release area and fracture depth

Dry-snow slab avalanches releasing on slope angles minor than 30° are rarely observed (Margreth, 2007; Schweizer et al., 2003). In terrains with inclination above 45° continuous release of loose snow avalanches is more likely and the formation of weak layers is prevented. Therefore, formation of slab avalanches is assumed between terrain angles of 30° and 45° degrees (Margreth, 2007; Schweizer et al., 2003).

The 3-day sum of new snow depth at the measuring station in Zuoz (1710 m.a.s.l) was used to define the fracture depth in *T1951*. The station measured 1.18 m on the 21st January, which is even higher than the 1.01 m extrapolated with extreme statistic for 300 year return period. The value corresponding to a 30 year return period (scenario *T30*) at the same station is 0.73 m. (Appendix B. Extreme value statistics). For the back-simulation of scenario *T22J,* data from a measuring station in Zernez (1471 m.a.s.l.) was available. The 3-day new snow depth measured on the 22nd January 2018 is 0.75 m, which would correspond to a return period of 20 years (Appendix B. Extreme value statistics). Although the report on the winter 1951 (SLF, 1951a) indicated 0.7 cm

new snow depth increase for 100 m altitude difference, no information on how the value was extrapolated was available. Therefore, a value of 0.5 cm for 100 m altitude increase used in the Swiss guidelines was used (Salm et al., 1990). All the fracture depths (d0*) were corrected for altitude and mean slope angle according to standard procedure in the Swiss guidelines (Salm et al., 1990).

Table 2 to Table 4 in the following sections provide an overview of the information on avalanche formation as well as explanations for each scenario. For the study area of La Punt and Susauna, release areas in *T1951* are labeled with the letter A and modified or added areas for scenario *T300* are described with B. In the same way, areas from *T300* modified or added for *T30* are described with letter C. For the study area Zernez, release areas are labelled from the top of the ridge to the treeline and not based on scenarios. The resulting areas are shown in the results (4.2 Forest cover change and avalanche simulations) and shortly presented in the following sections. Detailed information on fracture depth, release area and volume of each scenario at each study area is available in the Appendix C.

3.3.1.1 La Punt

The release areas in *T1951* were selected based on the evaluations of slope and forest damages for the hazard map in La Punt by Pitsch (2015). In the report additional areas further down the avalanche tracks are used to simulate snow entrainment. However, the extended version of RAMMS already accounts for this process and therefore the original release areas by Pitsch (2015) were modified. Dwarf mountain pines were assumed to have no stabilizing effect on the snow cover for extreme snowfalls. The release area A3 was used in the *T1951* and *T300* scenario (Table 2).

Table 2: Release areas, 3-day sum of new snow depth at station Zuoz (1710 m.a.s.l.) and assumptions on wind drift for the scenario *T1951*, *T300* and *T30* in La Punt.

La Punt	***T1951***	***T300***	***T30***
$d0^*_{1710}$	1.01 m	1.01 m	0.73 m
Release area	A1, A2, A3, A4, A5, A6, A7, A8, A9	A1, A2, A3, A4, B10, B5, A6, A7	A1, A2, A4, C5, C6
Wind drifted snow:	0	0	0
Notes:		B10 below constructions added. B5 smaller due to snow supporting structures	A3 in dwarf mountain pine deleted. Forest gaps in steep slopes added (C5-C6)

The avalanche released one day before the end of the heavy snowfall. Therefore, I did not use the 1.18 m for the fracture depth definition. However, the height measured on that day in the early morning was 0.73 m, which would not correspond to an extreme event. With peak snowfall inten-

sities of 10-15 cm per hour (Laternser and Ammann, 2001), I find realistic to use an intermediate value such as 1 m, which also corresponds to a return period of 300 years.

For the scenario *T300* supporting structures were considered as suggested by Pitsch (2015). The release area A5 was therefore reduced to account for the supporting structures in the upper part (B5). The areas A8 and A9 are completely stocked and are not accounted in the simulations of *T300*. Although the forest damages in 1951 show that no avalanche released from the gully in the middle (B10), the current forest condition and slope indicate possible release for the scenario *T300*. Release area in dwarf mountain pine (A3, B10, A5-A7) are not used in *T30.* Forest openings larger than 30-60 m in the line of slope (Frehner et al., 2005), were defined as release areas for *T30* as this openings (C5-C6) were not part of the entrainment from avalanches releasing above anymore.

3.3.1.2 Susauna

The release areas mapped on counter slopes pictures (SLF, 1951b) after the 1951 event were not completely situated in slopes above 30° according to inclination maps from the swissALTI3D terrain model. However, the accuracy of the model in this area (see Section 3.2.2 Remote sensing) is very low. For this reason, a plan of contour lines based on field measurements from the canton of Grisons (Übersichtsplan Kanton Kanton Graubünden, 2018b) was used as control, which showed these slopes as mostly above 30°.

With the current state of the protective structures in Susauna, no avalanche release is possible. Release areas for the scenarios in 2018 (*T300 and T30*) do not account for these constructions and aim to investigate whether the actual forest stands can prevent avalanches to reach the village. Nevertheless, the area of A3 was reduced and the road constructed after 1951 was considered, which divides A5 and prevents avalanche release.

The avalanche occurred the night before the end of the heavy snowfall. However, during the night the snowfall diminished strongly (Laternser and Ammann, 2001) and the value of 1.2 m is used for the fracture depth. Additional 50 cm were added to account for the wind drifted snow according to the description of strong north-west winds and the formation of a cornice (Simon Luzi, 2018; SLF, 1951b). Although the stone walls were revealed to be too small, the structure height and the presence of structures against wind drift on the ridge (Simon Luzi, 2018) lead to the conclusion that the fracture depth in A3 and A4 was smaller. Therefore, I did not account for wind drifted snow in these areas. The release zone A1 was not mapped in the counter slope pictures but it must be mentioned that the sight to the north-west part of the ridge is hidden by the forest. Due to the topography, open forest structure and the detected forest destruction further downwards, avalanches most likely released in this area as well. In scenario *T30* the protective function of dwarf mountain pine both as avalanche prevention as well as possible detrainment along the track is taken into account. As a result, no avalanche release in A1 is considered (Table 3).

Table 3: Release areas, 3-day sum of new snow depth at reference station Zuoz (1710 m.a.s.l.) and assumptions on wind drift for the scenario *T1951*, *T300* and *T30* in Susauna.

Susauna	***T1951***	***T300***	***T30***
$d0^*_{1710}$	1.18 m	1.18 m	0.73 m
Release area	A1, A2, A3, A4, A5, A6	A1,B2, B3, A4, A6	B2, B3, A4, A6
Wind drifted snow:	0.5 m except for A3, A4 due to protective structures	0.5 m	0 m

3.3.1.3 Zernez

The fall of a snow cornice on the south extension of Piz d'Urezza and the failure of the two underlying snow slabs were described as the triggering factor (SLF, 1951b). However, no detailed information on the extension and location of the failure was available. The avalanche on 22nd January 2018 in the track "Vallun Quadratscha" (Figure 5) showed a failure below the ridge (A1, A2) similarly to 1951 with secondary release in the slopes above the treeline (B1, B2). These areas were used for the simulation of all scenarios. Scenario *T1951* was investigated to determine whether the same areas as in 2018 (with higher fracture depth) would lead to the observed deposition or whether secondary release in additional areas (B, C) are necessary to back-simulate the event in 1951 (Table 4).

Table 4: Release areas and assumptions on wind drift for the scenario *T1951* and *T22J* in Zernez. 3-day sum of new snow depth is indicated at the reference station Zuoz (1710 m.a.s.l.) for *T1951* and in Zernez (1471 m.a.s.l) for *T22J*.

Zernez	***T1951***	***T22J***
$d0^*_{1710\ (1471)}$	1.18 m	0.73 m
Release area	A1, B1, sensitivity B2, C, D	A1, B (B1+B2), sensitivity A2
Wind drifted snow:	0.3 m on the ridge (A1)	0.3 m on the ridge (A1, A2)

3.3.2 Simulation parameters

The values of the following simulation parameters (Table 5) are based on the state of the art and first back-simulations of avalanches using the extended version of RAMMS (personal communication Perry Bartelt, January 2018; Christen et al., 2010a; Dreier et al., 2016). All the values presented here were kept constant in the simulations at the study areas of La Punt and Susauna. As the avalanche of 1951 in Zernez presented a much larger release volume and different snow cover conditions, some parameters were set differently. Cohesion was set higher as the simulated avalanches were slightly wet in the lower transition and deposition zone (Platzer et al., 2007). Due to the much larger area, resolution of the DTM was lowered from 4 to 5 m to reduce calculation time.

The avalanche reports of the study areas indicated some contradictory information on the release snow density, sometimes describing the new snow as heavier than the old snow (SLF, 1951b). However, the same release density (ρ = 200 kg/m^3) was selected in each area. Differently to the

Swiss guidelines, friction coefficients remain constant for topography, avalanche volume and return period. These may be lowered in the release areas to better simulate slab avalanche release on a gliding surface. This was the case in Zernez, where μ in the release area was set to 0.01 and ξ to 4000 m/s^2. This approach was not used in the area of La Punt as the avalanches started almost only on slopes with vegetation. Due to the coarse resolution of the DTM in the release area of Susauna and the resulting slope angles, friction coefficients were lowered to initiate avalanche release.

Table 5: Reference simulation parameters for all scenarios at the study areas of La Punt, Susauna and Zernez. Parameters that varied in scenarios of the study area Zernez are shown in brackets.

Parameter	Value
μ	0.55
ξ [m/s^2]	1800
Cohesion [Pa]	100 (150 Zernez)
Granule density ρ [kg/m^3]	450
DTM resolution [m]	4 (5 Zernez)
Release density $\rho_{release}$ [kg/m^3]	200
Release T [°C]	-5
Generate (α)	0.07
Decay (β) [1/s]	0.7
Act. Energy [kJ/m^3]	2
Mu Wet	0.12
Dry-Wet Transition [mm]	100
Cloud drag	2.0 (4 Zernez)
Frontal Air entrainment	3.0
K-Value after forest destruction	20%
Higher friction after forest destruction	yes
Use interception in forested area	yes

3.3.2.1 Entrainment

Descriptions of the 1951 avalanches (Section 2.4 Winter 1950-1951) indicate significant entrainment of new snow along the track, which has to be considered in the simulations.

The reference values of κ = 4 (erodibility) and ε = 0.4 (elasticity coefficient) apply for dry and cold snow cover (personal communication Perry Bartelt, January 2018; Bartelt et al., 2018; Christen et al., 2010a). As avalanches with snow entrainment from older layer were observed as well (Fragebogen für Schadenlawinen SLF, 1951b; SLF, 1951a), also the bottom layer was accounted for in the simulations. For this layer, κ and ε were set to lower rates (κ= 2.0, ε= 0.0) and the snow density slightly increased (250 kg/m^3). Currently, entrainment height (D) is defined with constant 0.5 m. A new approach is to correct the measured snow height for a slope of 25° and multiply the

result with a ratio of 0.75 that accounts for snow settlement (personal communication Lukas Stoffel, January 2018). This method was applied to 3-day sum of new snow depth for top layer and measured snow height before the heavy snowfall for the bottom layer. Although the three avalanches in 1951 released at different times, I choose an average of the calculated entrainment height (D) for all three cases and set the top layer to 0.7 m and the bottom to 0.5 m at the reference altitude of 1710 m.a.s.l.. For entrainment height the same gradient with increasing altitude as the Swiss guidelines (Salm et al., 1990) was used, which is 0.05 m per 100 m altitude difference. For the scenario *T30* the standard 0.5 m top layer entrainment was used as it was similar to the value calculated with the above described approach when using the 30 years return period snow height. For the bottom layer no entrainment was added. The resulting entrainment height for scenario *T22J* was 0.36 m at the reference altitude of 1471 m.a.s.l. The values used in all the simulations of reference scenarios are presented in Table 6 and 7.

In addition, the temperature of the entrained snow cover has to be defined. Descriptions of the events indicate that no warming occurred in La Punt and Susauna. However, for Zernez conditions were slightly different. The avalanche started as a cold dry slab but entrained warmer and slightly wet snow in the transition track (see Section 2.4 Winter 1950-1951). Pictures of the 2018 avalanche and measured air temperatures (Zernez weather station at 1471 m.a.s.l. and nearby station Piz Pülschezza at 2667 m.a.s.l.) seem to confirm this pattern. Therefore, temperature in the release zone is set equal to the other study areas but a gradient with snow getting warmer towards the deposition zone is chosen to display the observed conditions (Table 7).

Table 6: Erosion parameters for the simulations of reference scenarios *T1951*, *T300* and *T30* (subscription) for the avalanches in La Punt and Susauna.

	La Punt and Susauna (reference altitude 1710 m.a.s.l.)							
Parameter	D [m]	T [°C]	Delta D [m]	Delta T [°C]	Rho [kg/m^3]	W [%]	K	ε
Top	0.7*	-5	0.05	0	200	0	4	0.4
Bottom	0.5*	-2	0.05	0	250	0	2	0.0

*for the simulation of scenario *T30*, the top height entrainment is set to 0.5 m and the bottom to 0 m.

Table 7: Erosion parameters for the simulations of scenario *T1951* and *T22J* (subscription) for the avalanches in Zernez.

	Zernez (reference altitude 1471 m.a.s.l.)							
Parameter	D [m]	T [°C]	Delta D [m]	Delta T [°C]	Rho [kg/m^3]	W [%]	K	ε
Top	0.58*	-2	0.05	0.25	200	1	4	0.25
Bottom	0.38*	-0	0.05	0.25	250	1	2	0.0

* for the simulation of scenario *T22J*, the top height entrainment is set to 0.36 and the bottom to 0 m.

3.3.3 Sensitivity Analysis

Simulation results are shown with delineation of avalanche runout distances on orthophotos. Maximum pressures of flowing or powder avalanche at damaged buildings in 1951 or reference points set in the deposition zones are compared. The values in Table 5, Table 6 and Table 7 are indicated as reference parameters and are used to show sensitivity to forest structure and terrain roughness. Differences in deposition length with and without forest for each scenario at each test site are shown in the results. Forest destruction predicted by the model is compared to the destruction detected by comparison of orthophotos in 1946 and 1951.

Due to the extensive area of dwarf mountain pine in La Punt, the effect of considering these stands in extreme scenarios (*T300*) and more frequent scenarios (*T30*) is shown in the results. In Susauna I present the sensibility of runouts to the classification of forest. Thereby, the entire roughness of the forest file is set to “smooth” or to “knobby”. Simulations differences between a forest completely classified as “open forest” or “dense forest” are displayed as well. Moreover, the effect of changing erosion parameters (κ, ε) on avalanche runout, maximum pressure at monitoring points and forest destruction in the study area Susauna is compared to the forest effect. Entrainment sensitivity is carried out with reference K-Values in the forest file. The area of Zernez allows a comparison of the effect of changing forest structure on the runout of extreme avalanches releasing far above the treeline.

4. Results

4.1 Field data and remote sensing

4.1.1 DBH and height measured in the field

The data of all trees measured in the field showed exponential increase of DBH with increasing height similar to the power function used in RAMMS (Equation 5). However, for all tree species, the difference between the height predicted using Equation 5 and the data measured in the field was significant. The data showed that the natural logarithm linear regression (Figure 9) better represents the relation between DBH and height for all tree species, although the difference is not always very pronounced. A power model similar to Equation 5 but adjusted for each tree species did not outperform the linear regression and is not shown in the results. For Swiss stone pine, the difference between Equation 5 and the fitted line increases at larger DBH reaching more than 5 m after 50 cm DBH. The fitted line is almost equal to Equation 5 for larch but predicts around 2 m more height in the range of 5 to 50 cm DBH. The difference is due to the smaller height of Swiss stone pine for same DBH compared to larch. The fitted regression for spruce predicts greater heights for same DBH as Equation 5, although the last still lies in the lowest range of deviation from the mean (lower standard deviation line). Dwarf mountain pine height is overestimated when using Equation 5. Mountain pine presented very variable growth habits and was only represented in few samples, which made the fit of a regression line between DBH and height very uncertain with a high deviation range from the mean (Figure 9). When looking at a general regression for all tree species except dwarf mountain pine (general in Figure 9), the regression line that best fitted the data showed almost no difference with the prediction from Equation 5.

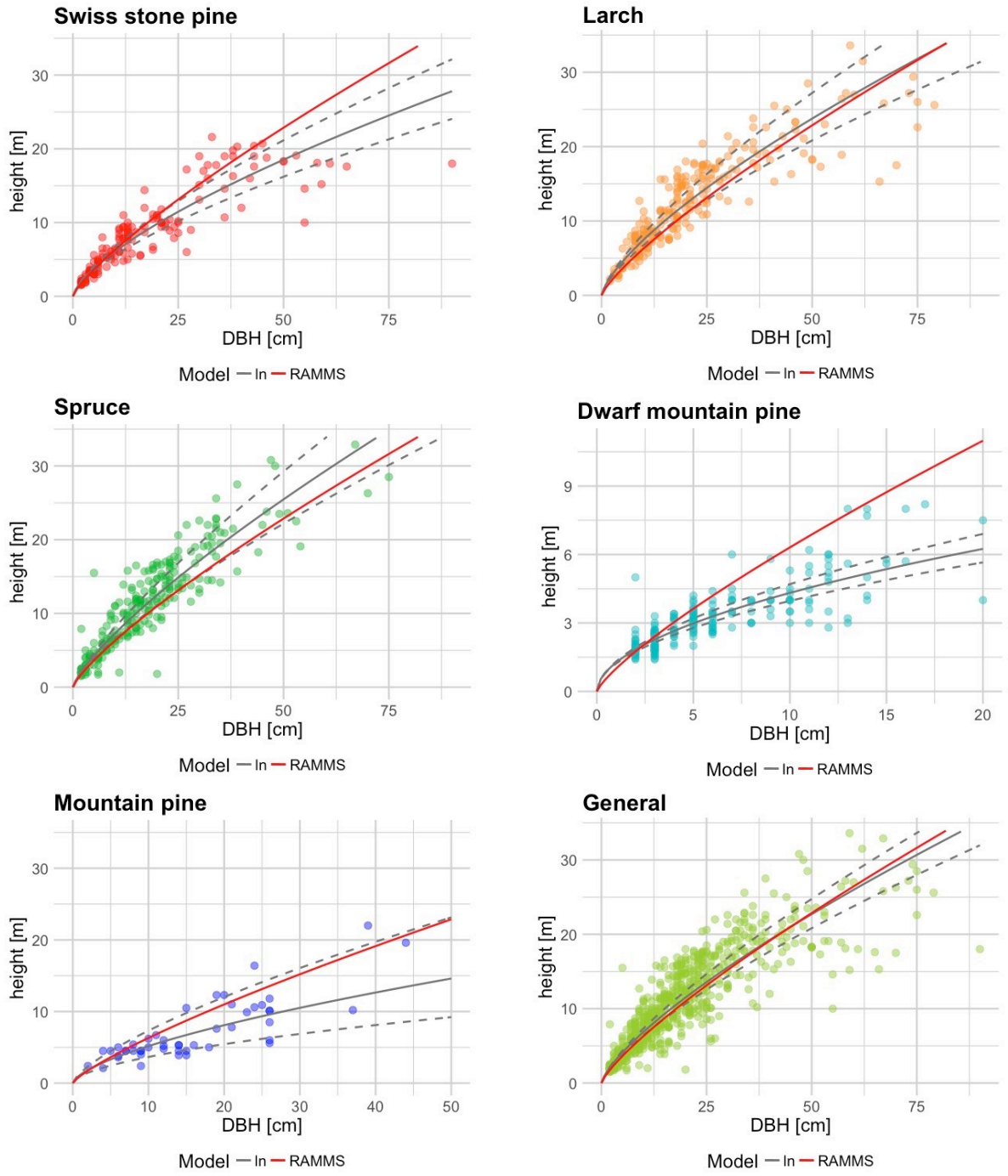

Figure 9: Linear regression (ln = natural logarithmic) with standard deviation (dotted line) between DBH and height for each tree species. RAMMS formula of height = $DBH^{0.8}$ is shown in red. The points in each graph represent the trees height and DBH measured in the field. The graph with a general regression shows the best fitted line for the tree species Swiss stone pine, larch, spruce and mountain pine grouped compared to the general formula in RAMMS.

For Swiss stone pine, larch and spruce the obtained regression between DBH and height explains the variation in the data quite well (See R^2 Table 8). For mountain and dwarf mountain pine the model R^2 is less than 0.8 and does not explain well the overall variation ($R^2_{\text{Dwarf mountain pine}}$ =0.72, $R^2_{\text{Mountain Pine}}$ = 0.64). Therefore, the equations are shown only in Appendix D.

Table 8: Regressions to predict height (H) from DBH according to the formula: $\ln(H) = a + b * \ln(DBH)$. Only regressions with a R^2 value above 0.8 are shown. Fitted parameters values and standard deviation (in brackets) as well as Akaike information criterion (AIC) and R^2 are shown.

$\ln(H) = a + b * \ln(DBH)$				
Tree species	**a**	**b**	**AIC**	**R^2**
Swiss stone pine	0.21 (0.05)	0.69 (0.02)	-8.9	0.89
Larch	0.36 (0.06)	0.72 (0.02)	-54.0	0.86
Spruce	0.20 (0.05)	0.78 (0.02)	97.9	0.84
General	0.21 (0.04)	0.74 (0.01)	221.27	0.83

Flowing avalanche loads on trees in the model is independent of tree height but the impact area for powder avalanche load is a function of DBH and tree height. In the examples (Figure 10), the difference in bending stress exerted by an avalanche at 20 m/s on spruce is small for larger DBH (10 MPa) but larger for small DBH (40 MPa). The tree height to DBH relation from the field data would lead to tree breaking in the class of 20 cm DBH, whereas with the overall relation tree break would start at a lower class (10 cm DBH). For larch the difference in bending stress is much smaller at larger DBH (3 MPa). This is due to the tree height in the fitted linear regression (LN), which is equal to the formula in RAMMS at larger DBH. Also at smaller DBH of 10 cm (Figure 10) the difference in bending stress is lower (26 MPa). The bending stress differences between the two methods are in the range of the maximum stress for larch, whereas for spruce they are outside the range. With higher velocities of the powder cloud, the difference between the two methods is larger and smaller for lower velocities.

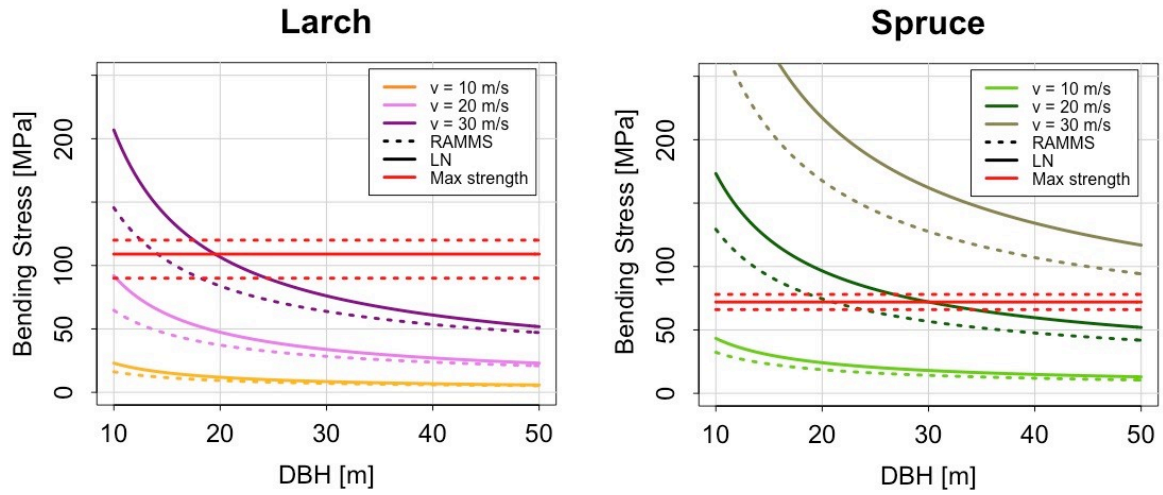

Figure 10: Bending stress for tree species considered in the forest module (larch and spruce) calculated with the overall height to DBH equation (RAMMS = dotted lines) and the single tree type equation fitted (LN = solid lines) according to Equation 4. As example representative values of the powder avalanche in the lower track of Zernez are used (mean slope angle = 35°, powder density = 3kg m^{-3}). The maximum bending strength of spruce in the model is 72 MPa and larch 109 MPa. For larch the plausible empirical range between 90 kPa and 120 kPa is shown with the red dotted lines. The range of maximum bending stress according to Grosser and Teetz (1985) is shown with the red dotted lines for spruce. Bending stress is shown for three powder velocities: 10, 20 and 30 m/s.

4.1.2 Canopy height model (CHM) accuracy

In both models, there is no significant difference in ΔHmax (CHM maximum height – field maximum tree height) depending on the study area, the forest type or canopy coverage. For this study, this means that a systematic error in detecting tree height in forests with different structures can be excluded. However, when using the 2016 model ΔHmax reaches values up to -25, indicating that for some sample plots almost no forest was detected with remote sensing. The ΔHmax is displayed for each study area, forest type and canopy coverage in Figure 11.

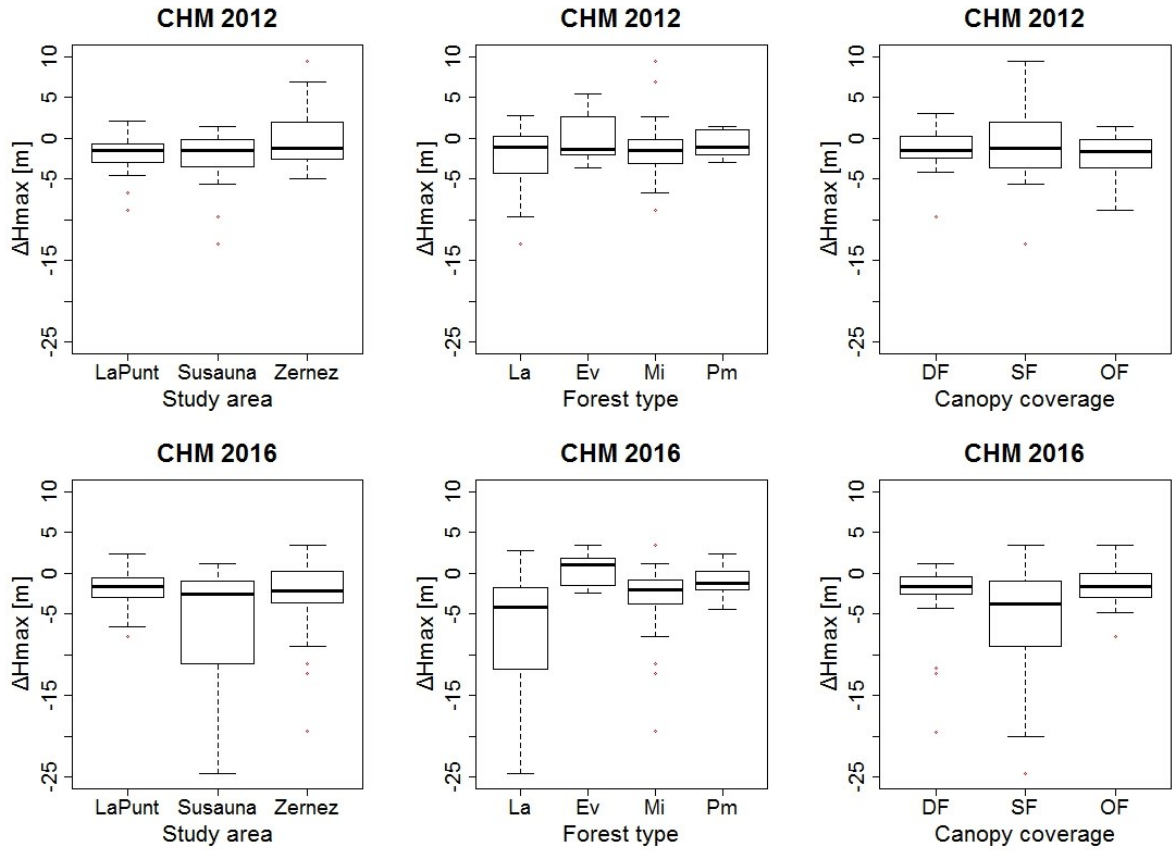

Figure 11: ΔHmax values (CHM maximum height – field maximum tree height) for the 2012 and 2016 models are shown in relation to the factors study area, forest type (La = larch, Ev = evergreen, Mi = mixed, Pm = dwarf mountain pine) and canopy coverage (DF =>70%, SF = 40-70%, OF = 20-40%) of each sample plot.

Correlation between maximum value of CHM and height measured in the field are significantly better for the 2012 data set (Spearman rank correlation rs = 0.91) than for the 2016 data set (Spearman rank correlation rs = 0.72). In fact, maximum tree height is underestimated in mean by 1.3 m with the 2012 model and by 3.4 m with the 2016 model. As it can be seen in Figure 12, some plots in Susauna and Zernez are detected almost no height in the CHM of 2016. Therefore, the following analysis applied the 2012 CHM.

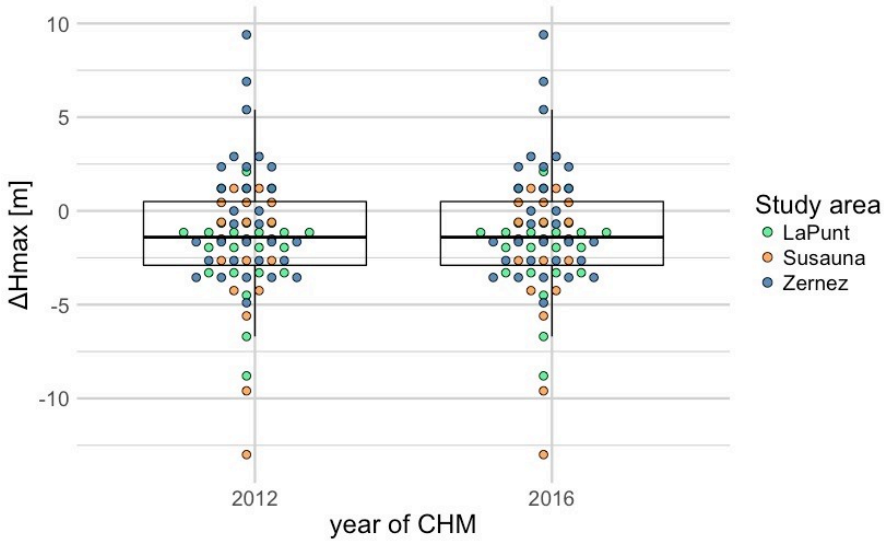

Figure 12: ΔHmax measured with the canopy height model of 2012 and 2016.

However, also in the model of 2012 there are sample plots where the maximum height is underestimated by 15 m or overestimated by 10 m. Indicators of canopy height model goodness (COMP = Completeness of Match and distance to nadir) and GPS position accuracy in the field are shown in relation to the ΔHmax per sample plot (Figure 13). There is no significant correlation between ΔHmax and the three variables (Pearson's rank correlation p-values: p_{COMP}= 0.60, p_{NADIR} = 0.13, $p_{Accuracy}$= 64). The sampling plots with most difference between maximum height in the field and canopy height model have very accurate or good GPS position. In the same way, completeness of match of 95% is detected where highest differences are measured. Highest differences in maximum height are in areas of the CHM with high nadir distance, although other sample plots show even higher nadir distances but better detection of maximum tree height (Figure 13).

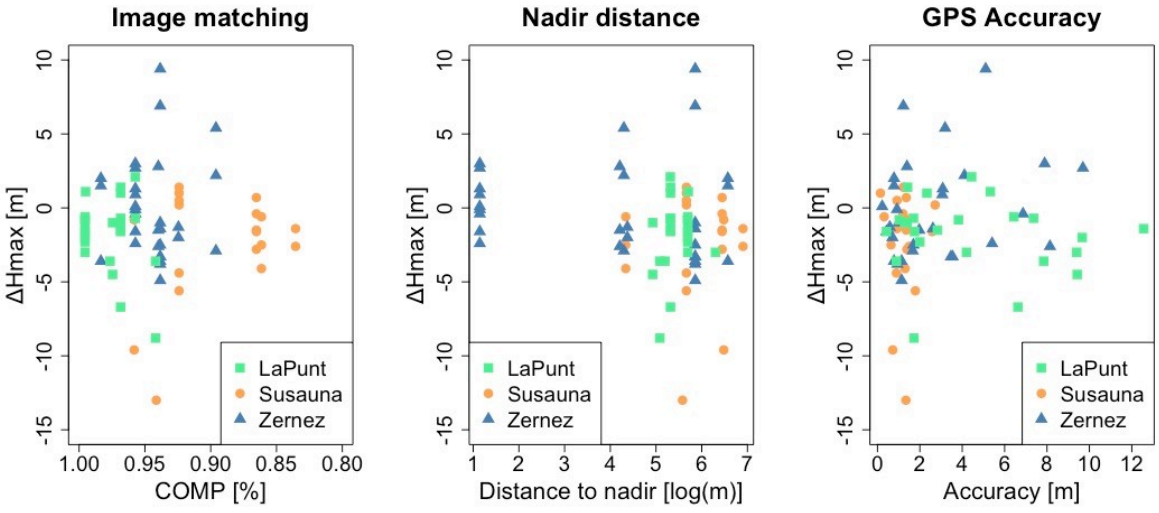

Figure 13: ΔHmax in relation to COMP (Completeness of match), distance to nadir and GPS Accuracy. A high COMP %, small NADIR distance and small GPS Accuracy indicate good accuracy in the methods.

Maximum tree height in each sampling plot is best represented by the 90th percentile of the CHM (Spearman's rank correlation 0.94). Also the height of (co-)dominant trees is described well by the 90th percentile (Spearman's rank correlation 0.9). Both models explain the variation significantly better when accounting for the effect of forest type (R^2_{Hmax} = 0.89, $R^2_{H(co\text{-})dominant}$=0.87). Although the correlation is linear, the maximum height measured in the field presents generally 5 m more than the 90th percentile of the CHM. However, the difference is smaller for larger stages. Similarly, the mean height of the (co)-dominant trees in each sampling plot is around 7 m higher in larch forests than the 90th percentile of the CHM. The offset for evergreen or mixed forests is around 5 m and for dwarf mountain pine stands it is almost 0 m. The underestimation of mean height when using the CHM is not constant as some sample plots also presents smaller heights in the field (Figure 14). For maximum tree height as well as for mean height of (co-)dominant trees, the difference between field measurements and the 90th percentile of the CHM showed to be smaller for larger tree heights.

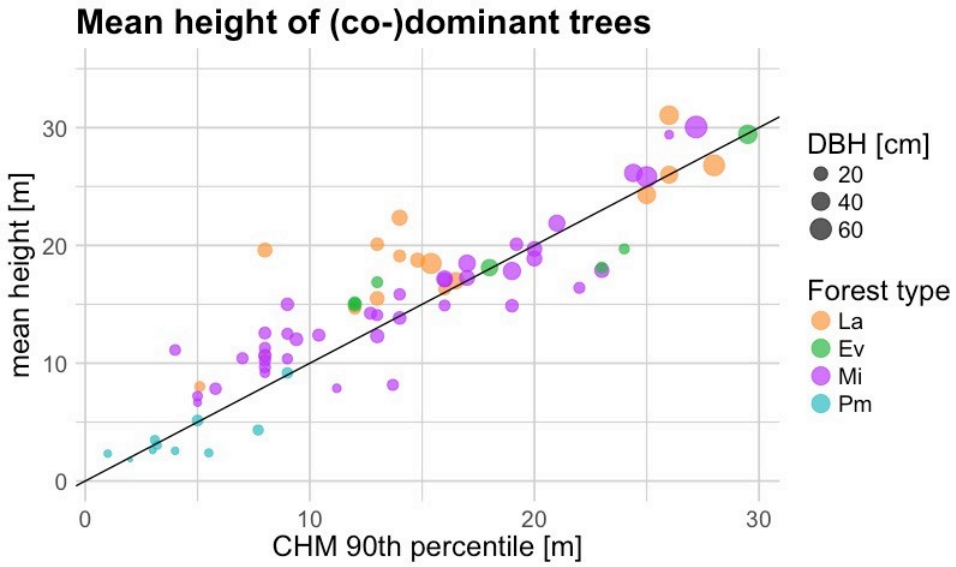

Figure 14: Correlation between mean height of (co-)dominant trees and the 90th percentile of canopy height model (CHM) for each sampling plot. Forest type (La = larch, Ev = evergreen, Mi = mixed, Pm = mountain dwarf pine) with the mean DBH range of the sample plot is displayed. The intersection line indicates where CHM and mean height would be equal.

4.1.3 Forest parameters with remote sensing

4.1.3.1 Crown coverage

The difference in crown coverage between the three field canopy coverage classes is significant. However, the intervals (95% confidence intervals) are slightly different when using the CHM model compared to the intervals described in RAMMS. For example, when using a 3 m height threshold for forest definition, the category "Open forest" is defined as below 46% in the CHM (compared to the value for estimation in the field or orthophotos of 20%). The same category with a threshold of 5 m is calculated as under 28% canopy coverage. Dwarf pine forest stands, which are manually classified as open stands, are mostly detected as well as open forest. Only for three plots, the canopy coverage calculated with the CHM is above 40%, which would classify them as scattered forests. The results present high variance, especially for the sample plots in scattered forests

(Figure 15). This may indicate difficulties of the canopy height model in detecting trees in these types of forests but also the uncertainty of the estimations in the field. When using 5 m height as threshold the result is very similar.

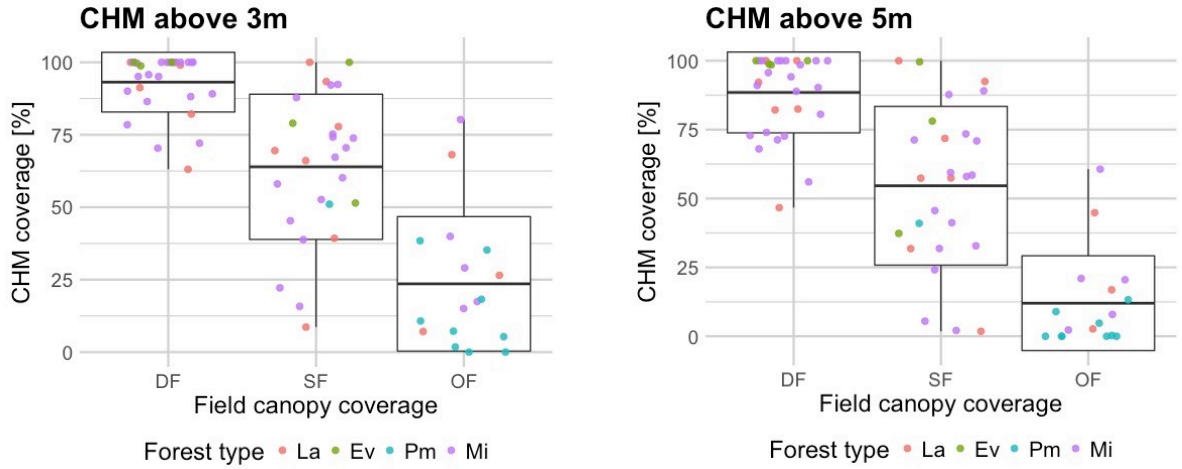

Figure 15: Canopy coverage calculated [%] with threshold height to define forest of 3 m (left) and 5 m (right). Mean values and 95% confidence intervals of the CHM coverage for each field canopy coverage class are shown in the plot (DF = > 70%, SF = 40-70%, OF = 20-30%). The dots represent each sampling plot according to forest type (La = larch, Ev = evergreen, Pm = dwarf mountain pine, Mi = mixed).

4.1.3.2 Roughness

The difference in maximum roughness values assessed with remote sensing data between the three field categories (smooth, knobby, rough) is not significant. In each field category, the mean value of the remote sensing method is smaller than 0.01, which stands for a smooth ground roughness. The ground roughness of each sampling plot classified in the field (field roughness) compared to the roughness classified with remote sensing (remote) is shown for each study area in Figure 16 to 18. When comparing the overall field roughness with the remote classification only 11 samples in La Punt, 6 in Susauna and 10 in Zernez have the same classification. In the study area of La Punt, 25% of the samples (6 samples) are classified as rough although in the field only smooth and knobby sample plots are observed. On the contrary, ground roughness is strongly smoothened by the remote sensing method in the other study areas. In Susauna 95% and Zernez 80% of the sampling plots are classified as smooth (remote) compared to the 32% and 23% observed in the field. If elements from the vegetation (stumps, saplings, trunks, shrubs) are not considered in the field classification of roughness, the comparison looks different. In La Punt 6 samples, 9 in Susauna and 17 in Zernez become smooth and samples number with same classification as remote sensing is higher (La Punt 13, Susauna 14 and Zernez 21). The high difference in Zernez is due to the large number of plots with regeneration or shrubs in understorey. Altough without considering regeneration and stumps the sample correctly classified are 54% in La Punt, 73% in Susauna and 70% in Zernez, it must be taken into account that these are all from the smooth field observation.

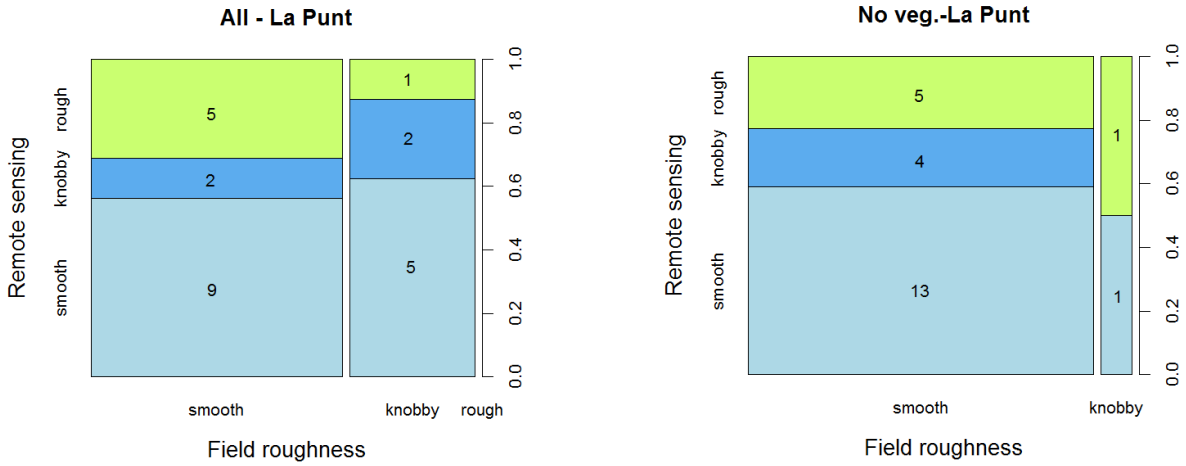

Figure 16: Field roughness with all elements (left) and without elements from the vegetation (right) compared to remote sensing roughness for study area La Punt. Column width indicates the relative amount of sample plots in each field roughness category. Numbers show the total amount of sample plots in each classification.

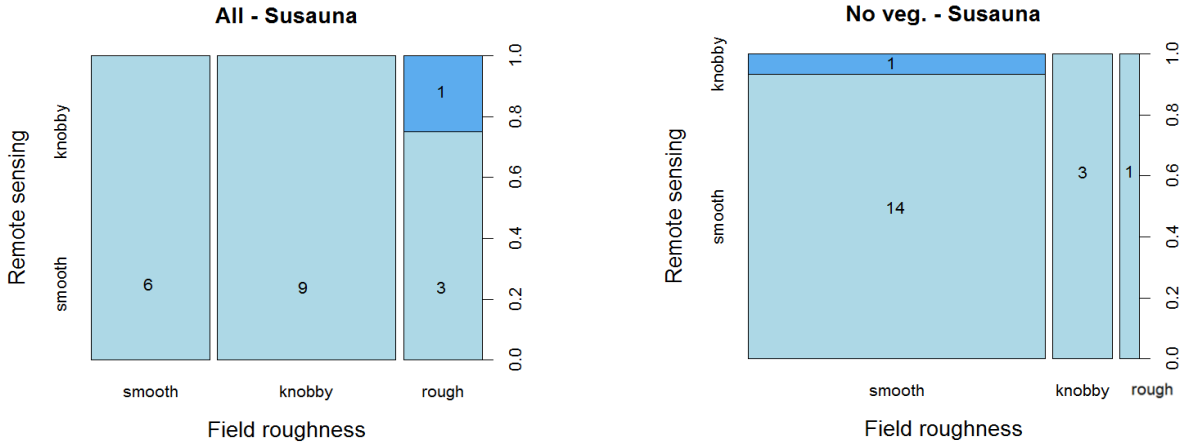

Figure 17: Field roughness with all elements (left) and without elements from the vegetation (right) compared to remote sensing roughness for study area Susauna. Column width indicates the relative amount of sample plots in each field roughness category. Numbers show the total amount of sample plots in each classification.

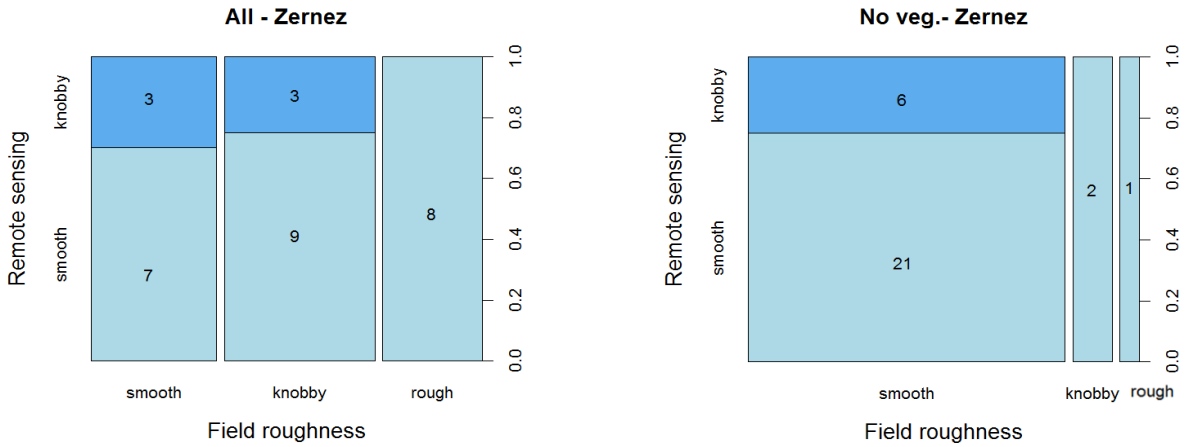

Figure 18: Field roughness with all elements (left) and without elements from the vegetation (right) compared to remote sensing roughness for study area Zernez. Column width indicates the relative amount of sample plots in each field roughness category. Numbers show the total amount of sample plots in each classification.

4.1.3.3 DBH

Best correlation between field data and remote sensing was found for the mean DBH of (co-) dominant trees and the 90th percentile of the CHM (H90) (Spearman's rank correlation = 0.82). Mean DBH of (co)-dominant trees is best predicted by a linear regression (Table 9) that accounts for differences in forest type.

Table 9: Equation to describe mean diameter at breast height (DBH) of (co-)dominant trees in each sampling plot. The explanatory variables are the 90th percentile value of the canopy height model (H90) and the forest type (La = larch, Ev = evergreen, Mi = mixed and Pm = dwarf mountain pine). Coefficients with standard deviation (in brackets), Akaike information criterion (AIC) and R^2 are presented here.

Equation	a	b	AIC	R^2
$\mathrm{DBH} = \exp(\mathrm{a}) + \mathrm{b} * \mathrm{H90}$	a_{La}= 1.58 (0.2)	0.74 (+-0.07)	40	0.82
	a_{Ev}= 1.32 (0.14)			
	a_{Mi}= 1.35 (0.09)			
	a_{Pm}= 0.86 (0.16)			

Larch presents higher intercept in the model as for same height in the CHM (predictor variable H90) the mean DBH is larger compared to mixed or evergreen forests. As shown in Table 9, these two forest types have very similar relation between the CHM and the mean DBH. As expected, dwarf mountain pine has much smaller DBH for same height compared to the other forest types. The difference in the fitted regression lines is graphically shown in Figure 45 (Appendix D). With increasing CHM height, the difference in the prediction of DBH for each forest type gets larger. For example, larch forests have in mean 20 cm larger diameter compared to evergreen and mixed forests at 90th percentile of 20 m in the CHM. This indicates that in an automatic prediction of DBH class from the canopy height model, the distinction between larch forests and the evergreen/mixed is essential.

The use of the regressions in Table 9 to predict the DBH of forest polygons in the area of Zernez is shown in Figure 19. More than the half of the forested area obtains the same DBH predicted with remote sensing as manually defined and few polygons are overestimated by 5-10 cm with remote sensing. Only three polygons present differences of more than 10 cm. In the larch forest with European alder in understorey at the lower timberline the DBH predicted is 40 cm larger than the manual classification (dark blue polygon in Figure 19).

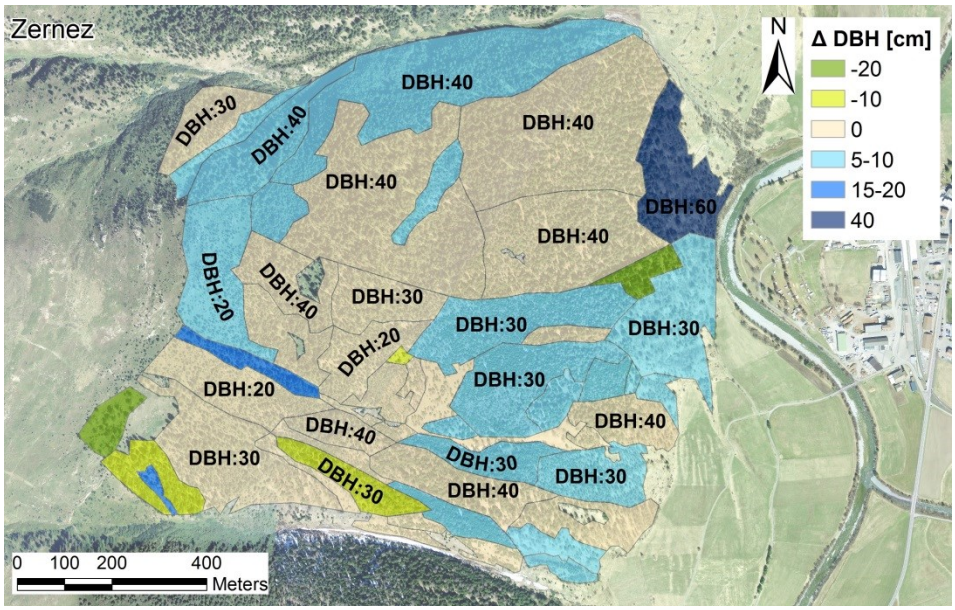

Figure 19: DBH calculated with remote sensing is displayed for major forest stands. Difference to manual classification in 2018 is shown as ΔDBH (DBH remote sensing – DBH manually).

4.1.3.K-Value

In the example of the study area Zernez, K-Values are generally underestimated when using an automatic classification with remote sensing data compared to the manual classification (field data, stand maps, orthophotos). The area presents much higher proportion of areas with scattered forest (60% compared to 30% with manual classification), almost no open (0.1% compared to 10% with manual classification) and 40% dense forest (compared to 50% manual classification).

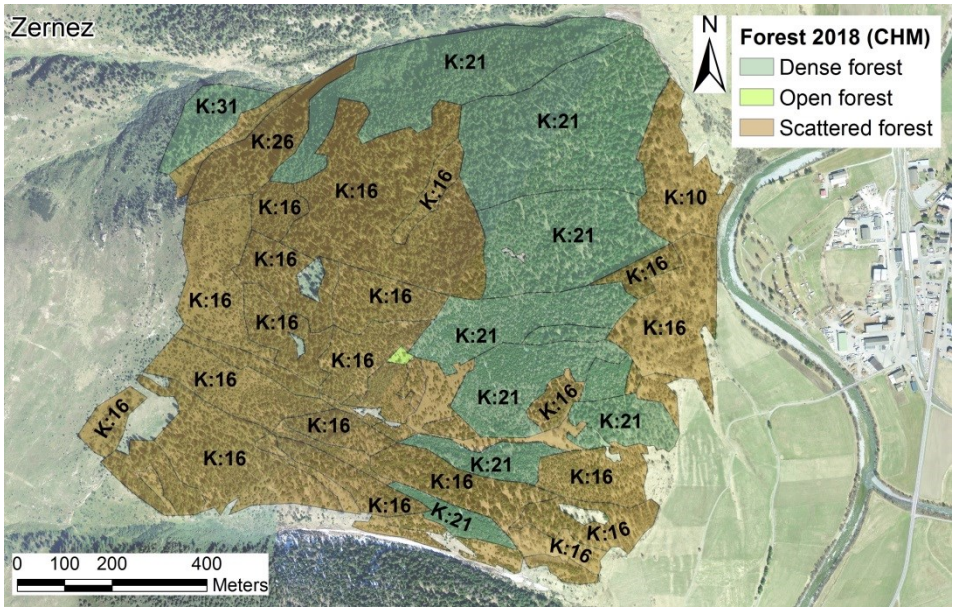

Figure 20: Forest classification for the example area Zernez using remote sensing data (canopy height model and SwissALTI3D terrain model). K-Values are shown for major forest stands.

The Δ K (K remote sensing – K manual classification) in Figure 21 shows mostly values between -10 and -5 $kgm^{-1}s^{-2}$. Polygons with underestimations of -20 to -15 $kgm^{-1}s^{-2}$ are also present. Areas where regeneration or understorey trees are classified as knobby or rough elements are generally classified smoother with remote sensing, which is directly reflected in smaller K-Values. The forest areas where the K-Value is overestimated (green) are small open stands between dense forest or dwarf mountain pine and larch stands in the avalanche track (Figure 21).

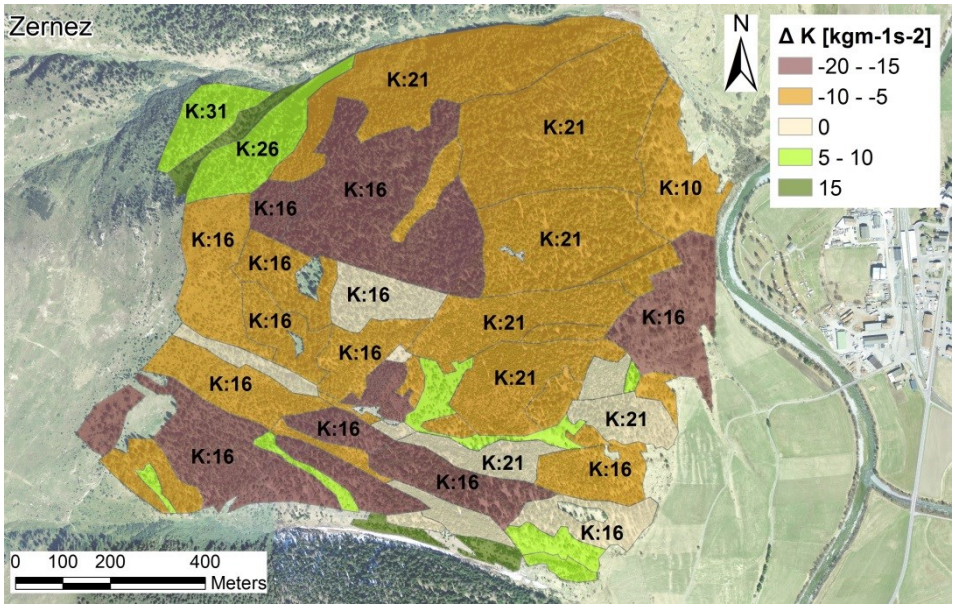

Figure 21: K-Values calculated with remote sensing are shown for major forest stands. Difference to manual classification in 2018 is shown as ΔK (K remote sensing – K manually).

4.2 Forest cover change and avalanche simulations

4.2.1 La Punt

4.2.1.1 Forest

In scenario *T1951* the area presented over 60% of scattered forest and 20 % of dense forest, which was mainly in the central area of God Arschaida. As it can be seen from the orthophoto of 1946 (Figure 22), the area below release zones A1-A2 and A3-A4 was extensively covered by shrubs or small dwarf mountain pines. However, image quality did not allow distinguishing for protective function according to different forest structures and the entire area was not considered in the simulations. The image quality and the field work in 2018, allows a more detailed classification of the stands as it can be seen in Figure 23. Compared to 1951, the area of open forest remained almost equal. The open larch forest on the west side has grown to a close and scattered forest but more open stands appear in the central area with mixed dwarf pine, larch and Swiss stone pine. The forest closure has increased the dense forest proportion by 2.5 times the area of 1951. The forest growth in the openings A8-A9 is considered as completely effective against avalanche release. The upper treeline in the east side has risen by 3 ha with a mixed dwarf mountain pine, Swiss stone pine and mountain pine forest (classified as scattered forest) but this growth is not considered as effective against extreme avalanches release (area A6-A7). Major differences in forest structure were visible for the east avalanche tracks. In 1951, the avalanche path below A5 was completely unforested and the path below A6 seemed completely stocked. In 2018 the situation is inverted. The path of B5 is stocked in the upper part and the forest closure narrowed the gully. The path of A6 is now very open.

Although around 1 ha of dwarf mountain pine with associated Swiss stone pine and larch has grown at the treeline in the central tracks (displayed as open forest), the stands are very open and are not likely to prevent avalanche release in extreme scenarios. The major difference to 1951 are the 14 ha of small dwarf mountain pine on the west side (displayed as young forest), which may prevent avalanche formation from A3 only in the case of small frequent avalanches (scenario *T30*). When not considering this area, the total forest increase from 1951 is around 4 ha. No consistent forest growth was detected in the areas A1-A2 and A4. Openings larger than 50 m in the line of slope in 2018 are present in the east side under the protective structures (release areas C5 and C6 in *T30*).

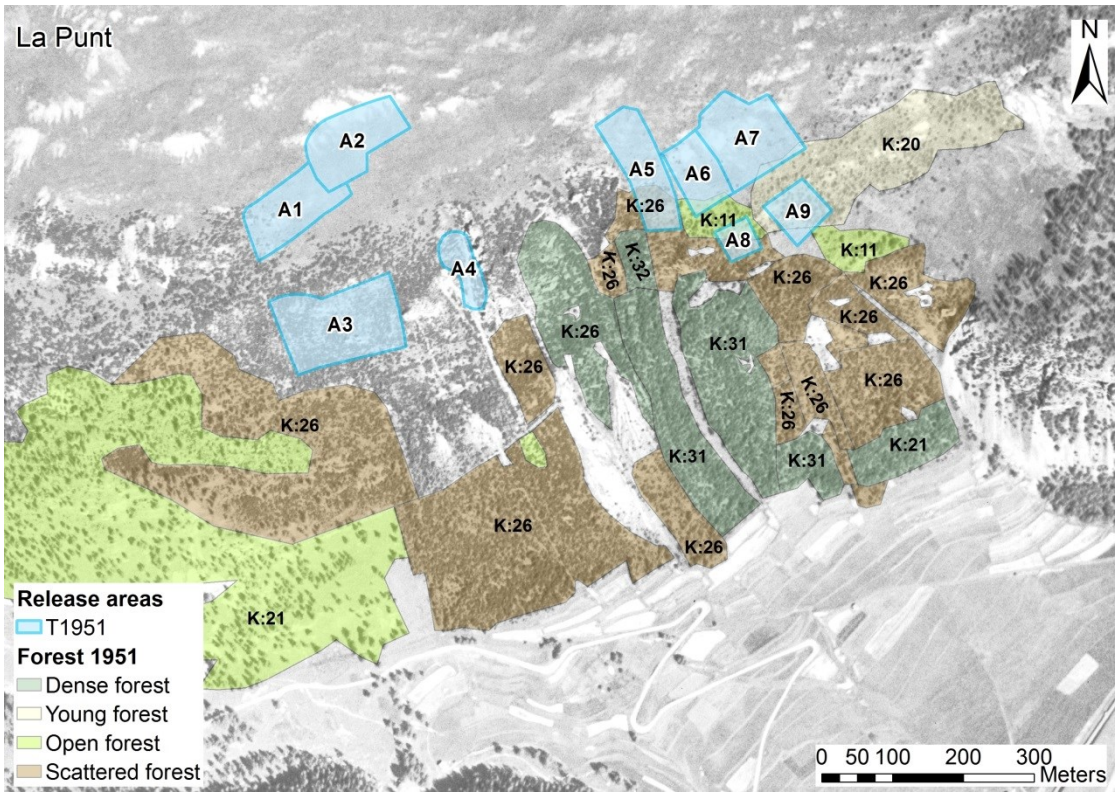

Figure 22: Forest classification for 1951. K-Values are shown for major forest stands. Release areas A1-A9 (scenario *T1951*) are represented in blue.

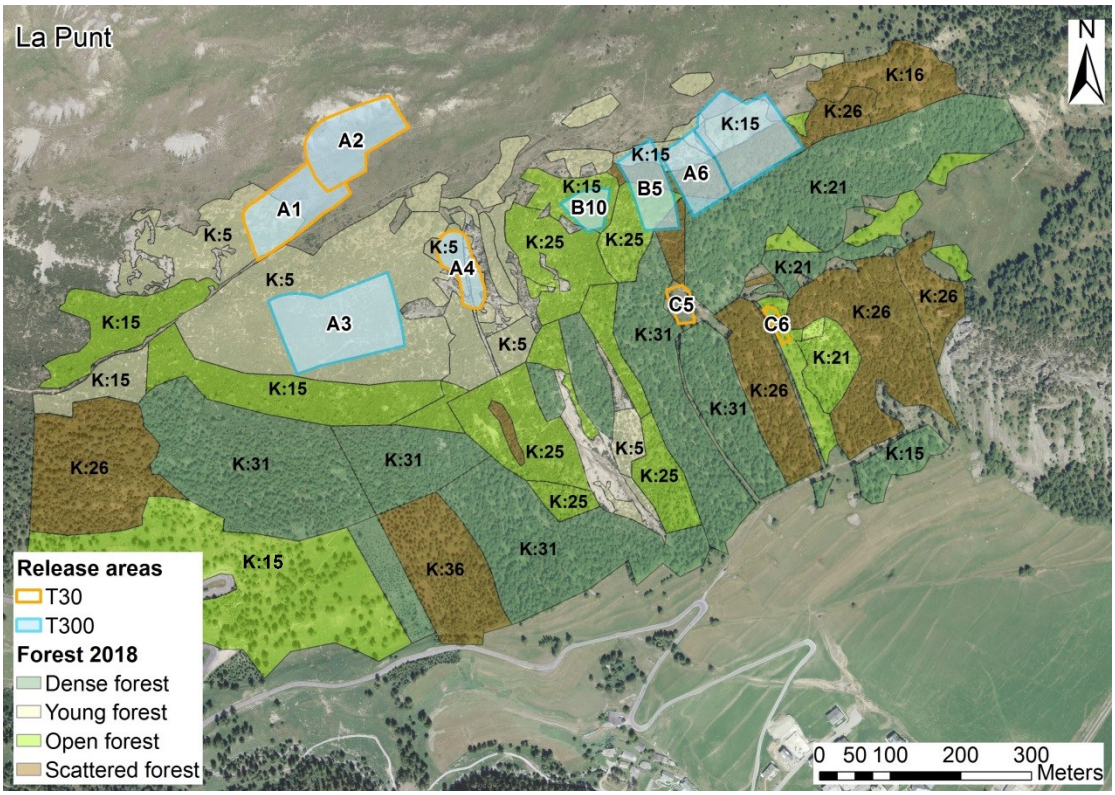

Figure 23: Forest classification for 2018. K-Values are shown for major forest stands. Release areas for *T300* are shown in blue. Small dwarf pine areas are displayed as young forest (yellow) and are not considered in the simulations for *T300*. Release areas for *T30* are represented with orange borders

4.2.1.2 Scenario T1951

The avalanches runouts of scenario *T1951* are different from the presumed but are similar to the avalanche hazard mapping of Pitsch (2015). The effect of forest on runout distance is mainly visible for the release area A5-A9, where the avalanche front stops in mean 80 to 120 m before when considering forest (Figure 24). There is little difference in deposition length with or without forest for the release areas A1-A3 due to the topography, which makes the avalanches stop on the counter slope. In both scenarios with and without forest the maximum pressure of the avalanche core at the shooting range is ca. 300 kPa or more (Table 10 on page 40). The cottage "Acla Buob" is at the side edge of the avalanche and in both cases the core pressure is 0. However, the maximum pressure of the powder avalanche is 27 kPa (Table 10), which is enough to damage the building. The forest destruction predicted by the model presents few differences with the destruction in 1951. For the release areas A4 and A5, the simulation predicts more destruction than detected. The damages in stands with dwarf mountain pine can also be recognised as lying to the ground of the trees instead of breaking.

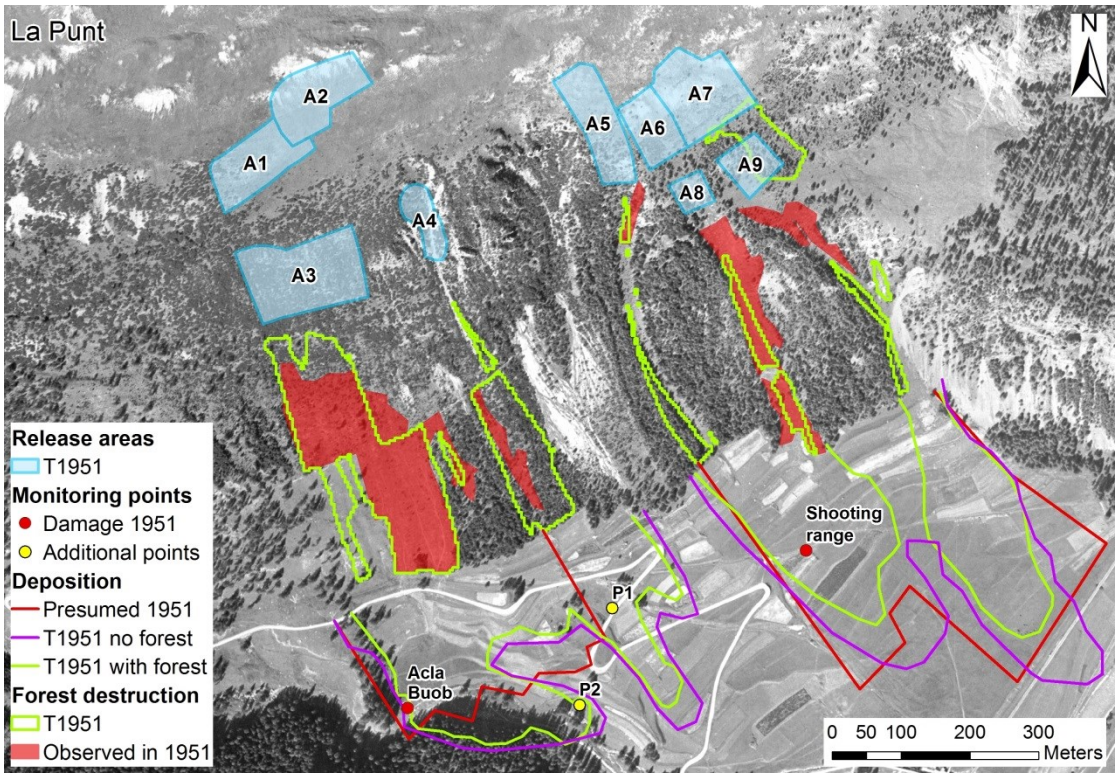

Figure 24: Flowing avalanche deposition with and without forest in scenario *T1951* and presumed deposition in 1951. Forest destruction detected by comparison of orthophotos is shown in red. Forest destruction simulated with reference parameters is shown in green. Damaged buildings and monitoring points are shown in red and yellow.

4.2.1.3 Scenarios 2018 (T300, T30)

The forest closure in A9 in scenario *T300* without forest leads to 70 m shorter deposition length compared to *T1951* without forest. When considering forest along the avalanche track in *T300*, the avalanche stops 120 m before than same scenario without forest and 70 – 80 m before compared to *T1951* with forest. Similarly, the forest growth in A8 shortens the deposition length in *T300* without forest of 30 m at the front compared to *T1951* without forest. The forest along the track leads to 60 m shorter runouts in *T300* but avalanches releasing from A6 flow 50 m longer when comparing both scenarios with forest (*T1951*, *T300*). The smaller detrainment rate due to open forest in the gully compared to the dense forest in 1951 affects the runout more than the reduced release area in *T300*. The decrease of A5 to B5 in *T300* has no impact on the deposition length compared to *T1951* without forest. The forest growth in the gully leads to 100 m shorter runout distances in 2018 compared to *T1951* with forest. In *T300* the braking effect of forest is around 80 m at the avalanche front. The change in forest structure since 1951 affects the runout distance of B5 more than the release area reduction.

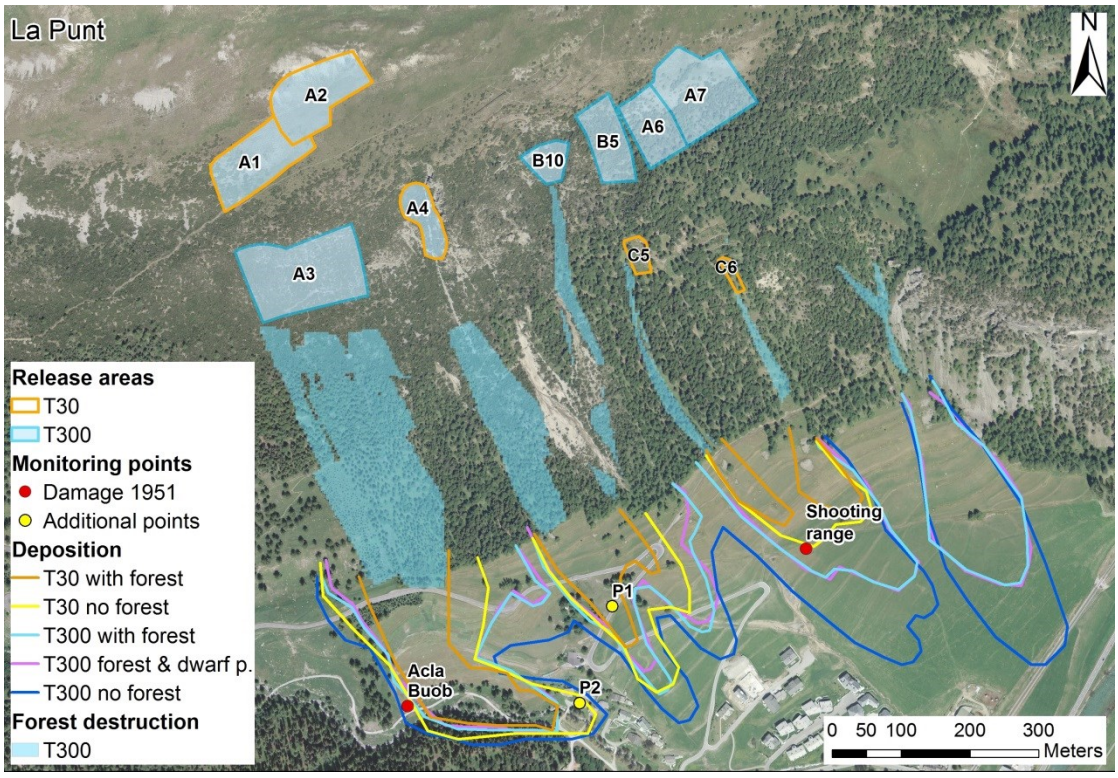

Figure 25: Flowing avalanche deposition with and without forest in 2018 for scenario *T30* and *T300*. For scenario *T30* release areas are displayed with orange outline. Release areas for *T300* are shown in blue. The depositions of scenario *T300* with forest and additional small dwarf mountain pine are shown as well.

Avalanches releasing from A2 and A4 stop 60 m before when considering forest in *T300*, which is also 30 m before compared to *T1951* with forest. Forest exerted the smallest effect in scenario *T300* on avalanches releasing from A1 and A3 with 20 m shorter deposition at the avalanche front. However, the effect of the counter slope should also be considered.

In the case of more frequent avalanches (scenario *T30*) the runout length at the front is reduced by 20 m for release from A1, 70-80 m for release from A2 and A4 and 20-40 m for avalanches releasing from the forest openings C5-C6.

In scenario T300 forest detrained maximum snow heights at the upper treeline were avalanches started. For avalanches initiating high above the treeline, the amount of snow detrained was highest in flatter slopes in mature and dense to scattered forests (Figure 26 (1)). When considering also small dwarf mountain pine forest polygons, forest area is substantially increased under release areas A1, A2 and A3 but the snow height detrained is generally minimal (Figure 26 (2)). Nevertheless, stands situated in flatter slopes at the treeline detrained snow heights equal to mature scattered forests (e.g under release A6, A7) despite being classified with the smallest K-Values of 5. Depositions in simulations that additionally account for small dwarf mountain pine in scenario *T300* are maximum 20 m shorter than those without (Figure 25).

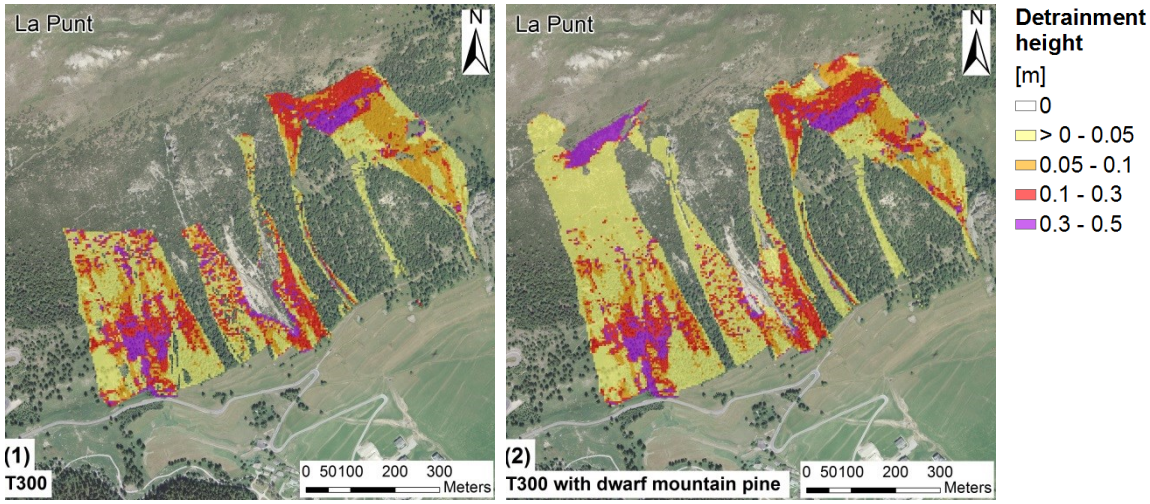

Figure 26: Forest snow detrainment in La Punt. (1) Snow detrained in scenario *T300*. (2) Snow detrained in scenario *T300* that additionally accounts for forest polygons of small dwarf mountain pine.

The forest structure in the transition zone in scenario *T300* reduces the pressure on P1 of the avalanches releasing from A2 and A4 by 70 kPa compared to the forest structure in 1951. Although the detrainment rate is similar in 2018, the total length over which mass is detrained by the avalanche increased by around 80 m. The avalanche pressure at the shooting range in 2018 compared to 1951 changes only little when comparing simulations without forest (30 kPa), whereas it is reduced by more than half when considering forest in the avalanche tracks. In this case, the detrainment rate is increased by forest growth in the gully since 1951. This indicates that the reduction of release area A5 to B5 has a much smaller impact on the maximum pressure of the flowing avalanche at the shooting range compared to the effect of forest along the track.

Table 10: Maximum flowing and powder avalanche pressures at damaged buildings in 1951 and monitoring points P1 (street Albula) and P2 (building in La Punt) in simulations of scenario *T1951* and *T300*. Pressures at each point for simulations with and without forest are shown.

		T1951		***T300***	
Point	Max Pressure	With forest	No forest	With forest	No forest
Shooting range	Flow [kPa]	295	478	130	446
Acla Buob	Powder [kPa]	27	35	10	35
P1	Flow [kPa]	280	329	210	329
P2	Powder [kPa]	5	16	5	16

4.2.2 Susauna

4.2.2.1 Forest

In 1951 almost 50% of the forest was scattered, with a higher rate of scattered forests near the timberline and in the east part. In the orthophoto dense stands are visible in the central and lower east part (Figure 28). In 2018 the total forested area without considering dwarf mountain pine stands is equal to 1951. However, the proportion of scattered and open stands increased mainly due to transitions from dense and young stands. Nowadays, almost half of the area is scattered. Compared to 1951 the forest at the upper treeline extended very little (0-20m) but indentations in the scattered forest are now fully stocked. As a result, the release area A2 was chosen smaller for scenario *T300* (Figure 27). In addition, around 4 ha of small dwarf mountain pine mixed with larches and Swiss stone pine are established at the upper treeline (young forest in Figure 28). A1 is now completely stocked with dwarf mountain pine and Swiss stone pine and is not considered in the simulation of *T30* (Figure 28). Dwarf mountain pine was also partially found in the understorey of the scattered and open stands in 2018. The reforestation after 1951 is visible in the young forest stands in the central track but the scattered forest at the lower timberline was not reforested after the destruction in 1951. The major change in forest structure compared to 1951 is on the orographic left side, where part of the scattered forest is now more open (Figure 28). However, due to the different image quality between 1946 and 2017 it is difficult to exclude any systematic error in classification.

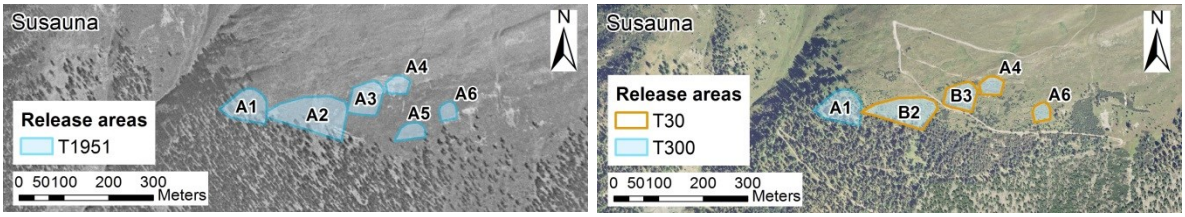

Figure 27: Release areas for *T1951* (left) and scenario *T300* (right) are displayed in blue. Release areas in scenario *T30* (right) are displayed with orange borders.

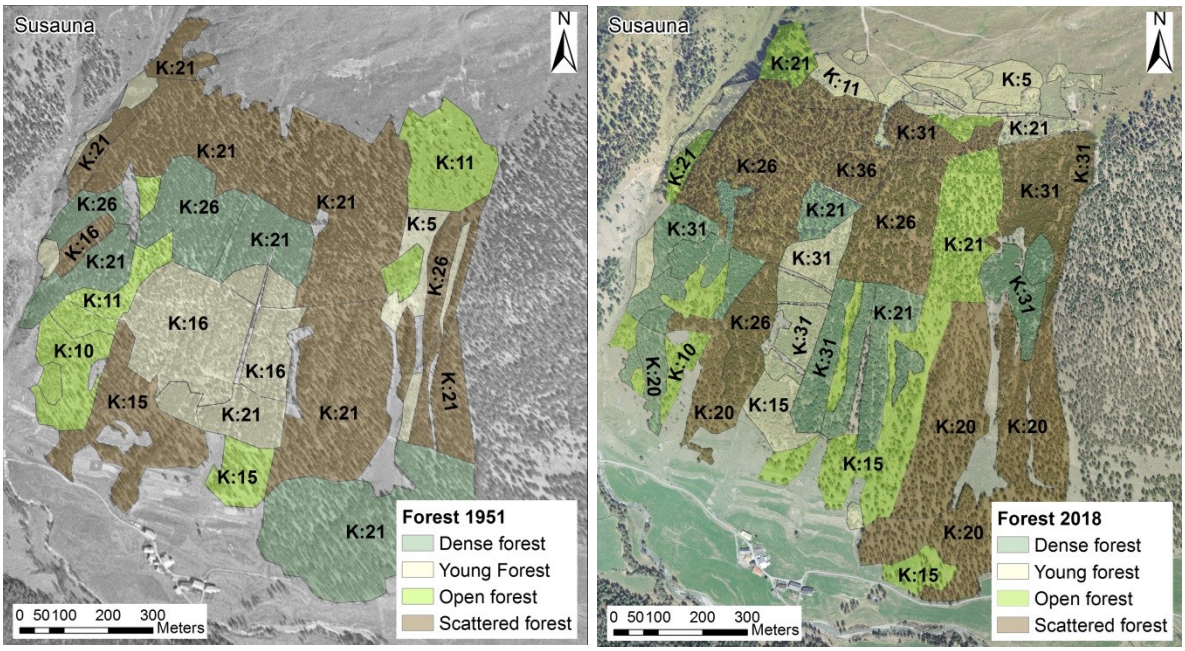

Figure 28: Forest classification for 1951 (left) and 2018 (right). K-Values are shown for major forest stands. In 2018 dwarf mountain pine stands are displayed as young forest and are not considered in scenario *T300.*

4.2.2.2 Scenario T1951

Without forest avalanches flow 50 m (central track) and 60-140 m (sides) more than with forest (Figure 29 (1)). For the central track, there is also to consider the stopping effect of the counter slope on the opposite site of the valley. Forest destruction in the main track with simulation reference parameters generally matches the real damages of 1951. In the transition of A1 it was difficult to achieve destruction, even with the here presented largest version of A1. On the contrary, in the lower forest under A3-A5 forest destruction is slightly overestimated in the simulation. The forest destruction detected in the west deposition was most likely due to lateral spread of avalanches flowing into the west gully and not from avalanches releasing from A1. Simulations showed small sensitivity on canopy coverage classifications in the forest file. The central avalanche track deposition is shortened by 30 m when accounting for dense compared to open forest. In the avalanche tracks in the west and east side, the effect of the increased canopy coverage is stronger as deposition length is reduced by 60-70 m (Figure 29 (2)).

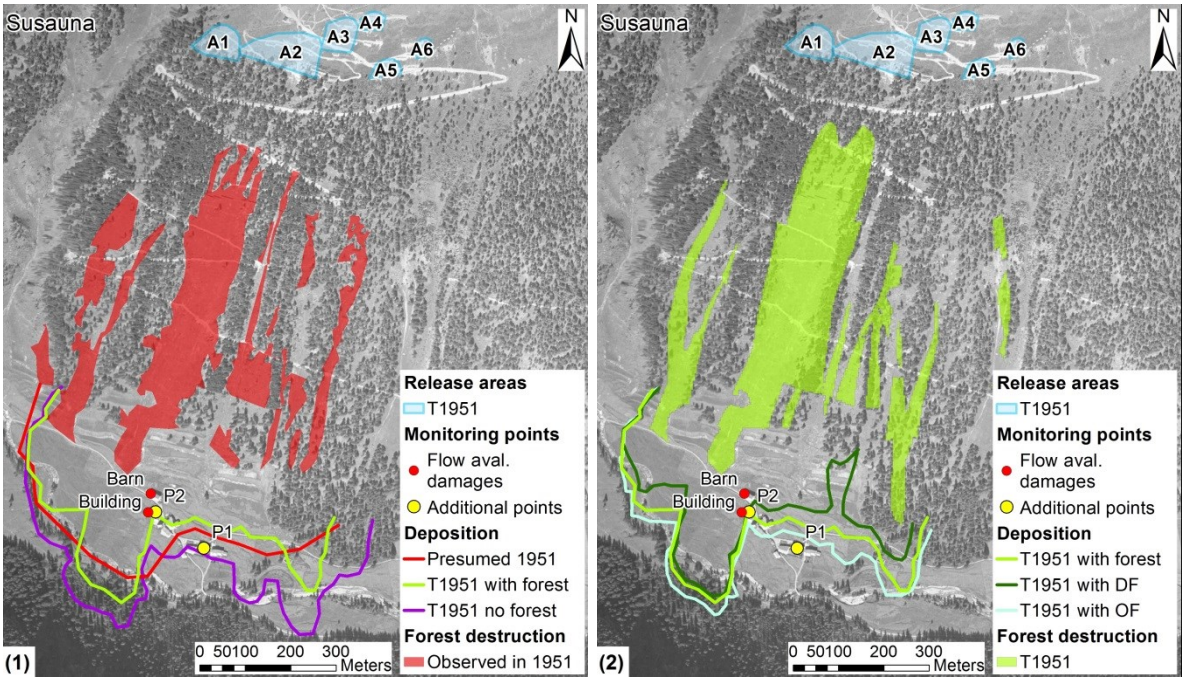

Figure 29: (1) Flowing avalanche deposition with and without forest and presumed deposition in 1951. Forest destruction detected by comparison of orthophotos is shown in red. (2) Flowing avalanche deposition depending on canopy coverage (DF = dense forest, OF = open forest). Forest destruction simulated with reference parameters is shown in green (*T1951*). Damaged buildings and monitoring points are shown in red and yellow.

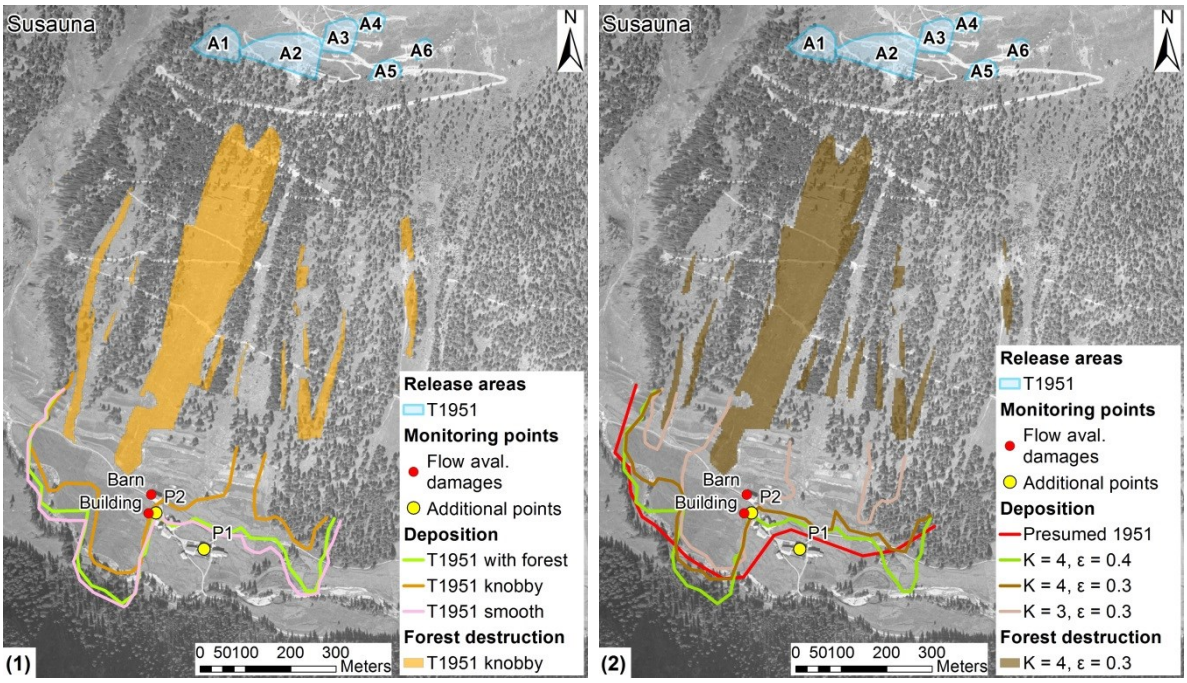

Figure 30: (1) Flowing avalanche deposition depending on forest ground roughness. Reference forest is shown in green. Forest destruction when considering knobby ground roughness is shown in orange. (2) Flowing avalanche deposition depending on erosion parameters. Reference erosion is shown in green (κ = 4, ε = 0.4). Forest destruction with lower erodibility (ε = 0.3) is shown in dark brown.

Changing roughness has a greater effect on the runout distance. Simulations with reference parameters but a “knobby” ground roughness, reduce the central avalanche runout of 40-60 m compared to reference simulations with forest ground roughness set manually (Figure 30 (1)).

Predicted forest destruction better matches the observation in the main track as well as in the lower transition track of A4-A5. When setting the entire forest to a smooth roughness the impact is very small as most of the forest in *T1951* was already classified as smooth. Simulations with same forest structure but with a reduction of the erosion from κ = 4, ε = 0.4 to κ = 3, ε = 0.3 display shorter runouts of 60-70 m for the central avalanche track. This effect is similar as for the change of manually classified ground roughness to a standard of "knobby" (Figure 30). When changing only the ε from 0.4 to 0.3 the runout in the same track is reduced by 30-40 m. Forest destruction using smaller values (ε = 0.3) approaches the observation in 1951 in the main and east track but is too small in the west transition zone of A1.

Dense forest reduces the maximum pressure of the flowing avalanche by more than 100 kPa at the barn and almost the half at the building (Table 11). The changes of the powder avalanche pressure due to more dense canopy area are small.

Table 11: Maximum flowing avalanche and powder pressures at damaged buildings in 1951 (barn, building) and 2 points untouched by the avalanche core in 1951 (P1 in the east part of the village, P2 = east part of building). Pressures at each point are shown for reference canopy coverage, only open or only dense forest.

		***T1951* sensitivity to canopy coverage**		
Point	Max Pressure	manually	Open forest	Dense forest
Barn	Flow [kPa]	481	639	362
Building	Flow [kPa]	256	396	135
P1	Powder [kPa]	4	5	3
P2	Powder [kPa]	31	44	25

Table 12: Maximum flowing avalanche and powder pressures at damaged buildings in 1951 (barn, building) and 2 points untouched by the avalanche core in 1951 (P1 in the east part of the village, P2 = east part of building). Pressures at each point are shown for reference ground roughness, completely smooth or knobby roughness in the forest file.

		***T1951* sensitivity to ground roughness of forest param-**		
Point	Max Pressure	manually	smooth	knobby
Barn	Flow [kPa]	481	498	165
Building	Flow [kPa]	256	269	39
P1	Powder [kPa]	4	5	1
P2	Powder [kPa]	31	33	18

Table 13: Maximum flowing avalanche and powder pressures at damaged buildings in 1951 (barn, building) and 2 points untouched by the avalanche core in 1951 (P1 in the east part of the village, P2 = east part of building). Pressures at each point are shown for reference erosion parameters and slightly lower values.

		***T1951* sensitivity to erosion**		
Point	Max Pressure	κ = 4, ε =0.4	κ = 4, ε = 0.3	κ =3, ε = 0.3
Barn	Flow [kPa]	481	247	82
Building	Flow [kPa]	256	47	23
P1	Powder [kPa]	4	1	0
P2	Powder [kPa]	31	13	5

The increase in roughness to the class “knobby” lowers the pressures at the barn and the building by 3 and respectively 6 times compared to reference simulations. Also the powder avalanche maximum pressure is reduced by more than half.

The reduction of ε to 0.3 leads to the half of the maximal flowing pressures at the barn. The effect on the powder avalanche is similar to the change of roughness to knobby. When changing also ε to 3 the avalanche core pressure diminishes by a factor of around 6 at the barn and more than 11 at the building. The effect is much higher than the sensitivity to forest roughness or canopy coverage.

4.2.3.3 Scenario 2018 (T300, T30)

The simulations of the scenario *T300* show, that avalanche runouts still reach the west part of the village of Susauna. The reduction of release area A2 (*T1951*) to B2 (*T300*) leads to 20-35 m shorter runout distances if forest is not considered in the simulation. In scenario *T300*, forest along the main avalanche track affects the runout distance by 110-140 m. The change of forest structure influences the deposition length more than the reduction of the release area. Simulations of avalanche release from B2, but with the forest structure in 1951, change the runout distance by only 40-50 m (Figure 31 (2)). The building in the position of the old barn is in the runout zone of avalanches releasing from B2 also in scenario *T30* without as well as with forest. Avalanches releasing from B3 and A4, A6 (scenario *T300*) do not reach the east part of Susauna when considering forest and stop 70-120 m before compared to same scenario without forest. The change in forest structure since 1951 leads to a reduction of the deposition length between 0-60 m compared to same release area and fracture depth but with forest structure in 1951. Also, it must be taken into account that no protective structures were considered in 2018. Avalanches releasing from A1 present around 70 m shorter runout at the front with forest in scenario *T300* compared to same scenario without forest. In the case of extreme avalanche release, the forest in the main track is subject to complete destruction (Figure 31 (1)).

The reduction of A2 to B2 has a small impact on the maximum core pressure at the barn and building. Simulation of B2 with the forest structure in 2018 changes the pressure at the barn by far the most (Table 14). This indicates that in the case of Susauna, the effect of changed forest characteristics along the path is greater than the smaller release areas in *T300*.

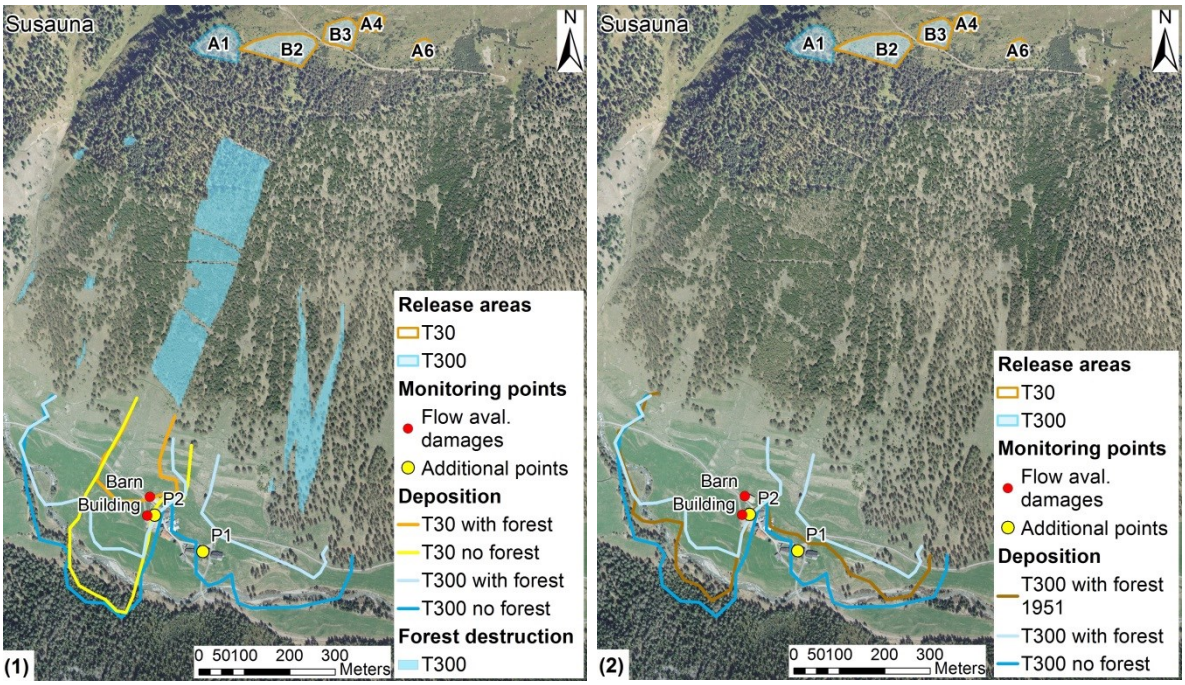

Figure 31: (1) Flowing avalanche depositions of scenario *T30* and *T300* with and without forest. Release areas for *T300* are displayed in blue and for *T30* in orange. (2) Flowing avalanche depositions of a scenario with release areas of *T300* but with forest file of 1951.

Table 14: Simulated maximum flowing avalanche and powder pressures at damaged buildings in 1951 (barn, building) and 2 points untouched by the avalanche core in 1951 (P1 in the east part of the village, P2 = east part of building). Pressures at each point are shown for scenario *T1951* and *T300* with and without forest.

		1951		***T300***	
Point	Max Pressure	With forest	No forest	With forest	No forest
Barn	Flow [kPa]	481	700	65	682
Building	Flow [kPa]	256	540	0	475
P1	Powder [kPa]	4	7	0	4
P2	Powder [kPa]	31	41	5	26

4.2.3 Zernez

4.2.3.1 Forest

In 1951 the scattered forest represented more than 60% of the area. Open stands were detected at the upper treeline and in the common avalanche tracks with exception of one stand near the grassland (Figure 33). When not considering small dwarf mountain pine stands in 2018 (young forest with K-Value 5), the forested area is almost equal to 1951 with only an increase of 3 ha, which corresponds to the afforestation at the treeline in the avalanche track “Vallun Quad-ratscha”. However, through the forest closure the dense stands area triplicated and the scattered forest diminished by around half. Open stands total area remained almost equal. Especially at the treeline, no significant change in structure was visible compared to 1951 (Figure 34). The open stand in the release area C is assumed to not prevent avalanche release in 1951 as well as in 2018. Release areas A1, A2 and B are situated far above the treeline and are not influenced by any changes in forest structure (Figure 32).

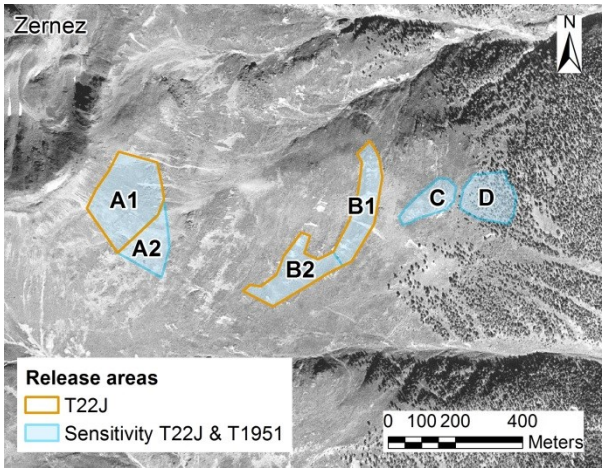

Figure 32: Release areas in 2018 (scenario *T22J*) are shown with orange borders. Sensitivity for release area in 2018 and 1951 is shown in blue.

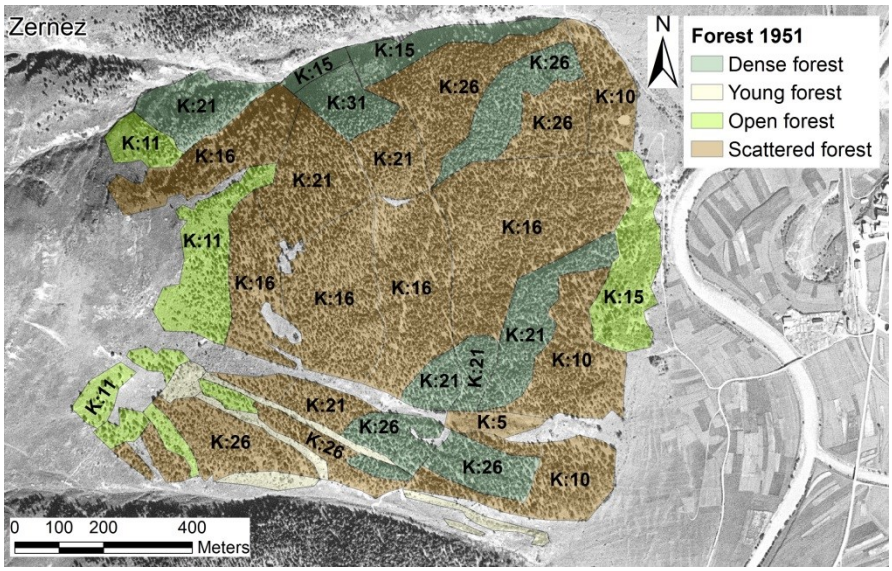

Figure 33: Forest file for simulation 1951. K-Values are shown for major forest stands.

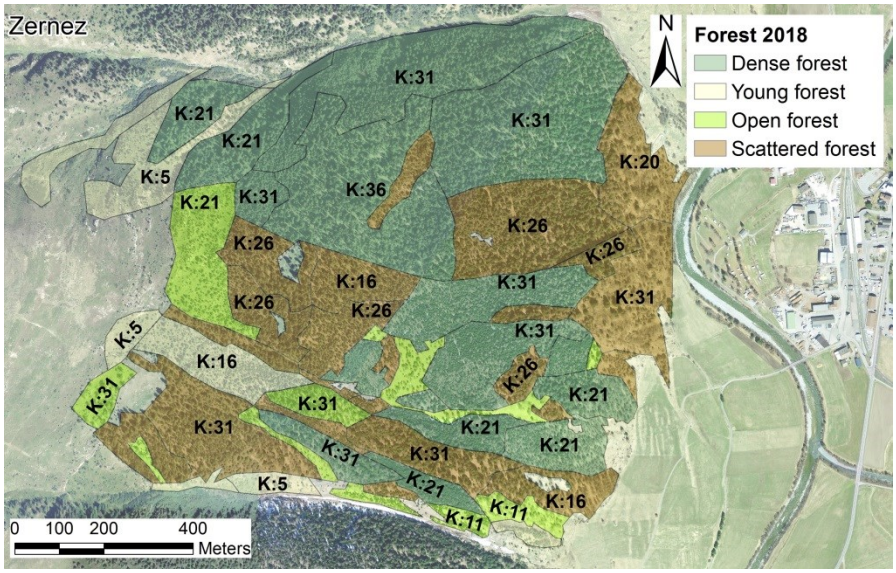

Figure 34: Forest file for simulation 2018. K-Values are shown for major forest stands.

4.2.3.2 Scenario T1951

Simulations of avalanches releasing from the area A1 and B (B1 and B2) as observed in 2018 do not reach the observed deposition length (Meliorationsamt und Vermessungsamt Graubünden, 1951) and do not entirely flow over the "new track" with forest destruction in 1951. Additionally, the avalanche in the track "Vallanzun" flows more than 270 m longer than observed. When considering the area B2 only as entrainment, the same runout is 140-240 m shorter (Figure 35 (2) and (3)). When adding secondary releases from area C, deposition length is similar to 1951 in the "new track" but 130 m longer in "Vallun Quadratscha" and around 170 m longer at the front in "Vallanzun". The forest destruction predicted does not match the observation of 1951 (Figure 35 (2)). Avalanches starting from A1 with secondary release in B1, C and D best match the presumed depositions (Figure 35 (3)). Despite the prediction of less forest destruction in the north stands at the upper treeline and in the sides of the transition, this scenario (release areas A1, B1, C and D) best matches the observed forest destruction in 1951. The interaction of release area C and D results in runout distances, which better represent the observation in 1951.

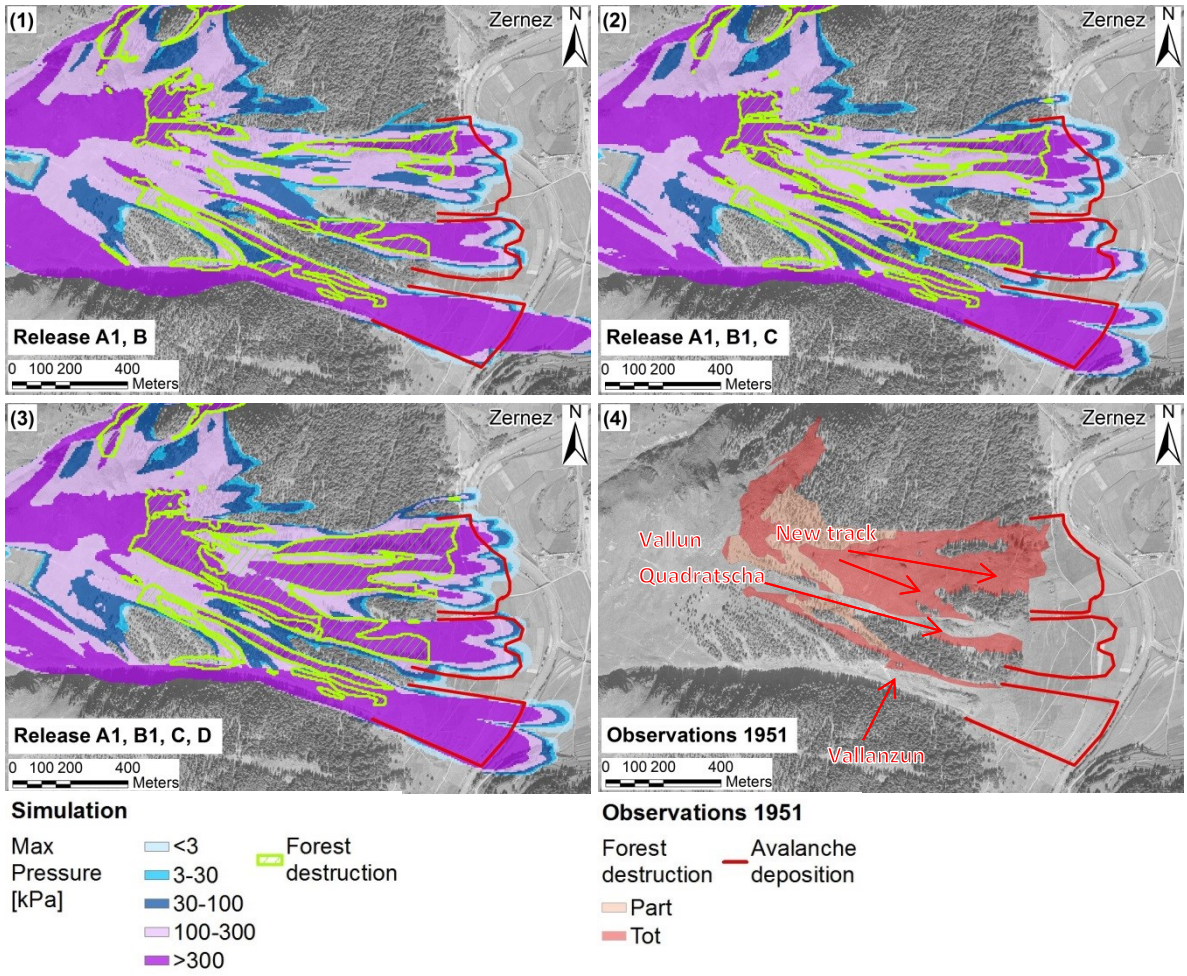

Figure 35: Flowing avalanche pressure in scenario *T1951* and deposition in 1951: (1) avalanches releasing from A1 and B (B1 + B2); (2) avalanches releasing from A1, B1 and C; and (3) avalanches releasing from A1, B1, C, D. (4) Forest destruction in 1951 detected by comparison of orthophotos. Predicted forest destruction for different release areas is shown in green (1)-(3).

In the case of avalanche formation in A1 and secondary release from B1, C and D, runout distances of simulations without forest are 0-40 m longer at the front in “Vallun Quadratscha” and 50-60 m longer in the “new track” than with the forest of 1951 (Figure 36). The avalanche reaches the valley bottom also on the north of the new avalanche track and stops at the beginning of the industrial zone of Zernez. No effect of forest in the track “Vallanzun” is observed. The forest structure used in the simulation of 2018 leads to 30-60 m shorter runouts in the “Vallun Quadratscha” and new track compared to the forest in 1951. The runout in the simulation is now 100-120 m shorter compared to simulations without forest. Avalanches simulated with the forest classification using remote sensing (CHM) are more similar to the 1951 deposition lengths. For the track “Vallun Quadratscha”, the remote sensing method leads to deposition lengths very similar to the ones obtained with classification of forest in 1951. Forest destruction predicted with manual classification (forest 2018) and remote sensing (forest CHM) presents almost no difference.

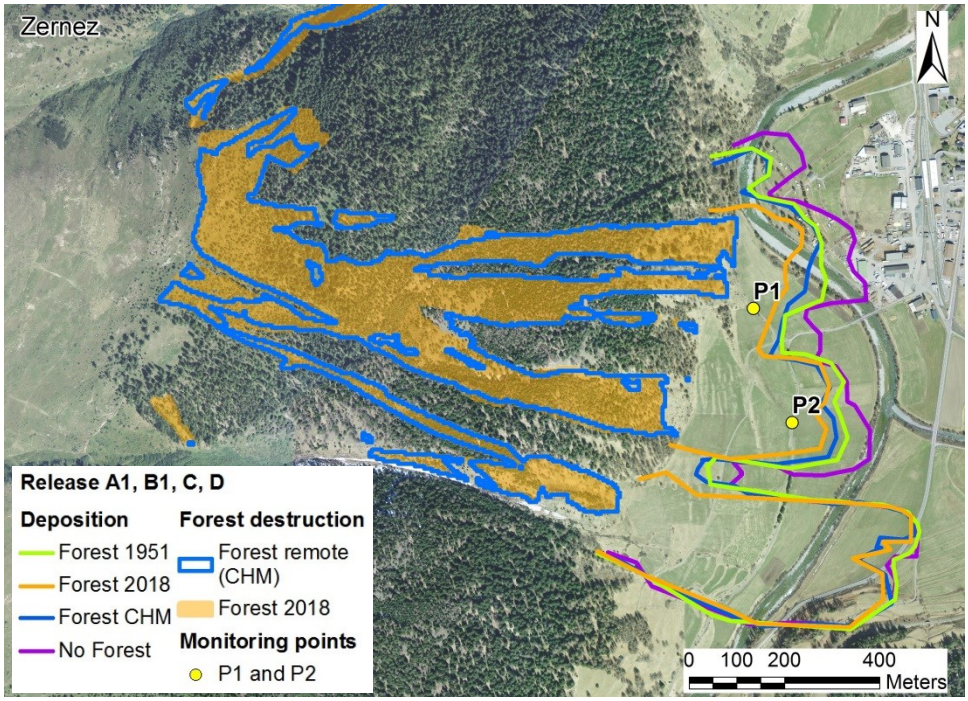

Figure 36: Sensitivity of runout distance to forest. Deposition length is shown for simulation with forest structure in 1951 and 2018 (manually classified = forest 2018, remote sensing = forest CHM). Forest destruction predicted with the remote sensing and the manual classification are shown in blue and orange.

The pressure of the avalanche core in the deposition of the new track is reduced around 3 times when considering the forest in 1951 and by more than 10 times when considering the forest in 2018. In the deposition of “Vallun Quadratscha”, the forest in the scenario *T1951* reduces the pressure by more than a third. The effect of the forest in 2018 is much larger (Table 15). Similarly to the runout observations in Figure 36, the avalanche pressure in simulations with automatic forest classification (CHM) resemble more to the scenario with forest in 1951 than to the forest manually classified in 2018. The difference between 2018 and 1951 is larger for the avalanche in “Vallun Quadratscha” than for the new track.

Table 15: Avalanche core pressure in the runout zone of the new avalanche track of 1951 (P1), and the track "Vallun Quadratscha" (P2). Pressures are shown for simulations with forest structure in *T1951*, 2018, classification in 2018 with remote sensing (CHM) and no forest.

		Forest sensitivity Release A1, B1, C, D			
Point	Max Pressure	*T1951*	*2018*	*CHM*	*No Forest*
P1	Flow [kPa]	71	18	64	204
P2	Flow [kPa]	208	72	130	342

4.2.3.2 Scenario 2018 (T22J)

Compared to observations in 2018, avalanches releasing from A (A1 + A2) and secondarly from B (B1 + B2) present 90-270 m longer runouts in the deposition from the track "Vallanzun" and on average 120 m in the track "Vallun Quadratscha"(Figure 37 (1)). With release only from A1 and B the avalanche front stops around 60-180 m after the limit observed in "Vallanzun" and 60 m in "Vallun Quadratscha"(Figure 37 (2)). Forest destruction predicted by the model with release from A1 and B matches the observation in 2018 (Figure 37 (3)). The forest destruction predicted in the track "Vallanzun" can be seen as bending on the ground instead of breaking of the young larches and dwarf mountain pines. Water content in the snow cover affects majorly smaller tracks such as the one between "Vallun Quadratscha" and "Vallanzun"(Figure 38 (2)). Similarly, avalanches of the simulation with smaller ε in the entrainment parameter stop exactly as observed in the track "Vallun Quadratscha" but do not flow in smaller tracks (Figure 38 (1)). The deposition of the "Vallanzun" is less affected by these changes but mostly by the change in the release area.

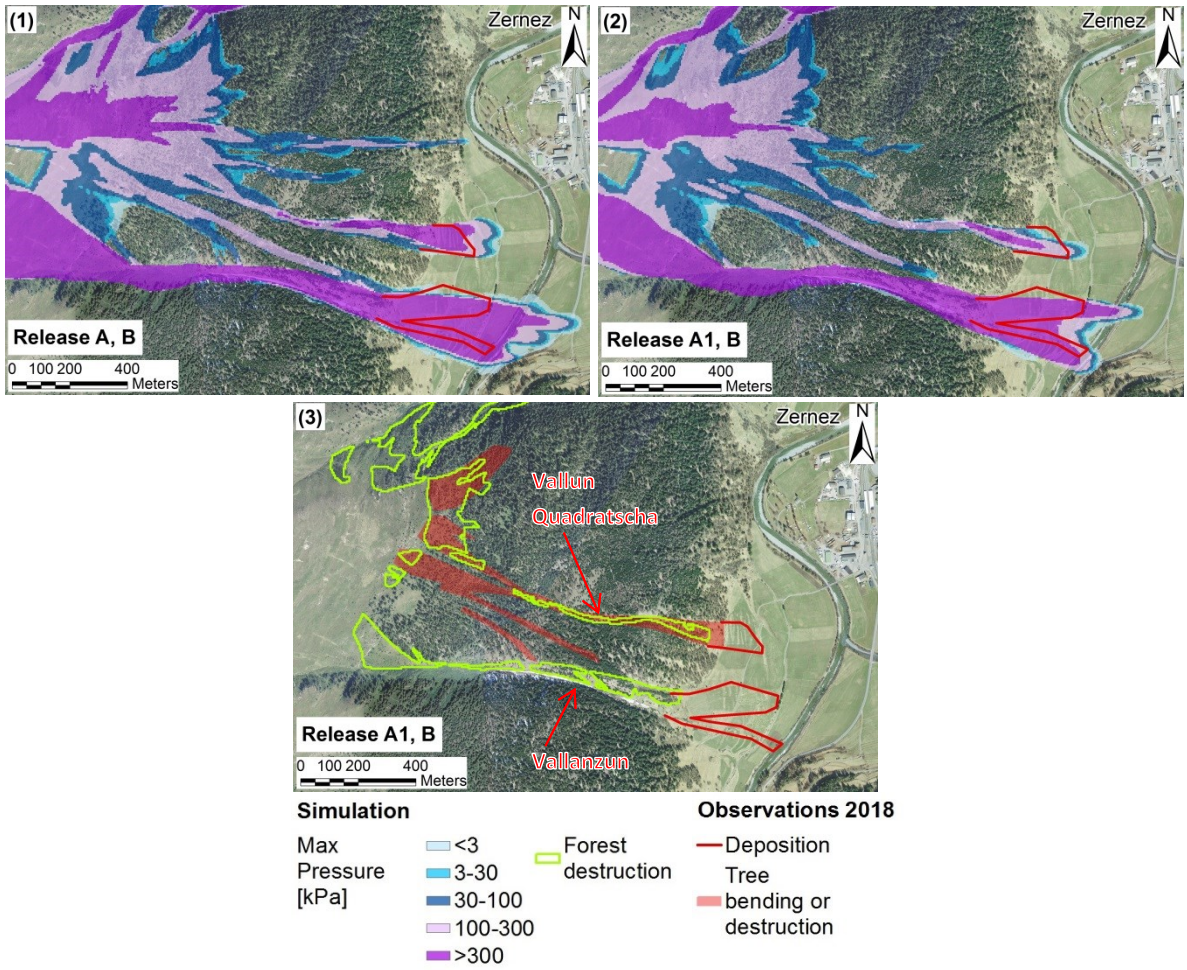

Figure 37: Flowing avalanche pressure in 2018 (scenario *T22J*): (1) avalanche release from area A (A1+A2) and B (B1+B2); and (2) avalanche release from area A1 and B (B1 +B2). (3) Predicted forest destruction with release A1 and B and observed tree destructed or bent by the avalanche. Deposition observed in 2018 is shown in red.

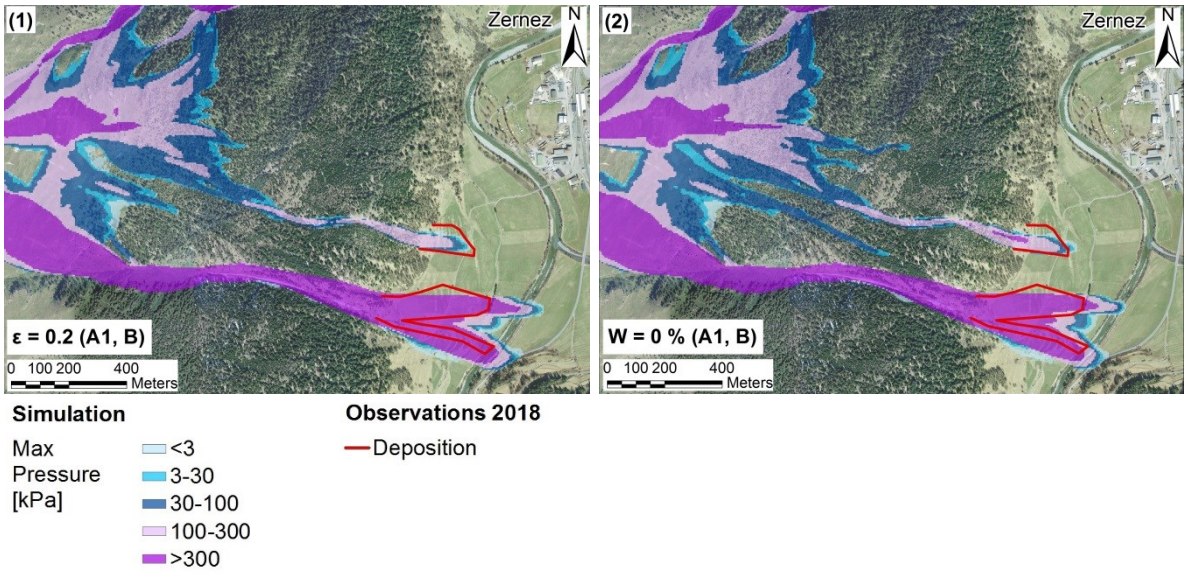

Figure 38: Flowing avalanche pressure in 2018 (scenario *T22J*) with variation of reference parameter for entrainment: (1) avalanche release from A1 and B but ε 0.2 instead of ε 0.2; and (2) avalanche release from A1 and B but no water content in the erodible snow cover instead of 1% water.

5. Discussion

5.1 Comparison of field data and remote sensing

5.1.1 DBH to height relation

The heights predicted with the simple relation (Equation 5) used in the forest destruction module of RAMMS, differed significantly from the field measurements for all tree species. These results disagree with the findings in Brožová (2018), where no significant difference between Swiss stone pine and the values calculated using Equation 5 was found. However, the study compared only DBH ranges of 0 cm to 20 cm, whereas in this study most of the Swiss stone pines measured varied between 1 cm and 60 cm DBH. Although the tree height to DBH relation was described with different and more complex models depending on site, stand, stage, forest type or tree type (Gureicke, 2001; Indermühle, 1978; Prodan, 1965), simple double logarithmic models as suggested by Sterba (2015) were shown to be reliable for the prediction of height from one variable (DBH).

The RAMMS relation (Equation 5) overestimates tree heights compared to the best double logarithmic model obtained from the field data for Swiss stone pine. In the case of larch, tree height is underestimated when using the formula in RAMMS. Thereby, the differences are more pronounced for Swiss stone pine, whereas for larch the difference is small and only in the middle DBH ranges. The best relation for spuce shows smaller height for same DBH compared to the estimation with Equation 5. Due to the smaller sampling number and large scattering of the data, it is not possible to draw any conclusions on mountain pine and dwarf mountain pine. When considering a general linear regression for multiple tree species together (Swiss stone pine, larch, spruce and mountain pine), there are only small differences between the best regression line of the data and Equation 5 at lower DBH ranges and no difference at larger DBH.

The difference in height prediction results also in variations of the calculated bending stress on trees. The results suggest, that accounting for individual DBH to height equations for different tree species (e.g. the logarithmic regressions fitted in this study) would be more accurate than the actual relation used in RAMMS. Although further analysis for different regions and forest stands are needed, the differentiation seems especially important for pure spruce forest stands, where the resulting difference in bending stress exceeded the range of maximum bending stress (between 66 and 78 kPa) proposed in Grosser and Teetz (1985). For mixed forest stands, a general equation such as the one currently applied in RAMMS seems reliable for predicting mean tree height from the DBH in forest polygons.

5.1.2 Canopy height model accuracy

The canopy height model of 2012 represented the maximum tree height for each sampling plot better than the 2016 model. Nevertheless, the best correlation between maximum tree height in the field and the 90^{th} percentile of the CHM 2012 showed as well a constant difference of 5 m with smaller differences for higher trees. When looking at mean height of dominant and codominant trees, the general difference was only 2 m with also a tendency in getting smaller at higher heights. As mentioned by Ginzler and Hoby (2015), this indicates that the model resolution allows

height estimations over forest stands but no precise estimations for single trees. The larger difference between CHM and field data in younger stages might be due to forest growth in the past 6 years.

5.1.3 Remote sensing and forest parameters

5.1.3.1 Terrain roughness

In the study area La Punt, the remote sensing method detected 25% of the sampling plots as rough, whereas in the field no rough classification was observed. The entire area of La Punt starting from the first forest stands with dwarf mountain pine up to the treeline presented very heterogeneous and rough structures in the SwissALTI3D terrain model. For the creation of DTMs with Lidar data, the pulses reflecting directly from the ground and not from the vegetation needs to be filtered (Hyyppä et al., 2000). Although it was shown that dense conifer forest canopy do not affect the accuracy of DTMs based on Lidar data (Reutebuch et al., 2003), dense shrub covers such as dwarf mountain pine seem to affect the accuracy of Lidar-derived DTMs (Gould et al., 2013). The Lidar resolution used to create the DTM by Swisstopo was coarser compared to other areas, which made it more difficult to filter dwarf mountain pines and vegetation in the selection of ground hits for the calculation of the DTM (personal communication Benoit Regamey, Swisstopo, 26.03.2018).

In the other study areas, the remote sensing method strongly smoothened the terrain roughness as in Susauna 95% and in Zernez 80% of the samples are classified as smooth compared to the 32 % (Susauna) and 23 % (Zernez) observed in the field. The difference was expected, as the remote sensing method does not account for vegetation (Sappington et al., 2007). When filtering saplings and stumps from the field roughness classification, the study area Susauna resulted in 74% and Zernez 70% of smooth samples. These values are much closer to the remote sensing classification but still not precise enough. It was observed, that also small non-biological roughness elements such as big rocks or stepped terrain in the sampling plots were not recognised with the remote sensing approach. This indicates that the swissALTI3D model resolution of 2 m is too coarse to detect small elements used in the classification of ground roughness. Brožová (2018) showed that roughness detection with terrain models of 0.5 m resolution better matched the field observations. The recording of a nationwide Lidar dataset will provide a DTM with more than 0.5 m resolution for Switzerland (Swisstopo ©, 2018). The data acquisition for the canton of Grisons and therefore for the study areas is planned for 2020 and 2021 (Swisstopo ©, 2018).

5.1.3.2 Diameter at breast height and K-Value

The classification of mean diameter at breast height for each forest polygon in the study area of Zernez presented only few differences with the manual classification. Although further studies are needed, this shows that the canopy height model can be used in a reliable way to obtain a quick estimate of the mean DBH of the forest polygons. As forest stand maps show the diameter of the 100 dominant trees per hectare, this method provides additional information for more accurate estimation of the DBH needed to account for forest in avalanche simulations.

The K-Value is mostly underestimated, which is due to the smoother terrain roughness as discussed in the previous section. While the runout distance predicted with this method was generally 30-60 m longer than with the manual classification in 2018 for the area of Zernez, it presented only few differences with the deposition predicted with the forest file of 1951. Also the maximum pressure of the flowing avalanche at the monitoring point in the "new track" (P1) presented a difference of around 10 kPa between simulations with forest from remote sensing (CHM) and in 1951. In the avalanche track "Vallun Quadratscha", the maximum pressure registered at the monitoring point (P2) was two times higher in 1951 compared to the simulations with remote sensing forest (CHM). This is mainly due to the afforestation at the upper treeline in the avalanche track "Vallun Quadratscha", which augmented the distance the avalanche flows through forest of around 700 m. Although the archive data only offers a vague indication, the depositions lengths obtained with forest files in 1951 that were generally smoother better matched the observations in 1951. As terrain and vegetation ground roughness are smoothened by snow accumulations (Frey and Thee, 2002; Schweizer et al., 2003) the K-Values obtained with remote sensing and its smoothing effect may better represent the real terrain for extreme snow conditions.

5.2 Simulations parameters and release areas

5.2.1 Release areas

The initial setting of release area and fracture depth strongly determine the avalanche runouts (Bebi et al., 2017; Vera Valero et al., 2017). In the case of Susauna, the areas were manually sketched on counter slope pictures and they were manually adjusted to match the flow paths observed with forest destruction in 1951. The forest destruction predicted for avalanches releasing in the east part suggests that fracture height was probably overestimated and the protective structures at the ridge may prevented more snow drift or retained more snow than assumed in this study.

Similarly, the runout distance obtained with the release at the extension of the Piz d'Urezza observed in January 2018 did not match the associated deposition in the track "Vallanzun". This suggests, that even though flanks were visible in the photo (Martin Keiser AWN GR, 2018) the associated mass was smaller compared to the rest of the release area. When changing the stauchwall and limiting the release area at the steeper zone (A1), the runout distance better matched the observations. Also, for the fracture depth one mean value is calculated for the entire area whereas in reality the fracture line is generally larger than the mean used in the simulation (Gruber and Margreth, 2001). In the case of Zernez, where the avalanche presents different flow paths after one release, the resulting mass allocation can also affect the avalanche dynamics.

5.2.2 Effect of digital terrain model accuracy on simulations

Simulations with lower DTM resolution of 10 m x 10 m had longer runout distances and different flow pattern than with the resolution of 4 m x 4 m (5 m x 5 m Zernez), which were used to present the results as suggested in Bebi et al. (2017). Although Bühler et al. (2011) showed very similar

runouts in simulations of flowing avalanches with 2 m and 25 m digital terrain model, the accuracy of the simulations strongly depends on DTMs resolution (Bartelt et al., 2011; Christen et al., 2008). According to Schweizer et al. (2003), snow heights of more than 0.3 to 1 m eliminate terrain roughness. The use of very detailed DTM is likely to not represent the smoothing of summer terrain due to high snow accumulations during winter (Bühler et al., 2011; Veitinger et al., 2014). This may be relevant only for dry-snow avalanches as Sovilla et al. (2012) showed, that small scale terrain roughness changed the flow direction of a large wet-snow avalanche and should therefore be considered in simulations .

The rough structure in the DTM of La Punt discussed in Section 5.1.3.1 was smoothened in the simulations by resampling to 4 m. The simulation in the study area of Susauna showed very strong acceleration of the avalanches in the east side (releasing from A3, A4) compared to the other avalanche tracks. This was also reflected in larger forest destruction at the lower timberline compared to observations. Despite the dependency on the release area and fracture depth definition discussed in the previous sections, this may result from a smoothing effect of the large coarser DTM band (see Section 3.2.3 Remote sensing) present in the study area. As these slabs started above the area with coarser DTM, they were initially slower than the other avalanches but then accelerated more when flowing on the coarser DTM.

The increase in the accuracy of the simulation under 5 m DTM is not significant but the simulation time increases strongly with higher resolution (Christen et al., 2008). Due to the large area in Zernez, DTM resolution was set slightly lower in order to reduce calculation time. Almost no difference in runouts distances between 4 and 5 m was observed. It was not possible to achieve same deposition for the three main avalanche tracks as presumed in 1951. The slab starting at the ridge and flowing through the “Vallanzun” track showed longer runout distances. Additionally to the uncertainties discussed in the sections above, topography in avalanche tracks with more frequent activity in the same winter are modified by previous depositions (Maggioni et al., 2013). Multiple releases in winter 2018 for this area were observed. Maggioni et al.(2013), showed different flow direction and deposition pattern in the simulations on winter terrain (digital surface model with snow height and previous depositions) compared to summer terrain (normal DTM). More frequent releases most likely followed also in 1951, which may influenced the deposition of the avalanche. Also, 3 m resolution may be more indicated for avalanches flowing in narrow gullies (Vera Valero et al., 2017) such as the “Vallanzun”.

5.2.3 Entrainment

Additionally to the release area, variations in the entrainment parameters can lead to differences in the predicted runouts (Vera Valero et al., 2017). Avalanche models that account for entrainment perform better in predicting avalanche runouts than those without (Sovilla et al., 2006). The entrainment height defines the snow cover that can potentially be eroded by the avalanche. Observations from winter 1999 showed, that avalanches on average entrained a snow height of

0.7 time the observed fracture depth (Sovilla et al., 2007). The approach used in this study to define possible entrainment height corrects the height based on altitude and a similar factor of 0.75. The entrainment height was kept equal in the simulations across the study areas as Sovilla and Bartelt (2002) showed, that the dynamic of mass uptake in the avalanche has more potential to influence runouts than the definition of entrainment height. In Susauna, the choice of slightly lower values for κ and ε was shown to decrease the runout distance of 60 -80 m and the maximum avalanche pressure at the monitoring points by more than 5 times. Especially for simulations in forested terrain, these parameters need to be chosen carefully before taking forest structure into account. In fact, the effect of lowering erosion parameters has the same magnitude as the increase of forest ground roughness by one class. The manuscript currently in edition by Bartelt et al. (2018) should provide valuable information for the estimation of such parameters.

The simulations in Zernez presented even more uncertainties as the avalanches most likely started as cold slabs and developed into slightly wet avalanches toward the end of the transition zone (Martin Keiser AWN GR, 2018; SLF, 1951b). This transition implies the entrainment of warm snow along the track (Vera Valero et al., 2015). The parameters were chosen based on the back-calculation of the 2018 event, where more information on the air temperature in release zone and warming in the deposition area was available. The use of slightly wet snow (1%) and a temperature gradient for warming of the snow cover toward the deposition showed runouts more similar to the observations. Recently, Valero et al. (2017) showed that for wet or avalanches starting in dry cold conditions and entraining warm snow the definition of fracture depth and entrainment height has a greater impact than changes in temperature and water content definition. Therefore, I find realistic the use of the same water content and snow temperature in the back-simulation of 1951 and to adjust only the entrainment height. Due to the avalanche observed in 2018 in the previous snowfall, in the track “Vallanzun” no bottom layer entrainment was used. Despite observations of earlier releases in more frequent avalanche tracks compared to unusual ones in 1951, (SLF, 1951a), no exact information on the track “Vallanzun” was available. In the case of previous avalanche release in the same snowfall, the entrainment process was significantly different than the assumption used in this study. However, the speculations leave space to multiple options, which can’t be properly described in the model without exact information on the event.

5.3 Effect of forest structure

Forest showed a reduction of the runout distance of large snow avalanches in all three study areas (scenario *T1951* and *T300*) as well as smaller avalanches (*T30*) as observed in several studies (Takeuki et al., 2016; Takeuki et al., 2011; Teich et al., 2012). In the simulations with the extended version of RAMMS, the forest effect is considered with the detrainment of snow mass from the avalanches by trees as well as with a reduction of the snow cover on the forest ground. Thereby, the snow mass uptake along the avalanche track is decreased, which influences the runout and maximum pressures of the avalanches. The potentially erodible snow layer was reduced for example to the 56% in dense mixed forests and to the 90% in open larch forests. These values corre-

spond to a forest with smooth terrain but with an increase in terrain ground roughness (higher K-Value) the snow depth in the model is additionally reduced. Accounting for snow interception only as a function of canopy coverage categories (dense, scattered and open forest) instead of the K-Value would represent the effect of snow interception more accurately but further field campaigns are needed to better parametrize this process.

5.3.1 La Punt

The canopy density of the 3 ha of forest grown on the east slopes varies slightly in the stand (40-70%), which corresponds to the lower ranges indicated for prevention of avalanche release (Margreth et al., 2008; Schneebeli and Bebi, 2004). However, due to the presence of larch, Swiss stone pine, mountain pine associated with dwarf mountain pine the stand is not regularly stocked and the avalanche control in the area is not ensured (Margreth et al., 2008). Therefore, only the release areas A8-A9 were affected by the forest closure. The major effect of forest on avalanche runout was observed for avalanches releasing from the east slopes both in 1951 and 2018 (A5-A9 or B5, A6-A7). The simulations showed, that the snow height detrained by the forest was highest at the treeline where avalanches started. For avalanches releasing above the treeline, highest detrainment values were observed in flatter slopes in mature forest. This is a result of the assumption used in the forest module, that detrainment is proportional to the braking power of the forest (K-Value) and the inverse velocity of the avalanche (Feistl et al., 2012; Feistl et al., 2014b), which is small where avalanches initiated. This leads to the same conclusion as Teich et al. (2012), that the effect of forest on runout length mainly depends on the distance the avalanche flows before entering forest. The forest closure in the east slopes (release areas A8-A9) resulted in 50-120 m shorter runouts in 2018 compared to 1951 without considering forest along the avalanche track. The effect of forest in the avalanche flow path was nearly equal or was smaller as a consequence of thinning in the gullies. Differently, the reduction of the release area A5 to B5 due to the presence of protective structures had no impact on the deposition length or maximum pressure at the shooting range. The forest growth in the gully improved the effect of forest since 1951 substantially as the maximum pressure at the shooting range was reduced by almost half and the runout by ca. 90 m.

As in the study area small dwarf mountain pines were observed to be completely bent on the ground under the high snow load, they should not be considered as avalanche control neither as additional resistance in the transition zone of extreme snow avalanches. This has been suggested since the 19th century, where mountain dwarf pine extensive stands were generally regarded as promoting factors for avalanche release with extreme snow heights rather than prevention (Frey, 1977). The loose branches may increase the instability of the snow cover and in particular the development of depth hoar (Frey, 1977). Differently, with lower snow heights they may stabilize the snow cover and exert a small braking effect on avalanches. In Sitko (2008), areas completely covered by dwarf mountain pines under a high snow cover were also considered to have a promoting effect on slab avalanche release. Even with smallest K-Values, small dwarf mountain pine

stands showed detrainment height equal to mature scattered forests when the avalanche releasing from A1 and A2 (scenario *T300*) flew into the stands on flatter slopes at the upper treeline. More frequent avalanches (scenario *T30*) were more subject to the effect of forest in the transition of A1-A2 and A4 as the release areas were strongly reduced (A3 not considered) and the total length the avalanche flows through forest increased by 360 m when considering dwarf mountain pine. Therefore, it is strongly suggested to use different forest classifications in the simulation of extreme avalanches compared to more frequent ones.

5.3.2 Susauna

In scenario *T1951* changes in canopy coverage affected the runout distance similarly as the changes in ground roughness in the avalanche paths in the west and east slopes. Differently, the runout length of the main avalanche track was diminished more by higher ground roughness (knobby) than by higher canopy coverage (dense forest). Maximum flowing avalanche pressures were also more sensible to roughness than canopy coverage. This matches the expectations, as the K-Value is increased by 10 $kgm^{-1}s^{-2}$ with an increase of one class of roughness (for example from smooth to knobby), whereas for an increased canopy coverage (for example from scattered to dense) the value is augmented by 5 $kgm^{-1}s^{-2}$. The forest growth at the upper treeline only diminished the release area A2 for extreme avalanche release. However, the runout shortening in *T300* was mostly due to the changes in forest structure in the transition zone since 1951 as simulations with same release areas but forest structure of 1951 showed 50 to 100 m longer runouts at the front. This is a result of the high stumps as well as the higher tree density observed in the young forest in 2018, that implied the definition of higher detrainment coefficients. Differences between the forest in 2018 and 1951 with exact equal release area and fracture depth were in the same range also for the avalanche tracks at the sides. The current forest structure lead to the less plausible result, that extreme avalanches stopped at the beginning of the deposition area in the east side. Similarly to 1951, the forest alone does not prevent avalanches releasing from the area B2 to reach the west side of the village of Susauna, even smaller ones with higher frequency. Also, the steel structures at the upper treeline protect the afforestation in the main track, which is subject to complete destruction in the case of large avalanche release. Only on the east side, avalanches releasing from B3, A4 and A6 in scenario *T30* completely stopped into the forest before reaching the valley bottom.

5.3.3 Zernez

The simulation showed shorter runout distance of the avalanche front in the track “Vallun Quadratscha (0-40 m) and “new track” (50-60 m) in simulations with forest in 1951 compared to simulations without. Considering the forest structure in 2018 had a more important effect on runout, with an average of 100 m shorter runouts compared to simulations without forest. The initial release volume was extreme and the first slab (release A1) started more than 1’000 m above the treeline but the division of the avalanche after the release into several tracks resulted in only a small fraction of the mass flowing in direction of the forest. The secondary release areas (B1, C, D) started at 300 m, 90 m and at the treeline respectively. The observed runout shortening in all

scenarios with forest is in agreement with Teich et al. (2012), where forest effect on runout distance is suggested for large avalanches releasing at the maximum distance of 700 m from the treeline. Although all scenarios presented detrainment heights in the lowest range, the rather long distance the avalanches flow through forest before depositing on the grassland (around 1300 m for the track "Vallun Quadratscha" and "New track") was shown to result in sufficient snow mass detrainment to reduce maximum pressures and runouts. Due to the multiple assumptions that had to be made for the classification of the forest in 1951, ground roughness was systematically smoother. However, the runout distance with the forest of 1951 better represented the observations in 1951, at least in the new avalanche track. This indicates, that smoother ground roughness is more appropriate also in this case.

5.3.4 Forest damage

In the area of Zernez, it was more difficult to back-simulate the same avalanche flow and deposition observed in 1951 together with the forest destruction, even when adding secondary release areas. In the results, the flowing avalanche reached pressures above 100 kPa in the areas where forest destruction was observed in 1951. Observations and model calculations show, that avalanches with flow heights of more than 2-3 m and pressure above 50–100 kPa can destroy mature forest stands with DBH of ca. 30 cm (Margreth et al., 2008). Back-simulations of avalanches in 2009 showed maximum pressures of 60-200 kPa for larch and 10-140 kPa for spruce at the position of broken trees in the avalanche paths (Tiri, 2009). Powder snow avalanches with pressures above 3-5 kPa can also destroy entire forests (Margreth, 2004; Margreth et al., 2008). Therefore, it is presumed that in this case the model underestimates the bending stress caused by the avalanche in the lower transition track. Alternatively, the maximum bending strengths used in the extended version of RAMMS may be too high. These refer to the average values suggested by Grosser and Teetz (1985) and uses 72 MPa for spruce, 93 MPa for pine and 134 MPa for birch. The value of 109 MPa for Larch is based on observations and first back-simulations of forest avalanches with the extended version of RAMMS. Tree pulling experiments on unfrozen soils calculate lower bending strength for stem breakage of spruce (36 MPa), birch (41 MPa) and scots pine (37 MPa). The same study suggests that bending strength needed for stem breakage of scots pine on frozen soils is almost double (63 MPa) than the strength in unfrozen soils (Peltola et al., 2000). Also, trees in unfrozen terrain are mostly uprooted and not broken (Peltola et al., 2000). In the case of the study area of Zernez, the indications from the avalanche report (SLF, 1951b) describe unfrozen terrain and uprooted trees in the lower track. Although due to the different growth and experimental conditions the threshold values presented by Peltola et al. (2000) should not be directly applied for mountain forests, it points to the conclusion that the forest in Zernez was destructed more easily due to the unfrozen terrain.

In addition, Feistl et al, (2015) suggest the magnification of the bending stress exerted by the avalanche to account for different conditions that are neglected in the model. The bending stress calculated corresponds to avalanches flowing on the normal terrain surface without considering

the existing snow cover height (Feistl et al., 2015; Feistl et al., 2014a). The load exerted by the avalanche can be 50% higher when it flows on a snow surface of 0.8 m and impacts the tree further up (Feistl et al., 2015). In the case of extreme winters such as 1951, this effect should be considered. Furthermore, broken stems or uprooted trees at the upper treeline were entrained by the avalanche. The impact of such components should be considered as additional impact to the flowing avalanche (Egli, 2005). Also in this case, Feistl et al. (2015) suggest to increase the impact pressure by 1.5 to 2 times. A magnification factor above 1 should also be applied for mature trees with heights above 20 m since the natural frequency of the tree is similar to the loading frequency of the powder avalanche (Bartelt, 2017). However, in the user interface there is no magnification option for the bending stress yet. This can be achieved by lowering the DBH as the bending stress of the avalanche core is inversely proportional to the square of the DBH of the tree. For example, by reducing the mean DBH of a forest stand from 30 cm to 20 cm the resulting bending stress is on average 2.3 times higher. For a change from 20 cm to 10 cm the factor is around 4. In the case of powder avalanches, the relation is also dependent on tree height and width.

Other factors, such as higher soil root strength of spruce in open forests compared to closed forests (Foetzki et al., 2004), the dependency of root anchorage on soil type, depth (Nicoll et al., 2005) and conditions (frozen/unfrozen) for each tree species (Peltola et al., 2000) or less snow cover height in evergreen than deciduous forests (Schneebeli and Bebi, 2004) may also generate differences between observations and simulations. Considering all this factors would require very detailed information for each forest polygon and would not be realistic in the use for practitioners. In general, the tree forest destruction predicted by the model matches the major destructions observed in the field well. In cases where it is underestimated, it is suggested to reduce the DBH of the forest polygon to obtain the observed destruction and not account for erroneous detrainment. Dwarf mountain pine is bent on the ground by avalanches flowing over the area (Frey, 1977) and the destruction shown in the results can be regarded as bending. Similarly, young trees under 5 m height (Kajimoto et al., 2004) or smaller than 6 cm DBH have flexible trunks (Johnson, 1987) and the forest destruction predicted in similar stands can also be regarded as bending on the ground.

6. Conclusions

The forest changes since 1951 affected only a small proportion of the possible release areas in La Punt and Susauna. In the study area Zernez, forest structure at the timberline did not significantly change since 1951. However, in all study areas forests were able to reduce runout length and maximum pressure of extreme avalanches. Considering forest in the back-simulation of the 1951 avalanches resulted in 70-120 m shorter runouts in La Punt and Susauna and 40-50 m in Zernez. The forest in the avalanche path affected the avalanche runouts more in 2018 than in 1951. Exceptions were detected in La Punt, where the protective function of the forest in a gully decreased since 1951 due to thinning. Avalanches with larger release volumes were influenced less by the forest despite the longer flow distance in forested terrain. In the case of La Punt and Susauna, the changes in forest structure do not guarantee the protective function against extreme events as avalanche depositions are expected to extend approximately to the same areas with endangered buildings of 1951. Differently, the growth of dwarf mountain pine stands mixed with larch, Swiss stone pine and mountain pine at the upper treeline in La Punt and Susauna is expected to reduce release areas of small and more frequent avalanches. Simulation results with forest condition in 2018 lead to the conclusion, that small avalanches stop before settlements. Only one building in Susauna is located at the front edge of small avalanches runouts.

The braking power of avalanches (K-Value) is strongly determined by ground roughness. In 2018, more detailed information for the classification of ground roughness was available, which resulted in the assignment of higher K-Values to the forest stands. Based on the assumptions applied for 1951, the ground roughness classification was generally smoother. Simulations results in 1951 were shown to approximately match the observed forest destruction, damages on buildings or-depositions observed in 1951. Therefore, the assignment of a smooth or lower ground roughness in the definition of the detrainment coefficients (K-Values) is presumed to be more adequate, at least in the case of extreme and infrequent events. This may be especially relevant for subalpine forests with species composition similar to the study areas and no particular terrain conditions (eg. talus forests). Despite being classified with the smallest K-Values, dwarf mountain pine forest stands should be considered only in the simulation of small and frequent avalanches but further studies are needed to confirm these observations. Therefore, it is suggested to differentiate between forest classification for the simulation of avalanches with different size and return period.

The analysis of the 1951 events showed, that it is possible to back-simulate forest destruction by avalanches. However, the underestimation of forest damages by large avalanches, suggest that the maximum bending strength for the tree species used in the extended version of RAMMS may be too high. This may be particularly relevant for the case where trees are uprooted instead of broken as it was observed in Zernez in 1951. Also, the prediction of powder snow avalanches destruction uses a DBH to height relation, which could be improved to account for different tree species or for differences between larch, spruce and mixed forests. Further studies on extreme forest avalanches could provide more information also on the effect of snow height on the ground

or the additional load of uprooted and broken trees for the forecast of forest damages. The back-calculation of well-documented events with more information is necessary to reduce uncertainties in the model application.

Avalanche runouts and maximum pressures are influenced in the same magnitude by changes in snow entrainment parameters as by changes in the classification of the forest ground roughness, whereas the effect of changes in canopy coverage is smaller. The further use of the extended version of RAMMS in the back-simulation of large avalanches will add more safety in the definition of the entrainment parameters, which have to be choosen carefully before taking the effect of forest in simulations into account.

The classification of forest parameters using remote sensing data leads to an underestimation of the K-Value compared to the manual classification in 2018. This is mostly due to the actual resolution of the remote sensing data, which does not allow a good detection of ground roughness. However, for the consideration of the forest effect on large and extreme snow avalanches, the procedure with remote sensing may represent a valuable option as terrain roughness is smoothened by snow accumulations. In future, remote sensing data with higher resolution will be available and will provide new opportunities for a more detailed detection of the forest parameters needed in the simulations.

7. Aknowledgements

I take this occasion to express my gratitude to my supervisor Dr. Peter Bebi, head of the group mountain ecosystems, for the opportunity to write my master thesis in his group at the SLF. I also would like to thank Dr. Peter Bebi for the supervision of my thesis, the support in the data evaluation and the suggestions in the writing process.

I would like to thank also my co-supervisor Dr. Perry Bartelt, head of the group RAMMS at the SLF, for his patient advises and explanations in the back-simulation of the avalanches.

I'm thankful to all people from the SLF who helped me, particularly Marc Christen, Dr. Yves Bühler and Lukas Stoffel for the help with remote sensing data and avalanche simulations.

In addition, I thank Martin Keiser from the cantonal office of forestry for the suggestion on the study areas and the archive information, pictures on forest conditions and avalanche events. My appreciation goes also to the forest office and community of Zernez for the archive data. A special thanks goes to Simon Luzi from Chinuos-Chel for his recollections on the events of 1951 in Susauna.

Furthermore, I'm grateful to my family and Matteo for the help in the field work and the support during the writing process. Thanks also to the people who made working and staying in Davos a great experience.

8. References

Ammann, W., 2000: Der Lawinenwinter 1999-Ereignisanalyse. Swiss Federal Institute of Snow and Avalanche Research. p 588.

Anderson, G. and McClung, D., 2012: Snow avalanche penetration into mature forest from timber-harvested terrain. *Canadian Geotechnical Journal*, 49(4), 477-484.

Archive Zernez, 1951: Zernez: picture of the avalanche of 21st January 1951.

Bartelt, P. and Stöckli, V., 2001: The influence of tree and branch fracture, overturning and debris entrainment on snow avalanche flow. *Annals of Glaciology*, 32, 209-216.

Bartelt, P., Buehler, Y., Christen, M., Deubelbeiss, Y., Salz, M. and Schumacher, L. 2011: RAMMS:AVALANCHE User Manual v1.4, SLF Davos.

Bartelt, P., Bühler, Y., Buser, O., Christen, M. and Meier, L., 2012: Modeling mass-dependent flow regime transitions to predict the stopping and depositional behaviour of snow avalanches. *Journal of geophysical research*, 117, F01015

Bartelt, P., Buser, O., Vera Valero, C. and Bühler, Y., 2016: Configurational energy and the formation of mixed flowing/powder snow and ice avalanches. *Annals of Glaciology*, 57(71), 179-188.

Bartelt, P., Vera Valero, C., Feistl, T., Christen, M., Bühler, Y. and Buser, O., 2017: Modelling cohesion in snow avalanche flow. *Journal of Glaciology*, 61(229), 837-850.

Bartelt, P., Christen, M. and Buser, O. 2018: Snow Entrainment: Avalanche Interaction with an Erodable substrate. Unedited- in process.

Bartelt, P., January 2018: [Personal communication on the simulation parameters for slab avalanches in the extended version of RAMMS].

Bates, D. M. and Pinheiro, J. C., 1998: LINEAR AND NON LINEAR MIXED EFFECT MODELS. *Annual conference on Applied Statistics in Agriculture*.

Bebi, P., Kulakowski, D. and Rixen, C., 2009: Snow avalanche disturbances in forest ecosystems—State of research and implications for management. *Forest Ecology and Management*, 257(9), 1883-1892.

Bebi, P., Bartelt, P., Christen, M. and Schmid, T., 2017: Analyse der Lawinenereignisse von 1951 und der aktuellen Lawinengefahr in La Punt-Chamues-ch unter Berücksichtigung des Waldeinflusses. Technischer Bericht zuhanden des Kantons Graubünden. WSL-Institut für Schnee und Lawinenforschung, SLF Davos - Unpublished.

BFF; SLF, 1984: Richtlinien zur Berücksichtigung der Lawinengefahr bei raumwirksame Tätigkeiten. Bern, Bundesamt für Forstwesen (BFF); Davos, Eidg. Institut für Schnee- und Lawinenforschung (SLF).

Brändli, U. B., 2010: Schweizerisches Landesforstinventar. Ergebnisse der dritten Erhebung 2004 - 2006. Birmensdorf, Eidgenössische Forschungsanstalt für Wald, Schnee und Landschaft WSL, Bundesamt für Umwelt, BAFU, Bern. p 42.

Brožová, N., 2018: Forest Effects on Avalanche Dynamics: Evaluation and Improvement of the Avalanche Model RAMMS. (Master Thesis), Universität für Bodenkultur Wien.

Bründl, M. and Margreth, S., 2015: Chapter 9: Integrative Risk Management. The Example of snow Avalanches. In: Snow and Ice-Related Hazards, Risks and Disasters. 263-301.

Bühler, Y., Christen, M., Kowalski, J. and Bartelt, P., 2011: Sensitivity of snow avalanche simulations to digital elevation model quality and resolution. *Annals of Glaciology*, 52(58), 72-80.

Christen, M., Bartelt, P., Kowalksi, J. and Stoffel, L., 2008: Calculation of dense snow avalanches in three dimensional terrain with the numerical simulation programm RAMMS. *International snow science workshop*.

Christen, M., Bartelt, P. and Kowalksi, J., 2010a: Back calculation of the In den Arelen avalanche with RAMMS: interpretation of model results. *Annals of Glaciology*, 51(54).

Christen, M., Kowalski, J. and Bartelt, P., 2010b: RAMMS: Numerical simulation of dense snow avalanches in three-dimensional terrain. *Cold Regions Science and Technology*, 63(1-2), 1-14.

Christian, R. and Streibig, J. C., 2009: Non linear regression with R. Edited by Giovanni Parmigiani, Springer New York.

Crawley, M. J., 2007: The R Book. John Wiley and Sons Ltd. 942.

Dreier, L., Bühler, Y., Ginzler, C. and Bartelt, P., 2016: Comparison of simulated powder snow avalanches with photogrammetric measurements. *Annals of Glaciology*, 57(71), 371-381.

Egli, T., 2005: Wegleitung Objektschutz gegen gravitative Naturgefahren. Vereinigung Kantonaler Feuerversicherungen (Hrsg). Bern.

Feistl, T., Bebi, P., Bühler, Y., Christen, M., Teich, M. and Bartelt, P., 2012: Stopping behaviour of snow avalanches in forests. *Proceedings, International Snow Science Workshop, Anchorage Alaksa*, 420-426.

Feistl, T., Bebi, P., Margreth, S. and Bartelt, P., 2014a: Forest damage by wet and powder snow avalanches. *Proceedings, International Snow Science Workshop*, Banff, 657-664.

Feistl, T., Bebi, P., Teich, M., Bühler, Y., Christen, M., Thuro, K. and Bartelt, P., 2014b: Observations and modeling of the braking effect of forests on small and medium avalanches. *Journal of Glaciology*, 60(219), 124-138.

Feistl, T., 2015: Vegetation effects on avalanche dynamics. Ingenieurfakultät Bau Geo Umwelt, Lehrstuhl für Ingenieurgeologie. Technische Universität München, 1-19.

Feistl, T., Bebi, P., Christen, M., Margreth, S., Diefenbach, L. and Bartelt, P., 2015: Forest damage and snow avalanche flow regime. *Natural Hazards and Earth System Science*, 15(6), 1275-1288.

Foetzki, A., Jonsson, M., Kalberer, M., Simon , H., Mayer, A. C., Lundström, T. and Stöckli, V., Amman, Walter J., 2004: Die mechanische Stabilität von Bäumen: das Projekt Baumstabilität des FB Naturgefahren. *Forum für Wissen* 35-42.

Frehner, M., Wasser, B. and Schwitter, R., 2005: Nachhaltigkeit und Erfolgskontrolle im Schutzwald (NaiS). *Wegleitung für Pflegemassnhamen in Wälder mit Schutzfunktion*, Vollzug Umwelt. Bundesamt für Umwelt, Wald und Landschaft. Bern, 564.

Frey, W., 1977: Wechselseitige Beziehungen zwischen Schnee und Pflanzen - Eine Zusammenstellung anhand von Literatur. Mitteilungen des Eidg. Institutes für Schnee- und Lawinenforschung SLF, 34, 1–223.

Frey, W. and Thee, P., 2002: Avalanche protection of winthrow areas,: A ten year comparioson of cleared and uncleared starting zones. *Snow Landsc. Res.*, 77 1/2, 89-107.

Ginzler, C. and Hobi, M. L., 2015: Countriwide Stereo-Image Matching for Updating Digital Surface Models in the Framework of the Swiss National Forest Inventory. *Remote Sensing*, 7, 4343-4370.

Ginzler, C. and Hobi, M. L., 2016: Das aktuelle Vegetationshöhenmodell der Schweiz: spezifische Anwendungen im Waldbereich. *Schweizerische Zeitschrift fur Forstwesen*, 167(3), 128-135.

Ginzler, C., December 2018: [Personal communication explanatory variables for goodness of the canopy height model].

Gould, S. B., Glenn, N. F., Temuulen, T. S. and Spaete, L. P., 2013: Influence of a Dense, Low-height Shrub Species on the Accuracy of a Lidar-derived DEM. *Photogrammetric Engineering & Remote Sensing*, 79(5), 421-431.

Grosser, D. and Teetz, W., 1985: Einheimische Nutzhölzer., Centrale Marketinggesellschaft der deutschen Agrarwirtschaft GmbH (CMA), Bonn, und Arbeitsgemeinschaft Holu e.V., Düsseldorf. In: Feistl, T., Bebi, P., Margreth, S., Bartelt, P., 2014: Forest damage by wet and powder snow avalanches. *Proceedings, International Snow Science Workshop,* Bannff, p 662.

Gruber, U. and Margreth, S., 2001: Winter 1999: a valuable test of the avalanche-hazard mapping procedure in Switzerland. *Annals of Glaciology*(32).

Gruber, U. and Bartelt, P., 2007: Snow avalanche hazard modelling of large areas using shallow water numerical methods and GIS. *Environmental Modelling & Software*, 22(10), 1472-1481.

Gureicke, M., 2001: Growth dynamics of mixed stands of beech and European larch. *Technical report*, Fakultät für Forstwissenschaften und Waldökologie, Georg-August-Universität. Göttingen, Germany. In: Allometric relationships of selected european tree species. *Betula pubescens, Fagus sylvatica, Larix decidua, Picea abies, Pinus sylvestris.* European Commission, Joint research centre. 2003.

Hubler, H. and Rychetnik, J., 1991: Effects of forests near the timberline on avalanche fomration. *Snow, Hydrology and Forests in High Alpine Areas*, 205.

Hyyppä, J., Pyysalo, U., Hyyppä, H. and Samberg, A., 2000: Elevation accuracy of laser scanning-derived digital terrain and target models in forest environment. *Proceedings of EARSeL-SIG-Workshop LIDAR,*, Dresden/FRG, June 16-17.

Indermühle. 1978: Struktur-, Alters- und Zuwachsuntersuchungen in einem Fichten-Plenterwald der subalpinen Stufe. Ph.D. thesis, Eidgenössische Technische Hochschule Zürich.

Jamieson, B., Margreth, S. and Jones, A., 2008: Application and limitations of dynamic models for snow avalanche hazard mapping. *International snow science workshop 2008, Whistler*, 730-739.

Johnson, E. A., 1987: The relative importance of snow avalanche disturbance and thinning on canopy plant populations. *Ecology*, 68, 43-53.

Kajimoto, T., Daimaru, H., Okamoto, T., Otani, T. and Onodera, H., 2004: Effects of snow avalanche disturbance on regeneration of subalpine *Abies mariesii* forest, northern Japan. *Arctic, Antarctic, and Alpine Research*, 36, 436-445.

Laternser, M. and Pfister, C., 1997: Avalanches in Switzerland 1500-1990.

Laternser, M. and Ammann, J. W., 2001: Der Lawinenwinter 1951. *Schweizer Zeitschrift für Forstwesen*.

Maggioni, M., Bovet, E., Dreier, L., Buehler, Y., Godone, D., Bartelt, P., Freppaz, M., Chiaia, B. and Segor, V., 2013: Influence of Summer and Winter Surface Topography on Numerical Avalanche Simulations. *International Snow Science Workshop Grenoble – Chamonix Mont-Blanc*.

Margreth, S., 2004: Die Wirkung des Waldes bei Lawinen. *Forum für Wissen*, 21-26.

Margreth, S. 2007: Lawinenverbau im Anbruchgebiet. Technische Richtlinie als Vollzugshilfe. Umwelt-Vollzug Nr. 0704. Bundesamt für Umwelt,Bern.

Margreth, S., Burkard, A. and Buri, H., 2008. Beurteilung der Wirkung von Schutzmassnahmen gegen Naturgefahren als Grundlage für ihre Berücksichtigung in der Raumplanung. Teil B: Lawinen: PLANAT.

Martin Keiser AWN GR, 2018: Flug Unterengadin. Photos Zernez - Vallanzun und Vallun Quadratscha.

McClung, D. and Schaerer, P., 2009: Chapter 4: Avalanche Formation. In: The Avalanche Handbook. 73-106.

Meliorationsamt und Vermessungsamt Graubünden. 1951. Lawinenschaden in Zernez: Kanton Graubünden.

Meyer-Grass, M. and Schneebeli, M., 1992: Die Abhängigkeit der Waldlawinen von Standorts-, Bestandes- und Schneeverhältnissen. *Interpraevent 1992 Bern*, Tagungspublikation, Band 2, 443-455.

Nicoll, B. C., Gardiner, B. A., Rayner, B. and Peace, A. J., 2005: Anchorage of coniferous trees in relation to species, soil type, and rooting depth. *Forest Research*, Northern Research Station, Roslin, Midlothian, Scotland, EH25 9SY, UK.

Peltola, H., Kellomäki, S. and Granander, M., 2000: Mechanical stability of scots pine, norway spruce and birch: analysis of tree-pulling experiments in finland. *Forest Ecol. Manag.*, 135(1), 143-153.

Pitsch, N., 2015: Gefahrenbeurteilung. Intensitätskarten und Gefahrenkarte Lawinen La Punt. Gemeinde La Punt Chamues-ch, Gebiet Arschaida.

Platzer, K., Bartelt, P. and Jaedicke, C., 2007: Basal shear and normal stresses of dry and wet snow avalanches after a slope deviation. *Cold Regions Science and Technology*, 49(1), 11-25.

Prodan, M. 1965: Holzmeßlehre J D Sauerlander's Verlag, Frankfurt/M. In: Indermühle M., 1978: Struktur-, Alters- und Zuwachsuntersuchungen in einem Fichten-Plenterwald der subalpinen Stufe. Ph.D. thesis, Eidgenössische Technische Hochschule Zürich.

Regamey, B., 26.03.2018: [Personal communication from Swisstopo on the creation of SwissALTI3D terrain model in the study area of La Punt (e-mail communication).].

Reutebuch, S. E., McGaughey, R. J., Andersen, H.-E. and Carson, W. W., 2003: Accuracy of a high-resolution lidar terrain model under a conifer forest canopy. *Can.J.Remote Sensing*, 29(5), 527-535.

Rickenbach, D., 2018: [Procedure to calculate terrain roughness implemented in ArcGIS].

Saeki, M. and Matsuoka, H., 1969: Snow buried young forest trees growing on steep slopes. *J Jpn Soc Snow Ice*, 31, 19-23.

Salm, B., 1978: Snow forces on forest plants. . *Proceedins of the IUFRO Seminar Mountain Forests and Avalanches, Davos, Switzerland*, 157-182. In: Bebi, P., Kulakowski, D., Rixen, C., 2009: Snow avalanche disturbances in forest ecosystems-State of research and implications for management.

Salm, B., Burkhard, A. and Gubler, H. U., 1990. Berechnung von Fliesslawinen eine Anleitung für Praktiker: SLF.

Salm, B., 1993: Flow, flow transition and runout distances of flowing avalanches. *Annals of glaciology*, 18.

Sappington, J. M., Longshore, K. M. and Thompson, D. B., 2007: Quantifying Landscape Ruggedness for Animal Habitat Analysis: A Case Study Using Bighorn Sheep in the Mojave Desert. *Journal of Wildlife Management*, 71(5), 1419-1426.

Schneebeli, M. and Bebi, P., 2004: Snow and avalanche control. In: Hydrology. 397-402.

Schweizer, J., Jamieson, J. B. and Schneebeli, M., 2003: Snow avalanche formation. *Rev. Geophys.*, 41(4), 1016.

Schweizer, J., Bartelt, P. and van Herwijnen, A., 2015: Chapter 12: Snow avalanches. In: Snow and Ice-Related Hazards, Risks and Disasters, 395-436. 395-436.

Simon Luzi. 2018: [Inteview on the 1951 avalanche in Susauna and Chinuos-Chel with inhabitant of Chinuos-Chel].

Sitko, R., 2008: Využitie geoinformatiky pri identifikácii, hodnotení a rajonizácii funkcií lesa (Utilization of the geoinformatics for the forest functions identification, evaluation and zoning). In Brožová N., : Forest Effects on Avalanche Dynamics: Evaluation and Improvement of the Avalanche Model RAMMS (Master thesis). p 52.

SLF, 1951a: Schnee und Lawinen in den Schweizeralpen, Winter 1950/1951. Davos, Eidg. Institut für Schnee -und Lawinenforschung.

SLF. 1951b: Fragebogen für Schadenlawinen in La Punt, Susauna und Zernez. Eidg. Institut für Schnee und Lawinenforschung.

SLF, 2000: Der Lawinenwinter 1999. Ereignisanalyse. Davos, Eidg. Institut für Schnee -und Lawinenforschung, 588.

Sovilla, B. and Bartelt, P., 2002: Observations and modelling of snow avalanche entrainment. *Natural Hazards and Earth System Science*, 2(169-179).

Sovilla, B., Burlando, P. and Bartelt, P., 2006: Field experiment and numerical modeling of mass entrainment in snow avalanches. *J. Geophys. Res*, 111.

Sovilla, B., Margreth, S. and Bartelt, P., 2007: On snow entrainment in avalanche dynamics calculations. *Cold regions Science and Technology*, 47, 69-79.

Sovilla, B., Sonatore, I., Bühler, Y. and Margreth, S., 2012: Wet snow avalanche interaction with a deflectin dam: field observations and numerical simulations in a case study. *Nat. Hazards Earth Syst. Sci.*, 12(1407-1423).

Stoffel, L., Margreth, S., Schaer, M., Christen, M., Bühler, Y. and Bartelt, P. 2016: Powder Snow Avalanche Engineering: New Methods to Calculate Air-Blast Pressures for Hazard Mapping. Interpraevent 2016 - Conference Proceedings.

Stoffel, L., January 2018: [Personal communication: new assumptions on snow entrainment with RAMMS extended Module].

Takeuki, Y., Torita, H., Nishimura, K. and Hirashima, H., 2011: Study of a large-scale dry slab avalanche and the extent of damage to a cedar forest in the Makunosawa valley, Myoko, Japan. *Annals of Glaciology*, 52(58).

Takeuki, Y., Nishimura, K. and Patra, A., 2016: Observations and numerical simulations of the braking effect of forest on large-scale avalanches. *Unpublished- In Review*.

Teich, M., Bartelt, P., Grêt-Regamey, A. and Bebi, P., 2012: Snow Avalanches in Forested Terrain: Influence of Forest Parameters, Topography, and Avalanche Characteristics on Runout Distance. *Arctic, Antarctic, and Alpine Research*, 44(4), 509-519.

Teich, M., 2013: Snow avalanche in forested terrain. Dissertation, Department of Civil, Environmental and Geomatic Engineering, ETH, Zürich, Switzerland.

Teich, M., Fischer, J. T., Feistl, T., Bebi, P., Christen, M. and Grêt-Regamey, A., 2014: Computational snow avalanche simulation in forested terrain. *Natural Hazards and Earth System Science*, 14(8), 2233-2248.

Tiri, R., 2009: Interaktionen zwischen verschiedenen Baumeigenschaften und Lawinen. Masterarbeit an der Professur für Waldökologie, Departement Umweltwissenscahften, ETH Zürich.

Veitinger, J., Sovilla, B. and Purves, R. S., 2014: Influence of snow depth distribution on surface roughness in alpine terrain: a multi-scale approach. *The Cryosphere*, 8, 547-569.

Veitinger, J., Purves, R. S. and Sovilla, B., 2016: Potential slab avalanche release area identification from estimated winter terrain: a multi-scale, fuzzy logic approach. *Natural Hazards and Earth System Sciences*, 16(10), 2211-2225.

Veitinger, J. and Sovilla, B., 2016: Linking snow depth to avalanche release area size: measurements from the Vallée de la Sionne field site. *Natural Hazards and Earth System Sciences*, 16(8), 1953-1965.

Vera Valero, C., Jones, K. W., Bühler, Y. and Bartelt, P., 2015: Release temperature, snow-cover entrainment and the thermal flow regime of snow avalanches. *Journal of Glaciology*, 61(225), 173-184.

Vera Valero, C., Wever, N., Christen, M. and Perry, B., 2017: Modeling the influence of snowcover temperature and water content on wet snow avalanche runout. *Under rewiev for Nat. Hazards and Earth Syst. Sci.* , 36.

Waser, L. T., Fischer, C., Wang, Z. and Ginzler, C., 2015: Wall-to-wall Forest Mapping Based on Digital Surface Models from Image-Based Point Clouds and NFI Forest Definition. *Forests*, 6, 4510-4528.

Wirtschaftsplan S-chanf. 1955. Zusammmenstellung der Lawinenschäden an Waldbeständen der Gemeinde S-chanf, Forstkreis XI. Bericht an das Forstinspektorat Graubünden.

Wirtschaftsplan Zernez. 1924. Wirtschaftsplan Kleinwaldungen Zernez 1924 -43.

Internet and data sources

EVA report. 26.02.2018. Highest measured snow height values and extreme value statistics. Retrieved from http://eva.zamg.ac.at/evaplus/

Kanton Graubünden.2018a: Bestandeskarte http://map.geo.gr.ch/gr_webmaps/wsgi/theme/Waldbetriebsplan%20-%20Bestandeskarte.

Kanton Graubünden.2018b: Übersichtsplan Kanton Graubünden. Retrieved 09.01.2018 http://app.geo.gr.ch/gis-tools/gdds/inventar/detailinventar.php?datenbestand_id=21&sesid=6vcnanf96ge2aste8hbdvqs7i7&action=show&viewmode=intranet.

Kanton Graubünden.2018c: Schutzbautenkataster. Retrieved 03.01.2018 http://map.geo.gr.ch/gr_webmaps/wsgi/theme/Verbauungen%20und%20Schutzbauten.

Swisstopo ©.1946: Orthophotos. Geoprocessed by Mauro Marty in October 2017

Swisstopo ©.1956: Orthophotos. Geoprocessed by Mauro Marty in October 2017

Swisstopo ©.2017: Orthophotos and maps.

Swisstopo ©. 2018. LiDAR Data Acquisition. Retrieved 21.03.2018, from https://www.swisstopo.admin.ch/de/wissen-fakten/geoinformation/lidar-daten.html

Appendix

A. Sample plots location

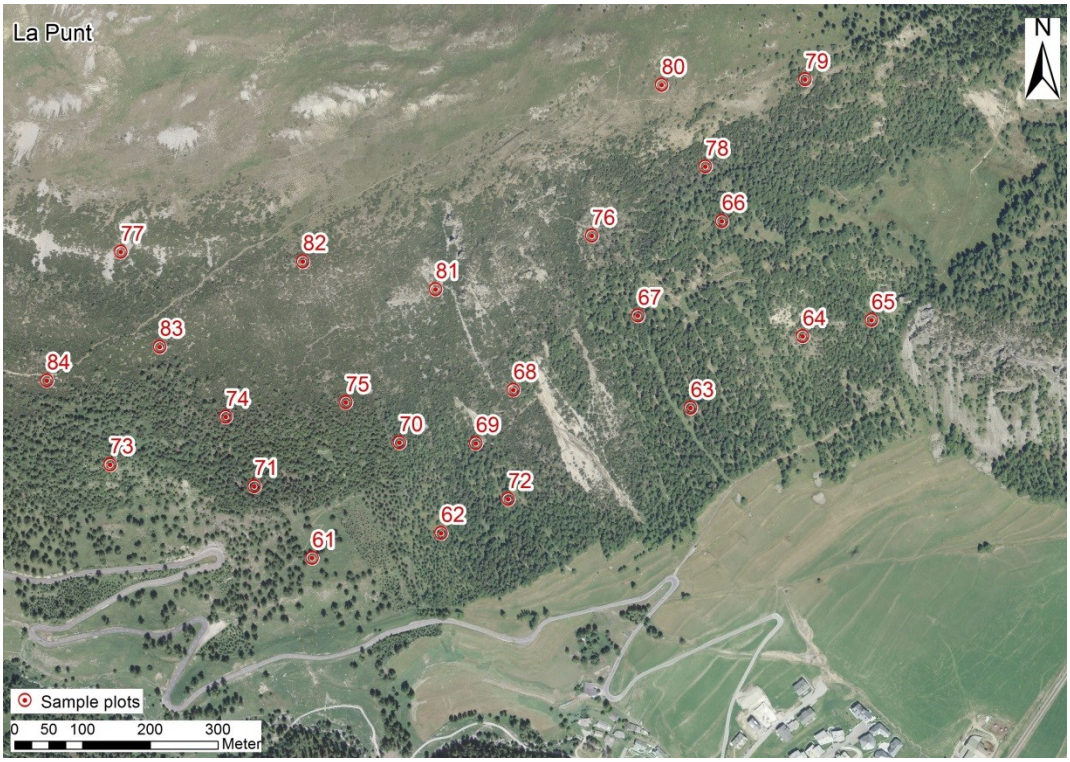

Figure 39: Field sample plots in the study area La Punt.

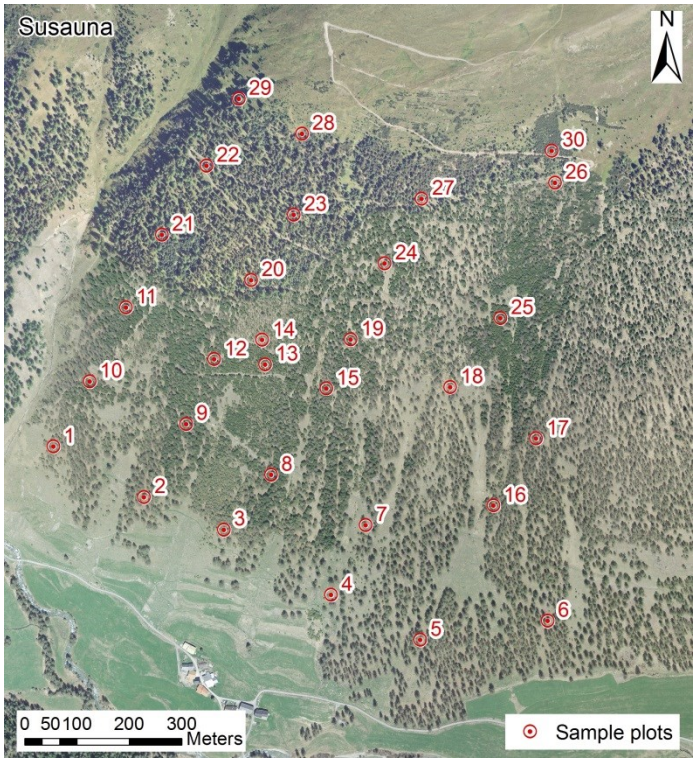

Figure 40: Field sample plots in the study area Susauna.

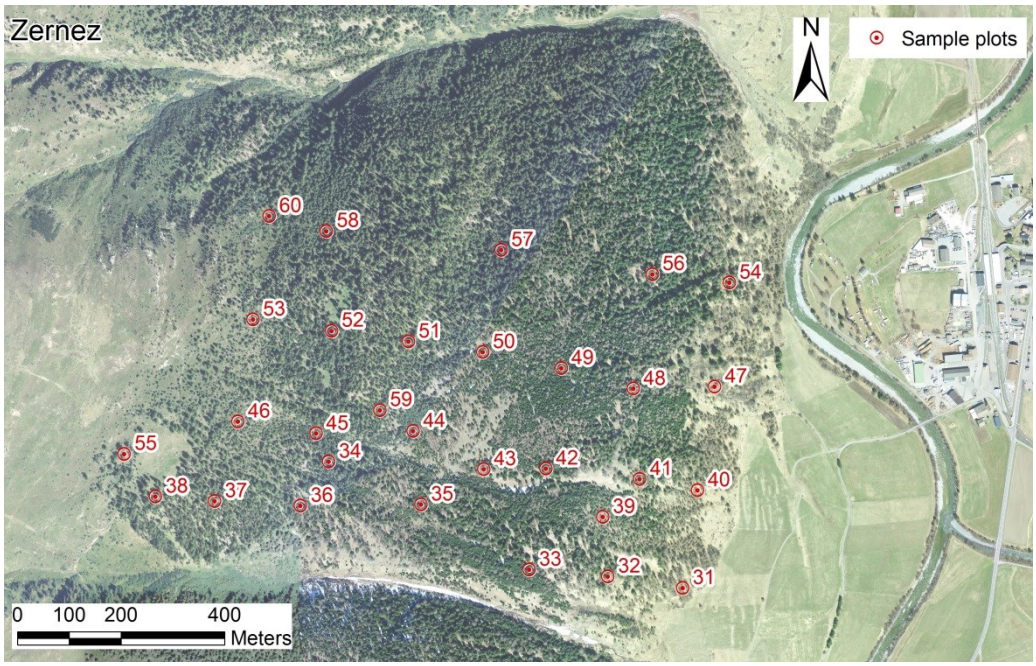

Figure 41: Field sample plots in the study area of Zernez.

B. Extreme value statistics

Name	ZUOZ		
Owner	SLF (WSL-Institut fuer Schnee- und Lawinenforschung SLF)		
Coordinates: lat/lon/height	46.60/9.96/1710m	**Period of Measurements**	1944 - 2018
Region	SCHWEIZ (SLF)	**Missing / Selected Years**	0/75
EVA+ Station Number	5019907	**Total Period of Measurments**	1944 - 2018
Original Station Number	5019_7ZU	**Extreme Value Distribution**	GUM / MLE

SLF
ENA
SNV
PNL

Highest Measured Values

Rank	1		2		3		4		5	
	Date	**[cm]**	**Date**	**[cm]**	**Date**	**[cm]**	**Date**	**[cm]**	**Date**	**[cm]**
1 day	1951-01-21	60	1981-10-27	56	1995-01-11	56	1991-12-22	55	1959-10-29	48
2 days	1951-01-20	99	1996-11-14	68	1995-01-11	60	1999-04-16	59	1991-12-21	58
3 days	1951-01-19	118	1950-01-03	70	1996-11-13	68	1983-01-15	66	1991-12-20	65
5 days	1951-01-19	118	1991-12-18	82	1950-01-01	70	1992-12-04	68	1996-11-11	68
10 days	1951-01-12	142	1991-12-13	82	1979-11-07	80	1981-10-18	77	1944-11-03	73
15 days	1951-01-12	147	1944-10-30	87	1968-01-13	85	1979-11-02	84	1991-12-08	82
Month	1951-01-13	200	1999-01-26	125	1944-11-10	124	1949-12-06	124	1996-11-14	124
Year	1951	463	1950	359	1945	331	2014	323	2001	319

Computed values for different Return Times (Extreme Value Distribution: GUM / MLE)

Return Time	5	10	20	30	50	100	150	200	300	[YEARS]
1 day	38	45	51	54	58	64	68	70	73	[cm]
2 days	48	56	64	68	74	81	86	89	93	[cm]
3 days	51	60	68	73	79	88	92	96	101	[cm]
5 days	56	66	75	80	86	95	100	104	109	[cm]
10 days	66	76	87	93	100	110	116	120	126	[cm]
15 days	75	87	99	105	114	125	131	136	142	[cm]
Month	105	121	137	146	157	173	182	188	197	[cm]
Year	277	319	359	383	412	451	474	490	513	[cm]

Figure 42: Highest measured values and computed values with Gumbel distribution at the measuring station Zuoz (EVA EVA report, 26.02.2018).

Name	ZUOZ		
Owner	SLF (WSL-Institut fuer Schnee- und Lawinenforschung SLF)		
Coordinates: lat/lon/height	46.60/9.96/1710m	**Period of Measurements**	1944 - 2018
Region	SCHWEIZ (SLF)	**Missing / Selected Years**	0/75
EVA+ Station Number	5019907	**Total Period of Measurments**	1944 - 2018
Original Station Number	5019_7ZU	**Extreme Value Distribution**	GUM / MLE

SLF
ENA
SNV
PNL

Highest Measured Values

Rank	1		2		3		4		5	
	Date	[cm]	Date	[cm]	Date	[cm]	Date	[cm]	Date	[cm]
1 day	1951-01-21	60	1981-10-27	56	1995-01-11	56	1991-12-22	55	1959-10-29	48
2 days	1951-01-20	99	1996-11-14	68	1995-01-11	60	1999-04-16	59	1991-12-21	58
3 days	1951-01-19	118	1950-01-03	70	1996-11-13	68	1983-01-15	66	1991-12-20	65
5 days	1951-01-19	118	1991-12-18	82	1950-01-01	70	1992-12-04	68	1996-11-11	68
10 days	1951-01-12	142	1991-12-13	82	1979-11-07	80	1981-10-18	77	1944-11-03	73
15 days	1951-01-12	147	1944-10-30	87	1968-01-13	85	1979-11-02	84	1991-12-08	82
Month	1951-01-13	200	1999-01-26	125	1944-11-10	124	1949-12-06	124	1996-11-14	124
Year	1951	463	1950	359	1945	331	2014	323	2001	319

Computed values for different Return Times (Extreme Value Distribution: GUM / MLE)

Return Time	5	10	20	30	50	100	150	200	300	[YEARS]
1 day	38	45	51	54	58	64	68	70	73	[cm]
2 days	48	56	64	68	74	81	86	89	93	[cm]
3 days	51	60	68	73	79	88	92	96	101	[cm]
5 days	56	66	75	80	86	95	100	104	109	[cm]
10 days	66	76	87	93	100	110	116	120	126	[cm]
15 days	75	87	99	105	114	125	131	136	142	[cm]
Month	105	121	137	146	157	173	182	188	197	[cm]
Year	277	319	359	383	412	451	474	490	513	[cm]

Figure 43: Highest measured values and computed values with Gumbel distribution at the measuring station of Zernez (EVA EVA report, 26.02.2018)

C. Release areas for each study area and scenario

La Punt

Table 16: Release areas for scenario 1951 in La Punt with mean fracture depth (d_0) area, mean slope and volume. Total volume 83'475 m^3.

1951	***A1***	***A2***	***A3***	***A4***	***A5***	***A6***	***A7***	***A8***	***A9***
d0	0.85	0.92	0.7	0.67	0.91	0.92	0.9	0.95	0.97
Area [m2]	9'664	10'816	17'376	4'096	10'000	6'416	12'848	2'352	4'608
Slope	37.1	35.5	41.7	43.4	34.4	33.9	34.4	32.5	31.9
Volume [m^3]	10'459	12'249	16'506	3'853	11'221	7162	14'073	2'666	5'286

Table 17: Release areas for scenario T300 in La Punt with mean fracture depth (d_0) area, mean slope and volume. Total volume 74'079 m^3.

T300	***A1***	***A2***	***A3***	***A4***	***B5***	***A6***	***A7***	***B10***
d0	0.85	0.92	0.7	0.67	0.89	0.92	0.9	0.69
Area [m2]	9'664	10'816	17'376	4'096	6'368	6464	12'848	2'832
Slope	37.1	35.5	41.7	43.4	34.4	33.9	34.4	41.8
Volume [m^3]	10'459	12'249	16'506	3'853	6'988	7'213	14'073	2'738

Table 18: Release areas for scenario T300 in La Punt with mean fracture depth (d_0) area, mean slope and volume.Total volume 22'353 m^3.

T30	***A1***	***A2***	***A4***	***C5***	***C6***
d0	0.67	0.72	0.52	0.51	0.60
Area [m2]	9664	10'816	4'096	1'472	736
Slope	37.1	35.5	43.4	41.4	35.7
Volume [m^3]	8187	9635	2981	1003	544

Susauna

Table 19: Release areas for scenario 1951 in Susauna with mean fracture depth (d_0) area, mean slope and volume Total volume 47'753m^3. In the release areas the frictional coefficients are lowered to $\mu = 0.5$ and $\xi = 2500$ m/s^2.

1951	***A1***	***A2***	***A3***	***A4***	***A5***	***A6***
d0	1.53	1.56	1.48	1.24	1.24	1.28
Area [m2]	5'632	11'472	4'736	1'792	2'000	1'360
Slope	32.7	32.5	28.1	31.7	38.5	37.7
Volume [m^3]	10'289	21'410	7'994	2648	3'191	2'221

Table 20: Release areas for scenario T300 in Susauna with mean fracture depth (d_0), area, mean slope and volume. Total volume 38'357 m^3. In the release areas the frictional coefficients are lowered to $\mu = 0.5$ and $\xi = 2500$ m/s^2.

T300	***A1***	***B2***	***B3***	***A4***	***A6***
d0	1.53	1.64	1.90	1.65	1.28
Area [m2]	5'632	7'376	3664	1'792	1'360
Slope	32.7	31.5	28.8	31.7	37.7
Volume [m^3]	10'289	14'321	8'002	3524	2'221

Table 21: Release areas for scenario T300 in Susauna with mean fracture depth (d_0), area, mean slope and volume. Total volume 14'625 m^3. In the release areas the frictional coefficients are lowered to $\mu = 0.5$ and $\xi = 1500$ m/s^2.

T30	***B2***	***B3***	***A4***	***A6***
d0	0.85	0.99	0.87	0.67
Area [m2]	7'376	3'664	1'792	1'360
Slope	31.5	28.8	31.7	37.7
Volume [m^3]	7427	4'186	1'852	1'160

Zernez

Table 22: Release areas for scenario 1951 in Zernez with mean fracture depth (d_0), area, mean slope and volume For secondary areas, release time after first release is shown. Total volume without sensitivity (A1, B1, C and D) is 140'597 m^3. In the release areas the frictional coefficients are lowered to $\mu = 0.01$ and $\xi = 4000$ m/s^2.

1951	***A1***	***B1***	***B (B1 + B2)***	***C***	***D***
d0	1.34	1.04	1.05	0.93	0.98
Area [m2]	42'528	23'828	46'536	11'904	19'648
Slope	35.9	35.2	35.4	37.6	35.3
Volume [m^3]	71'610	30'891	59'944	14'294	23'802
Secondary release	-	25	25	38	42

Table 23: Release areas for scenario 1951 in Zernez with mean fracture depth (d_0), area, mean slope and volume For secondary areas, release time after first release is shown. Total volume without sensitivity (A1, B) is 84567 m^3. In the release areas the frictional coefficients are lowered to $\mu = 0.01$ and $\xi = 4000$ m/s^2.

T22J	***A1***	***A (A1 + A2)***	***B (B1&B2)***
d0	1.12	1.27	0.82
Area [m2]	42'576	58'824	46'536
Slope	35.9	33.01	35.5
Volume [m^3]	59'853	91'389	58'074
Secondary release	-	-	25

D. Regression models

Table 24: Linear natural logarithmic regression between tree height and DBH for the tree types measured in the field. The general regression accounts for all the trees except dwarf mountain pine.

$$\ln(\text{height}) = a + b * \ln(\text{DBH})$$

Tree type	a	b	AIC	R^2
Swiss stone pine	0.21 (0.05)	0.69 (0.02)	-9	0.89
Larch	0.36 (0.06)	0.72 (0.02)	-54	0.86
Spruce	0.20 (0.05)	0.78 (0.02)	98	0.84
Dwarf mountain pine	0.23 (0.04)	0.53 (0.02)	-78	0.73
Mountain pine	0.16 (0.19)	0.64 (0.07)	18	0.64
General	0.21 (0.04)	0.74 (0.01)	221.27	0.83

Table 25: Fitted power regression between tree height and DBH for the tree types measured in the field. The general regression accounts for all the trees except dwarf mountain pine.

$$\text{height} = DBH^b$$

Tree type	b	AIC	R^2
Swiss stone pine	0.74 (0.01)	706	0.77
Larch	0.8 (0.00)	1197	0.43
Spruce	0.84 (0.01)	1246	0.95
Dwarf mountain pine	0.65 (0.00)	563	0.69
Mountain pine	0.73 (0.01)	228	0.65
General	0.80 (0.00)	3533	0.74

Table 26: Model regressions to predict DBH from the explanatory variable H90 (90th percentile of the CHM).

Model	Equation	a	b	AIC	R^2
linear	DBH = $a_{forest\ type}$ + b*H90	a_{La} =11.51 (3.69) a_{Ev}=-0.23 (4.25) a_{Mi} = 4 (2.78) a_{Pm} = -0.15 (4.29)	1.73 (+-0.18)	540	0.69
logarithmic	ln(DBH) = $a_{forest\ type}$ + b*ln(H90)	a_{La}= 1.58 (0.2) a_{Ev}= 1.32 (0.14) a_{Mi}= 1.35 (0.09) a_{Pm}= 0.86 (0.16)	0.74 (+-0.07)	40	0.82
Power	DBH= H90^$a_{forest\ type}$	a_{La}=1.27 (0.02) a_{Ev}= 1.14 (0.04) a_{Mi}=1.23 (0.02) a_{Pm}=1.28 (0.2)	-	555	0.6

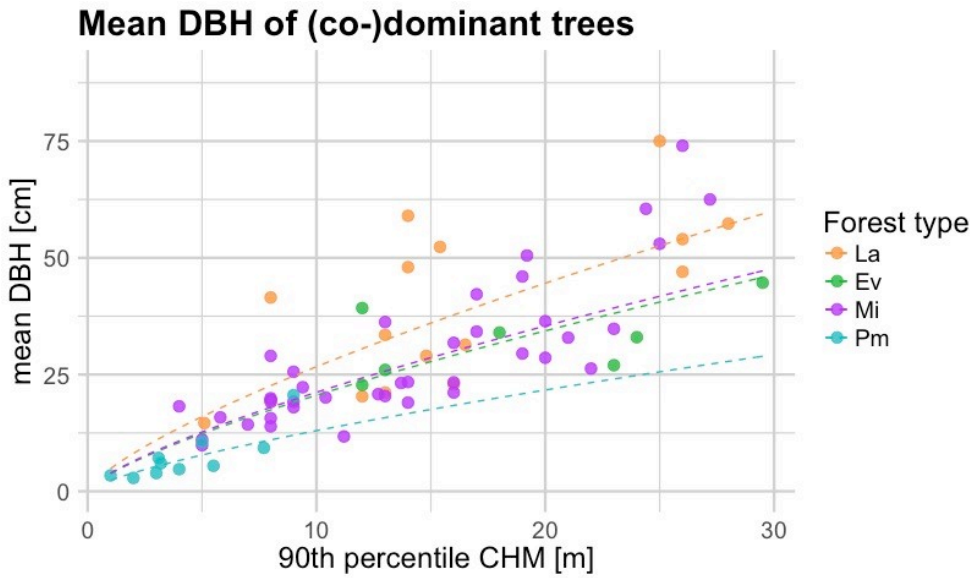

Figure 44: The dotted lines show the relation of mean DBH of (co-)dominant trees with the 90th percentile of CHM as explanatory variable for each forest type. The dots show the mean DBH measured in the field in relation to the 90th CHM value calculated in ArcGIS at each plot (La = larch, Ev = evergreen, Mi = mixed, Pm = dwarf mountain pine).

List of Figures

List of Tables